

Quantifying the Distribution of Rail Bending Stresses along the Track using Train-Mounted
Deflection Measurements

by

Saeideh Fallah Nafari

A thesis submitted in partial fulfillment of the requirements for the degree of

Doctor of Philosophy

in

STRUCTURAL ENGINEERING

Department of Civil and Environmental Engineering
University of Alberta

© Saeideh Fallah Nafari, 2017

Abstract

Heavy and frequent train loads generate large bending stresses in rail. These stresses contribute to the propagation of transverse fatigue defects, which are among the leading causes of broken rail derailments in North America. A thorough assessment of the rail structural condition requires reliable methods for estimating rail bending stresses. This is often challenging due to the many uncontrollable environmental, operational, and structural factors that affect the magnitude of rail bending stresses along the thousands of miles of track.

In this study, a new methodology was developed for estimating rail bending stresses over long distances using train-mounted vertical track deflection (VTD) measurements. Mathematical correlations between track modulus, rail deflection, rail stress, and applied load form the basis of the method. To develop the correlations, a new finite element modelling method was developed which allowed the simulation of a stochastically varying track modulus along the track. Track models with different track modulus distributions were developed and the resulting VTD and rail bending stresses under moving wheel loads were calculated. The mathematical correlations between the inputted track modulus, modelled VTD and rail bending stresses were quantified using statistical approaches.

Based on the results, equations were proposed to estimate the statistical properties of track modulus and rail bending stresses over track windows using the VTD measurements. A framework was also developed to estimate the probability distributions of maximum tensile and compressive bending stresses in the rail head and base, which are necessary for calculating the rail reliability under applied loading. The accuracy of the proposed equations was first verified using a numerical case study for which a random track modulus distribution was considered and artificial noise was added to the modelled VTD. Subsequently, datasets collected from a study

site were used to validate the methodology for estimating rail bending stresses. The rail-mounted strain gauges and the wheel impact load detector system at the study site provided information about the rail bending strains under known applied loads. This allowed validation of the maximum bending stresses estimated using train-mounted VTD measurements.

The thesis includes recommendations for future work.

Preface

This thesis is an original work by Saeideh Fallah Nafari. Four chapters of this thesis have been published or submitted for publication as follows:

A version of Chapter 3 has been published in Proceedings of the Institution of Mechanical Engineers, Part F: Journal of Rail and Rapid Transit, as Fallah Nafari S, Gül M, Roghani A, Hendry M.T, and Cheng J.J.R, “Evaluating the Potential of a Rolling Deflection Measurement System to Estimate Track Modulus”. Saeideh Fallah Nafari was responsible for developing the finite element models, all analyses and manuscript composition. Dr. Mustafa Gül was the supervisory author and was involved in concept formation, analyses and manuscript composition. Dr. Alireza Roghani, a former PhD student working with the Canadian Rail Research Laboratory (CaRRL), provided technical support for interpreting the analysis results. Dr. Michael Hendry, as the Associate Director of CaRRL, provided technical support throughout the study and was involved in concept formation and manuscript edits. Dr. J.J. Roger Cheng was the supervisory author and was involved in concept formation.

A version of Chapter 4 has been submitted to the Proceedings of the Institution of Mechanical Engineers, Part F: Journal of Rail and Rapid Transit for publication, as Fallah Nafari S, Gül M, Hendry M.T, and Cheng J.J.R, “Estimation of Rail Vertical Bending Stress using Train-Mounted Vertical Track Deflection Measurement Systems”. Saeideh Fallah Nafari was responsible for developing the finite element models, all analyses and manuscript composition. Dr. Mustafa Gül was the supervisory author and was involved in concept formation, analyses and manuscript composition. Dr. Michael Hendry provided technical support and was involved in concept formation and manuscript edits. Dr. J.J. Roger Cheng was the supervisory author and was involved with concept formation.

A part of Chapter 5 has been presented and published at the CSHM-6 workshop in Belfast in May 2015. The paper has been selected for publication in Structural and Geoinfrastructure Monitoring, a special issue of the Journal of Civil Structural Health Monitoring, as Fallah Nafari S, Gül M, Cheng J.J.R, “An Investigation of the Correlation between Train-Mounted Vertical Track Deflection Measurements, Track Modulus, and Rail Bending Moments”. Saeideh Fallah Nafari was responsible for developing the finite element models, all analyses and manuscript

composition. Dr. Mustafa Gül was the supervisory author and was involved in concept formation, analyses and manuscript composition. Dr. J.J. Roger Cheng was the supervisory author and was involved in concept formation.

A version of Chapter 6 will be submitted to the ASCE Journal of Transpiration Engineering, as Fallah Nafari S, Gül M, Hendry M.T, Otter D, and Cheng J.J.R, “A Case Study of the Assessment of Vertical Bending Stresses in Rail”. Saeideh Fallah Nafari was responsible for developing the finite element models, all analyses and manuscript composition. Dr. Mustafa Gül was the supervisory author and was involved in concept formation, analyses and manuscript composition. Dr. Michael Hendry provided technical support and was involved in concept formation and manuscript edits. Dr. Duane Otter, principal engineer from the Transportation Technology Center, Inc., provided the field data and technical support for interpreting the results. Dr. J.J. Roger Cheng was the supervisory author and was involved in concept formation.

Dedication

To my best friend, young talented engineer, Asieh Mosayebi who lost her battle to cancer.

May her beautiful soul rest in peace.

Acknowledgment

I wish to express my deepest gratitude to my dear parents for making many sacrifices to give me the opportunity to pursue my dreams. Words cannot describe my heartfelt feelings for their endless and unconditional love.

I am deeply grateful to my supervisors, Dr. J.J. Roger Cheng and Dr. Mustafa Gül, for their kind support, encouragement, and guidance. I was honoured to do my PhD research project under the direct supervision of Dr. Mustafa Gül, who has inspired and motivated me throughout my PhD program. He has been a wonderful teacher and had a great influence on my both personal and professional life.

I am greatly thankful to Dr. Derek Martin and Dr. Michael Hendry from the Canadian Rail Research Laboratory (CaRRL) (www.carrl.ca) at the University of Alberta for providing valuable feedback and technical support. I am also very thankful to Dr. Alireza Roghani, former PhD student working with CaRRL, for his constructive comments and help. I would like to acknowledge CaRRL for facilitating and funding my PhD project. CaRRL is funded by the Natural Sciences and Engineering Research Council of Canada (NSERC), Canadian Pacific Railway, Canadian National Railway, the Association of American Railways – Transportation Technology Centre Inc., the National Research Council of Canada, Transport Canada, and Alberta Innovates – Technology Futures.

I would like to thank Dr. Scott Walbridge from the University of Waterloo, and Dr. Yong Li from the University of Alberta for serving as my committee members, and providing suggestions and recommendations.

Last but not the least, I am grateful to my dear husband, Dr. Pouya Salem, whose love and inspiration has always given me the strength to achieve my dreams.

Table of Contents

CHAPTER 1: Introduction	1
1.1 Motivation and statement of problem	1
1.2 Objectives and scope	2
1.3 Research contribution	4
1.4 Organization of thesis	5
CHAPTER 2: Background and Literature Review	7
2.1 Rail stresses	7
2.1.1 Live bending stresses	8
2.1.2 Wheel-rail contact stresses	9
2.1.3 Thermal stresses	9
2.1.4 Residual stresses	10
2.1.5 Other stresses	11
2.2 Damage mechanisms controlling rail life	11
2.3 Rail defects	12
2.3.1 Head defects	12
2.3.2 Base defects	15
2.3.3 Web defects	15
2.4 Stress limits to prevent rail failures	16
2.4.1 Rail permanent plastic bending	16
2.4.2 Rail fracture	17
2.5 Track modulus: its meaning and its effects on rail deflections and stresses	26
2.6 Train-mounted systems to measure track modulus and assess rail condition	27
2.7 Summary	29
CHAPTER 3: Evaluating the Potential of a Train-Mounted Vertical Track Deflection Measurement System to Estimate Track Modulus	31
3.1 Overview	31
3.2 Introduction	31
3.3 MRail: a real-time vertical track deflection measurement system	33
3.4 Finite element model specifications and validation	35
3.5 Correlation between Y_{rel} and track modulus	39

3.6	Correlation between track modulus average and Y_{rel} average.....	42
3.7	Correlation between track modulus COV and Y_{rel} COV.....	46
3.8	Conclusions	48
CHAPTER 4: Estimation of Rail Vertical Bending Stress using Train-Mounted Vertical Track Deflection Measurement Systems.....		50
4.1	Overview	50
4.2	Introduction	50
4.3	Train-mounted VTD measurement systems.....	51
4.4	Estimating rail bending moment and stress from Y_{rel} measurements.....	52
4.5	Correlation between Y_{rel} and rail bending moments based on Winkler modelling.....	53
4.6	Finite element modelling.....	57
4.7	Validating the developed FEM	59
4.8	FEM results with a stochastically varying track modulus.....	59
4.9	FEM with varying track modulus versus Winkler model results.....	61
4.10	Correlation between Y_{rel} and bending moments based on finite element modelling.....	62
4.11	Correlation between probability distributions of Y_{rel} and rail bending moments	64
4.12	Conclusions	67
CHAPTER 5: An Investigation of the Correlation between Train-Mounted Vertical Track Deflection Measurements, Track Modulus, and Rail Bending Moments.....		69
5.1	Overview	69
5.2	Introduction	69
5.3	FEM specifications.....	71
5.4	Correlation between statistical properties of track modulus and Y_{rel}	73
5.5	Quantifying the spatial variation of the maximum rail bending moment	75
5.6	Numerical case study	77
5.7	Conclusions	81
CHAPTER 6: A Case Study of the Assessment of Vertical Bending Stresses in Rail.....		82
6.1	Overview	82
6.2	Introduction	82
6.3	Study site.....	84
6.4	Load data collected using the WILD system	86

6.5	Strain data collected using strain gauges.....	87
6.6	Analysis of datasets from the WILD system and strain gauges.....	88
6.7	VTD measurements using the MRail System	89
6.8	Comparing the Y_{rel} datasets from two MRail runs	91
6.9	Estimating rail bending strains from Y_{rel} data	95
6.10	Comparing the measured maximum tensile strains with the estimated range.....	97
6.11	Conclusion.....	98
CHAPTER 7: Conclusions and Recommendations for Future Research		100
7.1	Summary and conclusions.....	100
7.2	Recommendations for future research.....	102
References.....		104
Appendix A: Numerical Model Details		112

List of Tables

Table 2-1 Reduction factors to adjust allowable vertical bending stress based on the actual condition of the rail.....	17
Table 2-2 Allowable bending stresses for three types of AREMA (2013a) rail	20
Table 3-1 Track modulus distributions considered in the numerical models.....	37
Table 3-2 Correlation between the track modulus average and Y_{rel} average with respect to window size.....	45
Table 3-3 Correlation between track modulus COV and Y_{rel} COV with respect to window size	48
Table 4-1 Relative vertical track deflection, maximum positive and negative bending moments, and maximum tensile and compressive stresses in the rail head and rail base, calculated for different values of track modulus using the Winkler model.....	55
Table 4-2 Normal track modulus distributions considered in the numerical models.....	58
Table 4-3 Estimating the CDF of maximum negative bending moment using three predictor variables (Y_{rel} CDF, Y_{rel} average, and Y_{rel} COV) for a window length of 160 m.....	67
Table 5-1 Properties of the normal distributions considered for simulating the varying track modulus.....	71
Table 5-2 Summary of the calculations for quantifying the track modulus distribution from Y_{rel} measurements.....	80
Table 5-3 Summary of the calculations for quantifying the spatial variation of the maximum positive bending moment from Y_{rel}	80
Table 5-4 Summary of the calculations for quantifying the spatial variation of maximum negative bending moment from Y_{rel}	81
Table 6-1 Range of the multiple measurements of maximum tensile strains in rail under the loading set shown in Figure 6-7.....	89
Table 6-2 Statistical properties of track modulus and Y_{rel} for the zone with concrete cross ties at Calrin.....	94
Table 6-3 Average and standard deviation for the MRail data at the Calrin site in October together with the estimated average and StDev for the envelope profile of rail maximum positive bending moment and tensile strain.....	97

List of Figures

Figure 2-1 Illustration of a ballasted railway track structure.....	7
Figure 2-2 Terminology used to identify and classify rail stresses and defects in relation to the rail section.....	8
Figure 2-3 Wave action in loaded rail.....	11
Figure 2-4 S-N diagram for steel samples that have an ultimate strength of less than 1380 MPa (200 ksi) and are subjected to fully reversed alternating stresses.....	19
Figure 2-5 Crack-loading modes, a) opening mode or tensile mode, b) in-plane shearing or sliding mode, c) anti-plane shearing or tearing mode.....	21
Figure 2-6 Two-dimensional infinite centre-cracked plate subjected to uniform tensile stress ...	21
Figure 2-7 Growth trend of rail flaw.....	23
Figure 2-8 Fatigue crack growth rate (da/dN) vs. the applied stress intensity factor range (Δk). ...	24
Figure 3-1 Schematic of the MRail system used to measure Y_{rel} , a) the original MRail system, b) sensor system, c) the top view of the laser lines on the rail head, d) the new MRail system.....	34
Figure 3-2 The track structure model developed for numerical study.....	35
Figure 3-3 The MRail system installed in the back truck of a middle rail car.	37
Figure 3-4 The Wheel load set considered in the numerical models.....	37
Figure 3-5 Assignment of randomly selected stiffness values to the springs under the crossties along the track (ninety models were developed using the normal track modulus distribution, and ninety models were developed using the uniform track modulus distribution).....	38
Figure 3-6 Distribution of Y_{rel} along the rail calculated using finite element modelling for a track structure with the constant track modulus of 41.4 MPa.....	39
Figure 3-7 a) The vertical rail deflection profile under wheel loads and the relative vertical track deflection (Y_{rel}), b) correlation between the track modulus and Y_{rel} based on the Winkler model.	40
Figure 3-8 a) The track modulus distribution defined as input for the FEM, b) Distribution of the Y_{rel} calculated using FEM.	41
Figure 3-9 Estimation of the track modulus distribution based on the Y_{rel} data using the Winkler model (input track modulus distribution is normal with an average of 41.1 MPa and COV of 0.25).	42

Figure 3-10 Track modulus average vs. Y_{rel} average for: a) 160-m window length and b) 4-m window length.....	44
Figure 3-11 Comparison between the moving averages of inputted and estimated track modulus for: a) window length of 8 m, b) window length of 20 m, c) window length of 80 m.	46
Figure 3-12 Track modulus COV vs. Y_{rel} COV for: a) 160-m window length and b) 4-m window length, (COV: coefficient of variation, Y_{rel} : relative vertical deflection).	47
Figure 4-1 Illustration of the MRail system used to measure Y_{rel}	52
Figure 4-2 Tensile and compressive stresses in the rail head and base due to the positive and negative bending moments: a) positive bending moment, and b) negative or reverse bending moment.	53
Figure 4-3 Relationship between Y_{rel} and bending moment calculated using the Winkler model: a) the train and axle loads on a track structure with an RE136 rail size and a constant track modulus of 13.8 MPa, b) resulting VTD profile and measured Y_{rel} , and c) resulting bending moment profile showing the maximum positive and negative bending moments.....	54
Figure 4-4 Y_{rel} and maximum positive and negative bending moments calculated for different values of track modulus using the Winkler model: a) correlation of Y_{rel} and maximum positive bending moment, and b) correlation of Y_{rel} and maximum negative bending moment	56
Figure 4-5 Maximum tensile and compressive bending stresses in the rail head together with the maximum tensile and compressive bending stresses in the rail base, calculated for different values of track modulus using the Winkler model.....	56
Figure 4-6 Assignment of randomly selected stiffness values to the support springs along the track.....	58
Figure 4-7 Response of a track structure with an RE136 rail size and constant track modulus of 41.4 MPa calculated using FEM and VBA code: a) envelope profile of maximum negative bending moment, b) envelope profile of maximum positive bending moment, and c) distribution of Y_{rel}	60
Figure 4-8 An example of numerical models: a) track modulus distribution defined as the model input, and b) distribution of Y_{rel} calculated using FEM and VBA code.	60
Figure 4-9 Bending response for one of the simulations, envelope profile of: a) rail maximum positive bending moment, b) rail maximum negative bending moment, and c) maximum bending stress in the rail head and base.....	62

Figure 4-10 Rail maximum positive bending moment vs. Y_{rel} .	63
Figure 4-11 CDF of the rail responses for one of the simulations: a) CDF of Y_{rel} data, b) CDF of maximum positive bending moment, and c) CDF of maximum negative bending moment.	65
Figure 4-12 Correlation between the CDFs of Y_{rel} and maximum positive bending moment calculated for ninety models with different track modulus distributions. These comparisons were made separately at CDF levels of: a) 0, b) 0.2, c) 0.4, d) 0.6, e) 0.8, and f) 1.	66
Figure 4-13 Correlation between the CDFs of Y_{rel} and maximum negative bending moment calculated for ninety models with different track modulus distributions. These comparisons were made separately at CDF levels of: a) 0, b) 0.2, c) 0.4, d) 0.6, e) 0.8, and f) 1.	67
Figure 5-1 Wheel loads considered in the numerical models represent the two trucks in an adjacent railcar and locomotive.	72
Figure 5-2 A typical example of a simulation: a) Inputted track modulus, b) resultant Y_{rel} , c) resultant envelope profile of maximum positive bending moment, and d) resultant envelope profile of maximum negative bending moment.	72
Figure 5-3 Correlation between track modulus and Y_{rel} over 40-m long track windows: a) track modulus average vs. Y_{rel} average, and b) track modulus standard deviation vs. Y_{rel} average and standard deviation.	74
Figure 5-4 Correlation between track modulus and maximum positive bending moment over track windows of 40 m: a) average for maximum positive bending moment vs. track modulus average, b) standard deviation for maximum positive bending moment vs. track modulus average and standard deviation, and c) Peak for maximum positive bending moment vs. track modulus average and standard deviation.	76
Figure 5-5 Correlation between track modulus and maximum negative bending moment over track windows of 40 m: a) average for maximum negative bending moment vs. track modulus average, b) standard deviation for maximumnegative bending moment vs. track modulus average and standard deviation, and c) Peak for maximumnegative bending moment vs. track modulus average and standard deviation.	77
Figure 5-6 Input and output for a model with a 40-m track length: a) inputted track modulus distribution, b) resultant Y_{rel} with and without artificial noise, c) resultant envelope profile of the maximum positive bending moment, and d) resultant envelope profile of the maximum negative bending moment.	79

Figure 6-1 Causes of broken rail derailments on Canada’s main tracks from 2000 to 2014.....	83
Figure 6-2 Layout of CN’s Calrin WILD system including 16 instrumented cribs on both rails together with the location of rail base strain gauges.....	85
Figure 6-3 A photo of the WILD system and instrumented cribs along the north track at the Calrin site.....	85
Figure 6-4 Illustration of the MRail system used for measuring Y_{rel} at Calrin.....	86
Figure 6-5 Measuring wheel impact forces using the WILD system: a) illustration of a wheel passing over WILD instrumented zones, b) average wheel loads recorded for the passing wheel at the Calrin WILD site in August 2015, and C) peak wheel loads recorded for the same passing wheel.....	87
Figure 6-6 A sample strain time history from the August dataset collected using the rail base circuit at crib No. 5 long the north rail (tensile strains as positive values).....	88
Figure 6-7 Loading set used for comparing the strain datasets from August and February.....	89
Figure 6-8 a) MRail next to a locomotive during the May run, and b) MRail next to a tank car during the October run.....	91
Figure 6-9 a) Satellite map view of the study site, b) Y_{rel} data from May and October MRail runs (average of measurements on the north and south rails).....	91
Figure 6-10 Correlations between statistical properties of track modulus and Y_{rel} for the loading set shown in Figure 6-8a: a) track modulus average vs. Y_{rel} average, and b) track modulus standard deviation vs. Y_{rel} average and standard deviation.....	93
Figure 6-11 Correlations between statistical properties of track modulus and Y_{rel} for the loading set shown in Figure 6-8b: a) track modulus average vs. Y_{rel} average, and b) track modulus standard deviation vs. Y_{rel} average and standard deviation.....	94
Figure 6-12 Correlations between statistical properties of Y_{rel} and the envelope profile of rail maximum positive bending moment for the loading set shown in Figure 6-8b: a) average for maximum negative bending moment vs. Y_{rel} average, and b) standard deviation for maximum negative bending moment vs. Y_{rel} standard deviation.....	96
Figure 6-13 Y_{rel} data from the October MRail run at the Calrin site.....	97
Figure 6-14 Maximum tensile strains measured three times using the rail base strain gauges compared with the range estimated from the Y_{rel} data.....	98

CHAPTER 1: Introduction

1.1 Motivation and statement of problem

Canada, with more than 48,000 route kilometers of track, has one of the most extensive rail networks in the world. It is primarily a heavy freight railway network and carries more than 70% of the country's goods by mass [1]. As an efficient mode for transporting goods over long distances, freight railway transportation is of great importance for the promotion of economic developments within Canada. The railway industry has steadily increased the traffic volume, axle loads, and train speeds over time to meet the growing transportation needs. This trend has created further challenges for railway operators to ensure the safe operation of the railway network [2, 3].

The most serious categories of railway accidents in terms of potential risk to the public and of financial loss are main track collisions and derailments [4]. Main tracks are the tracks of subdivisions extending through and between stations [5]. In the Canada's railway network, rail issues such as broken rails, rail joint bars, and welds are among the leading causes of main track derailments. Of the reported main track derailments from 2005 to 2014, 13% on average were attributed to rail issues [4]. Many of these derailments occurred due to defects that propagated along or across the rail under applied stresses [4].

An estimation of rail stresses is necessary for assessing the condition of the rail and reducing failures [6]. Under normal operating conditions, rail steel is subjected to various stresses including residual, thermal, wheel-rail contact, and bending stresses [6-8]. The magnitude of these stresses is influenced by many uncontrollable environmental, operational, and structural factors along the thousands of miles of track [7, 9, 10]. Methods for estimating the spatial variation of rail stresses allow a more rigorous reliability analysis of rail, and therefore, the establishment of optimised solutions for rail issues [11, 12]. Many attempts have been made to

develop methods to measure rail stresses [13-19]. However, very few studies focus on evaluating rail bending stresses over long distances [20, 21].

New train-mounted systems that measure the vertical track deflection (VTD) under fully loaded axles offer new opportunities for estimating rail bending stresses over long distances and, thus, for characterizing the spatial variation of the bending stresses [20-22]. The VTD measurements under applied known loads allow the quantification of rail supporting stiffness, which is a stochastically variable parameter along the track [22-26]. Once track modulus is quantified as a measure of the rail foundation vertical stiffness [27], the rail deformed shape and range of bending stresses within the rail can be estimated for applied known loads. The mathematical correlations between VTD, track modulus, and rail bending stresses are the basis of this method for interpreting the VTD measurements [20, 21]. Although a number of train-mounted VTD measurement systems have been developed in recent decades [22-26], the mathematical correlations between VTD, track modulus, and rail bending stresses have not been thoroughly investigated, and the methods proposed to estimate track modulus and rail bending stresses from VTD measurements are overly simplistic [20, 21, 24, 25]. The relationships between VTD, track modulus and rail bending stresses are the focus of the study presented in this thesis. The study is aimed at developing methods for estimating the rail bending stresses from the VTD measurements along the track.

1.2 Objectives and scope

The main objective of this research is to develop a methodology to estimate the distribution of rail bending stresses along the track. The objective is defined based on the potential that train-mounted VTD measurement systems have for quantifying track modulus and rail bending stresses along long railway lines. The research project consists of three sets of objectives as follows:

Objective 1: Investigate the potential of train-mounted VTD measurements for quantifying track modulus over long distances

- develop a series of finite element models (FEMs) to simulate the stochastic nature of track modulus and calculate the track response under the moving load;

- examine the effect of track modulus variation on the modelled VTD;
- investigate the correlation between track modulus and VTD for track structures with different track modulus distributions subjected to a known loading condition;
- propose a methodology for quantifying the statistical properties of track modulus using VTD measurements.

Objective 2: Investigate the potential of train-mounted VTD measurements to quantify vertical bending stresses in rail over long distances

- utilize the developed FEMs with a stochastically varying track modulus to examine the effect of track modulus variation on rail bending moments and stresses;
- investigating the correlation between the modelled VTD and rail bending stresses considering track modulus distributions;
- investigate the correlation between the probability distributions of VTD, track modulus and rail bending stresses under a known loading condition;
- propose a methodology to estimate the probability distributions of vertical bending moments and stresses along the track.

Objective 3: Validate the methodology developed to quantify the rail bending stresses along railway lines using field measurements

- analyse the strain and wheel impact load detector (WILD) data collected by the Transportation Technology Centre, Inc. (TTCI) at the Calrin WILD site to establish a benchmark to validate the estimated rail bending stresses from VTD measurements;
- estimate the vertical bending stresses in a rail under a known loading condition from the train-mounted VTD measurements at the Calrin WILD site;
- compare the rail bending stresses estimated from VTD measurements with the stresses measured using strain gauges under a similar loading at the Calrin WILD site.

The train-mounted VTD measurement system used in this study was developed at the University of Nebraska-Lincoln in collaboration with the Federal Railroad Administration (FRA). The system, commonly referred to as the MRail system, was selected for this study because of its availability and the simplicity of the measurement technology. The approach presented for

estimating track modulus and rail bending stress from the MRail VTD data is applicable to other measurement systems. However, details of the framework for interpreting the VTD measurements for each system are different as the type of VTD measurement from moving cars (i.e., either relative or total) affects the frameworks.

Techniques for quantifying the distribution of the track modulus are investigated in this study, because stochastically varying track modulus is the main factor causing the spatial variation of rail bending stresses along the track. However, the application of the techniques for quantifying the track modulus is not limited to assessing rail bending stresses. Track modulus is widely accepted as an indicator of track performance [28-31]. Information about track modulus and the way it varies along the track makes it easier to identify the root causes of the structural issues of the track [28]. The results of the study on quantifying the track modulus distribution have widespread applications in assessing the structural conditions of the track and optimizing the way in which maintenance resources are allocated [29].

The methodology for estimating track modulus and rail bending stresses provides two fundamental tools for the structural health monitoring (SHM) of rails. This is a major step towards evaluating the rail structural integrity which is a complex task and needs a number of pieces to be completed. Some important pieces such as, methodologies for estimating thermal, residual and wheel-rail contact stresses over long distances are still under research.

This study aims to provide a practical method for estimating track modulus and rail bending stresses from VTD data, which are measured along thousands of miles of track. In this approach, the overall behavior of rail is more concerned rather than rail support stiffness and bending stresses at individual points along the track. As a result, the developed methodology considers the correlations between track modulus, rail deflections, and bending stresses over track windows.

1.3 Research contribution

There are a number of train-mounted VTD measurement systems that have been developed to estimate track stiffness [22-26]. When track stiffness and its variation are quantified along the track, it is possible to estimate the rail deformed shape and the range of bending stresses in the

rail under applied loads. Although, train-mounted VTD measurement systems have the potential to estimate the magnitude of rail bending stresses over long distances, the number of studies on the methods for interpreting the measured VTD data is very limited and the proposed methods for estimating the rail bending stresses from VTD data are overly simplistic. The main contribution of this thesis is that it presents a detailed methodology for estimating track modulus and rail bending stresses from VTD measurements. This is the first study that addresses the effect of a stochastically varying track modulus on the correlation between VTD, track modulus and rail bending stresses. Additionally, the proposed method makes it possible to estimate the probability distribution of maximum tensile and compressive bending stresses in the rail head and base along the track. The methodology for estimating track modulus and rail bending stresses over long distances is a major step towards evaluating the rail structural integrity which is a complex task and needs a number of pieces to be completed.

1.4 Organization of thesis

The thesis is organized into seven chapters including this first introductory chapter.

Chapter 2 covers the literature review on rail stresses and rail-related issues. Damage mechanisms controlling the rail life are described and a summary of rail defects is presented. This chapter provides the necessary background information on the key parameters that affect rail performance. The chapter includes a review of the most common rail failure modes and allowable limits for rail bending stresses to prevent these rail failures. There is also a section about track modulus as an important parameter influencing rail deflections and stresses and its relationship with track performance. A review of track modulus measurement techniques is also presented.

Chapter 3 presents the study conducted to evaluate the potential of a train-mounted VTD measurement system to estimate track modulus. Track modulus measurement techniques are reviewed and details are presented about the MRail system as a tool for the study. Subsequently, specification and validation of the finite element models (FEMs) used for the study are explained. This is followed by the study results about the correlation between VTD measurements and track modulus. The chapter includes a proposal for a new methodology to estimate the statistical property of track modulus over different track lengths. Finally, there is a

discussion about the drawbacks of the previous methods and the potential of the new proposed method for interpreting VTD measurements.

Chapter 4 presents the study conducted about the correlation between VTD measurements and rail bending stresses. The effect of the track modulus variation on rail deflections and bending stresses is discussed by comparing the differences between the results of a classic track model with constant track modulus, and the developed FEM with stochastically varying track modulus. There is also a description of the new methodology developed for estimating the probability distribution of rail bending stresses from VTD measurements.

Chapter 5 includes a complementary discussion on the correlation between VTD measurements, track modulus, and rail bending stresses. Equations are proposed to quantify the statistical properties of track modulus and rail bending stress from VTD measurements. The accuracy of the proposed equations is investigated using a numerical case study for which a random track modulus distribution is considered and artificial noise is added to the modelled VTD.

Chapter 6 presents the procedure followed to validate the estimation of rail bending stresses. Data sets collected in different time periods at a study site are analyzed. Information about the rail bending stresses under known applied loads is compared with the range of maximum bending stresses estimated from VTD measurements. The magnitudes of rail bending stresses are assessed in different time periods, and reasons for changes in the magnitudes are discussed.

Chapter 7 summarizes the findings of the studies presented in the other chapters along with conclusions and offers recommendations for future research.

CHAPTER 2: Background and Literature Review

2.1 Rail stresses

A railway's track structure provides a smooth and robust surface for the railcars passing over it. A track is designed and constructed with various configurations and components [10]. Figure 2-1 shows a typical ballasted railway track that is composed of two main parts: superstructure (rails, rail pads, fasteners, and cross ties) and substructure (ballast, sub-ballast, and subgrade) [7, 10]. In the track system, the rail is the component in direct contact with the railcars. The rail's functions are to guide the railcar wheels, provide a smooth running surface for passing trains, and sustain and transmit the train loads to the component below the rail in the track system [10].

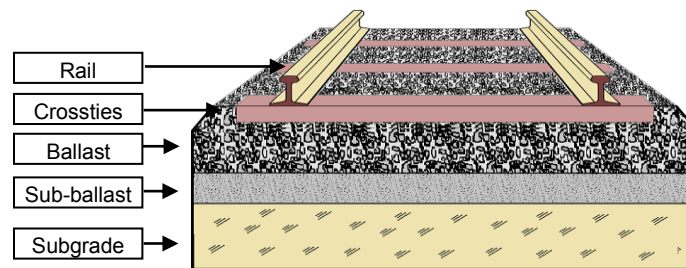


Figure 2-1 Illustration of a ballasted railway track structure.

A rail is subjected to various loads and stresses under normal operating conditions. Rail stresses are often studied in four main categories of live bending, wheel-rail contact, thermal and residual stresses [6, 32-35]. Terminology that is commonly used to describe the directions and plans of stresses in rail is presented in graph form in Figure 2-2 [36].

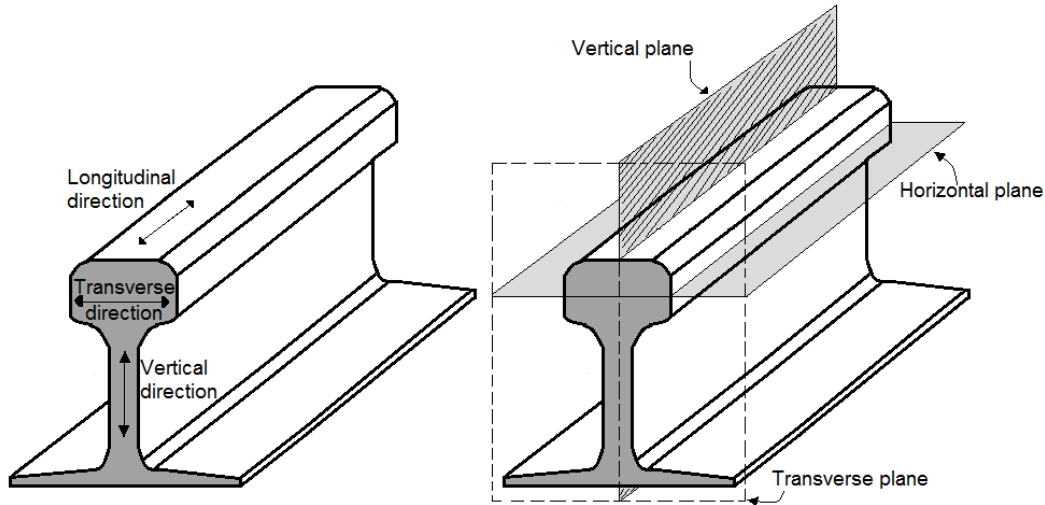


Figure 2-2 Terminology used to identify and classify rail stresses and defects in relation to the rail section (adopted from Reference [36]).

2.1.1 Live bending stresses

A rail is subjected to vertical and transverse (lateral) loads under moving trains. A vertical wheel load has three components: static, dynamic, and impact [37]. The static component arises principally from the weight of the vehicle. The dynamic component is a function of the vertical dynamics of the bogies interacting with the track geometry, and depends mainly on the vehicle speed. The impact component is an additional increase over the static and dynamic components that occur either when a wheel travels over a short vertical rail irregularity such as a dipped weld, or if a wheel contains wheel flats or is out of round [37]. The impact component is sometimes considered part of the dynamic component [7]. A rail also experiences transverse wheel loads from a vehicle's lateral dynamic behaviours, such as hunting or centrifugal forces on curves [8, 33, 38].

Rails bend vertically and transversely under wheel loads, and therefore, undergo vertical and transverse bending stresses. This leads to cycles of tensile and compressive longitudinal stresses in the rail head and base while the train is moving [38].

There are extra details that should be taken into account while analysing the magnitude of rail stresses. For instance, the rail head bends vertically on the web support which leads to tensile longitudinal stresses in the fishing surface of the rail head (bottom of the rail head) [34].

Moreover, the action line of vertical and transverse wheel loads does not pass through the shear centre of the rail. For this reason, a rail undergoes a torque about the centre of twist that in turn affects the longitudinal stress in the rail head and base [7].

2.1.2 Wheel-rail contact stresses

A rail and wheel can be considered as two cylinders that are in contact [33]. Vertical wheel loads and forces from traction, braking, and steering are applied to the rail through the small contacting surface and cause high contact stresses [6]. The Hertz theory is often suggested to estimate the contact stresses. The basis of this theory is that the contacting surfaces are continuous. This assumption leads to the contacting surface being modelled as an ellipsoid and the contact patch as elliptical [8, 38].

The contact stresses can be very significant in magnitude and cause rail defects such as head checks, spalling, shelling, and flaking. The magnitude of contact stresses decreases as the distance from the surface increases. For this reason, contact stresses mainly affect the early crack extension, and have a negligible influence on the crack propagation when the crack reaches a depth of greater than about 8-15 mm [39, 40].

2.1.3 Thermal stresses

A rail is not free to expand or contract in the longitudinal direction when subjected to thermal loads. As a result, tensile or compressive thermal stresses are generated in the rail longitudinal direction when the rail in-service temperature differs from the stress-free temperature (SFT). The SFT or rail neutral temperature is the temperature at which there is no thermal stress in the rail [41]. The SFT value that is initially equal to the installation temperature is not constant during the rail service and changes under operating conditions and maintenance practices [42]. Thermal stress in a rail is calculated using Equation 2-1 [43].

$$\sigma_T = E\alpha\Delta T \tag{2-1}$$

where E is the steel rail elastic modulus, α is the coefficient of linear thermal expansion for rail steel ($11 \times 10^{-6}/\text{c}^\circ$), and ΔT is the difference between the rail in-service temperature and SFT.

The magnitude of thermal stresses can be very high for continuously welded rail (CWR) track in which rails are welded together. In a conventional track with bolted rail joints, gaps between rails allow thermal expansion and contraction. However, the joints weaken the track structure and increase the track maintenance cost. For this reason, most modern railways utilize CWR track and eliminate the expansion joints [6, 41].

Longitudinal compressive thermal stress is the main reason that tracks buckle [8]. In CWR track, a rail and crosstie system behaves in a manner similar to that of a long slender column that can buckle under compression [6]. When high longitudinal compressive stresses in the rail overcome the lateral resistance from ballast, track buckling occurs [42]. This phenomenon is a direct threat to railway transportation safety as it can lead to derailments [6, 42]. To preventing high longitudinal compressive stresses, rail is welded under conditions that simulate high ambient temperature. As a result, rails undergo longitudinal tensile thermal stresses for most of the year, while compressive thermal stresses occur in hot summer months [33]. A comprehensive study on track buckling and methods for calculating rail reliability against buckling can be found in Reference [42].

Preventing track buckling by installing CWR track in relatively high temperatures has an adverse effect as it causes high tensile thermal stresses in a rail during cold temperatures. These tensile thermal stresses promote rail cracking and fracture [6, 8, 33, 35].

2.1.4 Residual stresses

Rail manufacturing processes, such as roller straightening, head hardening, and heat treatment, can cause residual stresses in a steel rail. Additionally, plastic flow under cyclic wheel load passages generates residual stresses in a rail during the rail's service life. There is also the possibility of localized residual stresses while rails are being welded. The characteristics of the residual stresses are highly variable along the rail cross section. Head-hardened rails can exhibit very high tensile vertical stresses in the rail web, tensile longitudinal stresses on top of the head and base, and compressive longitudinal stresses in the web and the side of the head [38, 44]. The distribution of residual stresses within the rail varies with the service life. For this reason, quantifying the effect of residual stresses on the propagation of transverse defects has never been

an easy task [2]. Studies have shown that transverse defects tend to initiate and propagate in regions of high tensile residual stresses in the rail head and base [38, 44].

2.1.5 Other stresses

A rail undergoes shear stresses due to applied wheel loads [8]. These shear stresses are known as the main cause of failures at the bolt holes in the rail web [7, 33]. In addition, transverse wheel loads move the rail head laterally relative to the rail base and produce tensile vertical stresses in the rail web [37].

Longitudinal loads are also applied to the rail through wave action under the passage of wheels and braking and accelerating actions. These loads affect the magnitude of longitudinal stresses in the rail [7, 38]. Figure 2-3 demonstrates the wave action in the loaded rail.

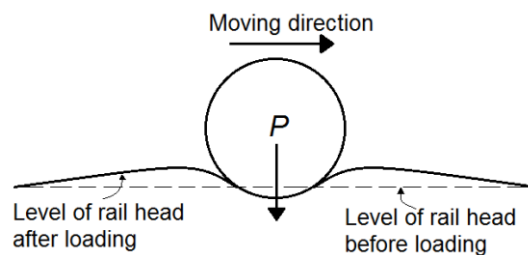


Figure 2-3 Wave action in loaded rail (adopted from Reference [7]), (P : wheel load).

2.2 Damage mechanisms controlling rail life

Wear, fatigue, and plastic deformation (plastic bending or plastic flow) are damage mechanisms controlling rail life [34, 45]. Wear is loss of material that arises from wheel-rail contact, corrosion, abrasive processes, and maintenance activities [39]. It reduces the rail cross-sectional area and moment of inertia, adversely affecting the rail's capacity to carry loads [43]. Fatigue refers to the weakening of a material under repetitive applied loading. Repeated stress cycles contribute to the initiation and propagation of defects, and as defects grow, the load-capacity of the rail is reduced. Excessive wear combined with the presence of a transverse fatigue defect is a direct threat to rail integrity [43].

Rail steel, particularly on heavy haul lines, is subjected to the heavy loads that sometimes exceed the rail elastic limit and trigger plastic deformation. Changes due to the plastic deformation

reduce the service life of a track [46]. Cumulative damage from plastic deformation is one of the causes of rail defects [11]. The surface and sub-surface plastic flows resulting from high normal and tangential stresses at the rail-wheel contact lead to the formation of wear flakes or the initiation of fatigue cracks [47, 48]. Comprehensive studies on plastic flow are presented in References [49, 50].

2.3 Rail defects

Rail defects are classified in many ways, such as location (e.g., head, web, or base), origin (e.g., manufacturing process, or traffic oriented), growth planes (e.g., transverse, horizontal, or longitudinal), or stresses involved in growth (e.g., residual, thermal, or live load stresses) [7, 36]. Major rail defects are classified here by location. Then, growth planes, origin, and stresses involved in growth are briefly reviewed for each defect.

2.3.1 Head defects

Surface defects

Gauge corner checks (head checking), running surface checks (flaking), burned rail, spall, shell, and squat are surface or near-surface initiated defects that are classified as rolling contact fatigue (RCF) defects. The development of these defects is mainly associated with excessive high normal and tangential stresses at the wheel-rail interface [6, 35, 36, 38]. Operating conditions (e.g., train speed, type of rolling stock and axle loads), environmental conditions, track layout and track geometry parameters (e.g., rail and wheel profiles, track curvature, super-elevation), rail metallurgy, and maintenance policy (e.g., lubrication and rail grinding practices) are factors that affect the initiation and propagation of RCF defects [39, 51]. RCF defects are of particular concern because they can mask ultrasonic signals and prevent the detection of larger and deeper internal defects. They may also lead to rail failure if not detected in time, particularly when growing in the rail transverse plane [37, 52]. For instance, a shell is a longitudinal crack parallel to the rail running surface that can turn downward perpendicular to the rail running surface and create a transverse defect known as a detail fracture [33, 38, 53].

Corrugation is another rail surface defect that has been widely studied [45, 54, 55]. It is a repeated wavelike pattern on the running surface of the rail [36]. Rolling contact fatigue, plastic deformation, and wear can cause corrugation [39, 45, 54, 55]. A detailed discussion about the mutual effects between RCF and corrugation can be found in Reference [54].

Different examples of rail defects on or near the rail-head surface are presented in Reference [36].

Defects growing in the rail-head transverse plane

Transverse defects are progressive fractures that occur along the rail transverse plane. The initiation and early growth of transverse defects are controlled by wheel-rail contact stresses. After the defects extend away from the rail surface, they propagate mainly due to live bending, thermal, and residual stresses [8, 35, 40]. Transverse defects are measured with respect to the cross-sectional area of the rail head. For instance, a 50% fracture indicates that signs of the defect growth are observed in half of the rail-head cross-section [36]. Transverse defects are classified as follows:

Transverse Fissure (also known as Tache ovale or shatter cracking). This starts from crystalline center or nucleus inside the head rail (e.g., shatter crack, inclusion, or blowhole) and extends at right angles to the rail running surface. For a transverse fissure, the initial imperfection is located more than 9.5 mm (3/8 in) from any surface of the rail head [7, 36].

Compound Fissure. This is a transverse separation at a right angle to the running surface. The possible origins include a longitudinal seam, segregation, or inclusion. A compound fissure starts from a horizontal separation that turns up, down, or in both directions [7, 36].

Detail Fracture. This is one of the most common and problematic defects in modern freight railroad tracks such as CWR, heavy haul lines, and lines with high-density traffic. Detail fractures form 75% of the rail defects found in CWR track in North America [2] and account for 4% of Canada's broken rail derailments [56]. Detail fractures originate in head checks and shelling near the upper gauge corner below the running surface [33]. The defect is called a reverse detail fracture (RDF) when the origin of transverse defect is at the lower gauge corner of the rail head. The RDF defect mainly occurs in poorly lubricated, curved, worn rail on a stiff

track carrying traffic with high axle loads [2]. The propagation life of an RDF defect is 20% shorter than that of a detail fracture. A comprehensive study on the propagation life of detail fractures has been conducted by FRA [2, 40]. Results of the study have shown that thermal and residual stresses, as well as rail curvature, are the factors with the most influence on the propagation life of detail fractures. Rail section, track foundation stiffness, location of wheel/rail contact, and average axle load are parameters that have moderate effects, whereas vehicle dynamics and the location of the flaw centre in the rail head slightly affect the propagation life. Higher average axle loads, higher curvature, a lower track modulus and lower rail moment of inertia decrease the propagation life of detail fractures by increasing rail bending stresses [40]. The propagation life of a detail fracture in a curve of three to six degrees is about half of the life of a similar defect in a comparable tangent track [40].

Engine burn fracture. This starts from a burn, with the transverse separation substantially at right angles to the running surface. The burn occurs when the slipping engine driver wheel heats a portion of the rail head, and rapid cooling forms thermal cracks. A shallow horizontal separation may be also observed at the zone where burned metal separates from the rail metal below the running surface. When the engine burn is cleaned insufficiently before welding, thermal cracks may remain and cause a subsequent progressive transverse separation called a welded burn fracture [36].

Defects growing in the rail-head longitudinal direction

Horizontal and vertical split head defects are separations in the rail head that develop along the rail's longitudinal direction. These defects originate from internal longitudinal seams, segregation, or inclusion [7, 33, 37]. If the defects are not detected in time, they may break off under the moving train. This becomes critical when the failure occurs on the gauge side of the rail because the wheel climb on the rail head may trigger derailment [37].

Horizontal split head. This defect extends longitudinally and horizontally along the rail horizontal plane, parallel to the rail running surface [33]. The defect starts on the field side of the rails with a distance of 6.25 mm or more from the rail running surface [36], and extends longitudinally along the rail for a distance of 50 to 100 mm [37]. Fatigue mechanisms and shear stresses contribute to the growth of horizontal split head defects [37].

Vertical split head. This defect extends longitudinally and vertically along the rail vertical plane, parallel to side of the head [33]. The defect initiates from the centre or the gauge side of the rail head and extends longitudinally for a distance longer than 0.5 m [37]. High impact loads and extremely eccentric loads contribute to the growth of vertical split defects [37]. The propagation life of vertical split head defects has been studied using two- and three-dimensional FEMs [57].

2.3.2 Base defects

Defects in the rail base are often categorized into two types of failure including a broken base and base fracture [36].

Broken base. This is a progressive fracture that initiates from a seam, segregation, or improper bending on the tie plate [7, 36]. Broken base sometimes refers to any break in the rail base [36].

Base fracture. This is normally caused by a nick or other type of damage to the rail base. It can develop in the rail transverse plane and result in a complete transverse failure of the rail section [36]. Transverse cracks may also appear in rails of switches, at the corner of the rail base due to corrosion pits or grinded flanges [38].

2.3.3 Web defects

Head and web separation, piped rail, and split web are progressive defects that develop longitudinally in the rail web.

Head and web separation is a fatigue defect that separates the head and web of the rail at the fillet under the head [36]. A crack in the fillet between the head and the web can arise from seams and segregations in the rolling process [7]. Acidic action from some material used in road crossings may also initiate a corrosion fatigue where the rail head and web are joined [36]. The development of head and web separation defects is often associated with eccentric overloading and wheel impacts from insufficient super-elevation on curves or improper canting of the rail [33]. In the joint area, head and web separation may appear in the fillet area at the end of the rail. Propagation of the defect in the joint area can be relatively quick under extreme stress conditions created by pumping or swinging joints [36].

Split web. This is a crack along the side of the rail web. It can be initiated from a seam or mechanical damage [36]. Heavy, eccentric wheel loads; improper super-elevation; insufficient web thickness; and excessively deep heat-number stamping may contribute to the formation of web cracks [7]. The main driving force for the propagation of the split web defect is occasional shock loads [33].

Piped Rail. This is a vertical split in the rail web. It starts from a seam, slag, or gas pocket inside the web that [7]. A piped rail is a rare defect in modern railway lines [36].

Bolt hole crack. This is a crack across the rail web that is initiated from a bolt hole. It can develop upward toward the rail head or downward toward the rail base. This defect may appear in a bolted-joint track where rail segments are attached, or at insulated joints where the CWR is divided into signal blocks [33]. A shear in the rail web is the driving force for the propagation of the cracks. Bolt hole cracks are among the most common and problematic defects in North America, forming 50 % of the defect population in bolted-joint rails (BJRs) [2, 33]. The risk of fracture for the cracks is higher when the joint is loose. The gap distance between the rail and the joint bars is a measure of the joint looseness [2]. The growth life of bolt hole cracks has been studied by numerical models [2, 58].

2.4 Stress limits to prevent rail failures

“Rail is defined as failed when it is broken, cracked or damaged and can no longer fulfil its design function” [6]. Broken and cracked rails refer to a complete and partial separation of the rail. Damaged rail implies that the rail serviceability is impaired due to changes in the design geometry and/or material properties. Such changes may eventually lead to the formation of cracks or breaks [6]. Two of the most common failure modes including rail permanent plastic bending and rail fracture, are reviewed here, as are the stress limits to prevent those.

2.4.1 Rail permanent plastic bending

Rail steel starts to yield when rail stresses exceed the yielding threshold. The Association of American Railroads (AAR) recommends a threshold limit value for live vertical bending stresses (σ_d) to prevent rail yielding [7]. This threshold is developed by reserving a portion of the rail

yield strength for thermal stresses, and applying reduction factors to rail yield strength to account for the effects of lateral bending, track conditions, rail wear and corrosion, and unbalanced elevation. The American Railway Engineering and Maintenance-of-Way Association (AREMA) also accepts this method for calculating allowable rail bending stresses. The threshold value is calculated using Equation 2-2 as follow [7, 59]:

$$\sigma_a = \frac{\sigma_y - \sigma_t}{(1+A)(1+B)(1+C)(1+D)} \quad (2-2)$$

where σ_y is the yield stress of the rail steel which is around 480 MPa (70,000 psi) and σ_t is the maximum thermal stress that is expected to develop in the rail. σ_t is assumed to be 140 MPa (20,000 psi) for the CWR and 50 MPa (7000 psi) for the jointed rail. A , B , C , and D are constants accounting for effects of lateral loads, track conditions, rail wear and corrosion, and unbalanced elevation. Recommended values for these constants are reported in Table 2-1 [7, 59]. The constants may need to be modified considering the actual condition of the rail [7, 59].

Table 2-1 Reduction factors to adjust allowable vertical bending stress based on the actual condition of the rail.

Constant	Severity Assumption
A (account for lateral bending)	20%
B (account for track condition)	25%
C (account for rail wear and corrosion)	15%
D (account for thermal stress)	15%

Plasticity of the extreme fibers of the cross section would hardly lead to rail failure. A more realistic approach was presented, which considers a rail as failed when the full depth of the rail section yields and a large permanent kink is formed [60]. In this approach, the effect of rail wear is addressed by reducing the rail cross-section area and moment of inertia [60].

2.4.2 Rail fracture

A brittle fracture in the rail transverse plane occurs when applied stresses to the rail exceed the rail's fracture stress. When a fracture occurs, the track support holds two separate parts together

until excessive misalignments are created as a result of the dynamic wheel loads from the repetitive passage of trains. The misalignment caused by a rail fracture can lead to derailments if not detected in time [6, 33].

Fracture stress (also known as remaining or residual strength) for an ideal rail without any flaws is usually considered to be ultimate tensile strength. However, no steel is completely flaw free. Flaws, which reduce fracture stress, may manifest as cracks, inclusions, voids, weld defects, or a combination of these discontinuities [34, 38]. By growth of defects and reduction in fracture stress can cause the applied stresses to eventually exceed the rail strength and cause brittle fracture [61].

When conducting a fracture analysis, it is important to consider the fatigue phenomena, since rail is subjected to cyclic loading. Three methods have been proposed for fatigue analysis including stress life, strain life, and fracture mechanics [62]. The stress life method is appropriate when the applied stresses are primarily within the elastic range of the material and the number of cycles to fracture is high (high cycle fatigue phenomena). Conversely, the strain life method is used when the material experiences a high level of stresses and plastic strains (low cycle fatigue) [62]. The fracture mechanics approach addresses the crack behaviour and propagation in the material by quantifying the correlation between applied stresses, material fracture toughness, and crack size and shape [62, 63]. The stress life and fracture mechanics approaches are reviewed here as they have been widely used to investigate rail fractures.

2.4.2.1 Stress life approach (fatigue limit concept)

The stress life method is based on the fatigue limit that is also referred to as the endurance limit or endurance strength. The fatigue limit is a stress level below which the material has an infinite life and no failure occurs [62]. For railway applications, infinite life is considered as two million cycles [10]. This suggests that the rail should be designed so that alternating stresses do not exceed the rail fatigue limit at two million stress cycles.

The S-N diagram, which shows the relationship between alternating stress (S) and the number of cycles to failure (N), is the basis of the stress life method. This diagram was obtained using controlled laboratory tests. Figure 2-4 shows the S-N diagram for steel samples that have an

ultimate strength of less than 1380 MPa (200 ksi) and are subjected to fully reversed alternating bending stresses. The fatigue limit in Figure 2-4 is about 50% of the ultimate strength when the number of cycles is greater than one million [33, 62].

The S-N approach is valid only if the plastic strains are small. When the alternating stresses are within the elastic range and the number of cycles to failure are high (high cycle fatigue), a very small component of the strain cycle is plastic. For this reason, the S-N approach is appropriate for analyzing high cycle fatigue stresses [62]. The line between low cycle fatigue and high cycle fatigue is 10^3 for steel material, as indicated in Figure 2-4.

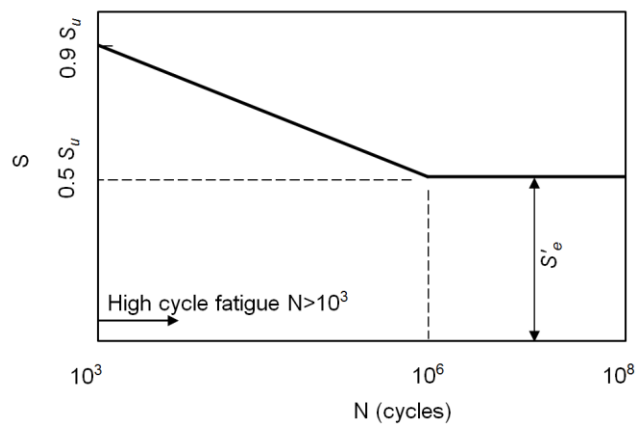


Figure 2-4 S-N diagram for steel samples that have an ultimate strength of less than 1380 MPa (200 ksi) and are subjected to fully reversed alternating stresses (S : alternating stress, N : number of cycles to failure, S_u : steel ultimate strength, S'_e : fatigue limit in the S-N diagram).

Rail bending stress is a high cycle fatigue stress and, thus, the fatigue limit in the S-N diagram can be considered as the allowable bending fatigue. However, the fatigue limit in the S-N diagram was obtained under controlled laboratory conditions, which means that modification factors are needed to account for real-world conditions [44, 62]. Correction factors addressing the effects of surface condition, size, shape, load, temperature, reliability and mean-stress are suggested to estimate the allowable fatigue bending stress under normal operating conditions [44]. The allowable bending stress calculated using the laboratory fatigue limit and modification factors for three types of AREMA (2013a) rail are reported in Table 2-2 [44].

Table 2-2 Allowable bending stresses for three types of AREMA (2013a) rail [44].

Properties/rail type	Standard strength	Intermediate strength	High strength
Yield strength	510 MPa (74 ksi)	552 MPa (80 ksi)	828 MPa (120 ksi)
Allowable bending fatigue stress	97 MPa (14.06 ksi)	98 MPa (14.18 ksi)	102 MPa (14.8 ksi)

The AREMA manual suggests the fatigue limit (S_e) of 386 MPa (56000 psi) for all types of rails, and proposes Equation 2-3 for calculating the allowable bending fatigue stress [59].

$$\sigma_a = \frac{S_e - \sigma_t}{(1+A)(1+B)(1+C)(1+D)} \quad (2-3)$$

where σ_a is the allowable bending fatigue stress and σ_t , A , B , C , and D are as defined in Equation 2-2. The assumption of severity factors reported in Table 2-2 and the σ_t of 138 MPa (20,000 psi) result in the allowable bending fatigue stress of 125 MPa (18000 si) for CWR. A detailed discussion on the allowable bending fatigue stress calculated using Equation 2-3 is presented in Reference [44].

2.4.2.2 Fracture mechanics approaches

Fracture mechanics is an established engineering discipline that addresses the propagation of cracks in materials. In this approach, magnitude and distributions of stresses near the crack tips are studied with respect to the crack size and shape, the material properties, and the applied stresses to the component [38, 62, 63]. Fracture mechanics has been widely used to study the crack growth life of transverse fatigue defects in the rail head [8, 32, 64]. Hence, principals of this approach are reviewed in this section.

Tensile stresses, perpendicular to the crack plane, generate stress amplification at the crack tip. This amplification is measured in terms of the stress intensity factor (K_I). The subscript of (I) shows that the crack-loading mode is the opening mode. Figure 2-5 demonstrates three crack-loading modes. The opening mode is of particular interest as it is the predominant mode in most engineering applications [62]. Hereafter, K is used instead of K_I as the other crack-loading modes are not the subject of this study.

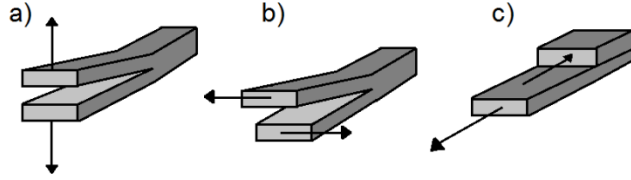


Figure 2-5 Crack-loading modes, a) opening mode or tensile mode, b) in-plane shearing or sliding mode, and c) anti-plane shearing or tearing mode (adapted from References [35, 62]).

Crack behaviour is influenced by factors such as crack and component geometries, service load spectra, stress distributions, and material characteristics [33, 61-63]. Many cracks in the rail head can be adequately represented as an ellipse. The stress intensity factor for an elliptical crack under arbitrary normal loading is discussed in References [65, 66]. A simple example from fracture mechanics analysis is presented in Equation 2-4 to show the relationship between the stress intensity factor, applied stress, and the crack size. This example, as shown in Figure 2-6, corresponds to a two-dimensional centre crack in an infinite plate that undergoes uniform tensile stress (σ) [62, 63].

$$K = \sigma \sqrt{\pi a} \tag{2-4}$$

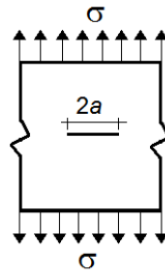


Figure 2-6 Two-dimensional infinite centre-cracked plate subjected to uniform tensile stress (σ), (a : half of the crack length).

When K reaches the fracture toughness of the material (K_c), the crack extends in a rapid and unstable manner without an increase in loading or applied energy, and a brittle fracture occurs. Equation 2-5 presents the relationship between the stress intensity factor, applied stress, and the crack size at the critical stage for the component shown in Figure 2-6.

$$K_c = \sigma_c \sqrt{\pi a_c} \tag{2-5}$$

where σ_c is the fracture stress and a_c is the crack length at instability (critical crack size). Rail fracture stress is dependent on the steel fracture toughness, size and location of cracks and magnitude and distribution of the loading condition [62].

Fracture toughness (K_c) is a material property that indicates the critical stress intensity factor (k) for a crack [62]. Fracture toughness generally decreases as the temperature decreases from room temperature. In addition, a higher yield strength or ultimate strength results in lower fracture toughness for all materials [62]. Typical values of K_c for rail steel are presented in References [33, 38, 67].

In most engineering applications, initial crack does not often instantaneously lead to a catastrophic failure. More commonly, the initial crack grows due to fatigue and wear. When the crack reaches a critical size, fracture occurs [38]. The damage tolerance concept was introduced to acknowledge this process. In this concept, the existence of a crack is accepted in rail steel. Then, the crack propagation life (also known as residual life or slow crack-growth life) is estimated in terms of the number of load cycles or cumulative tonnage that causes the crack to propagate from a barely detectable size to a critical size. Subsequently, information about crack propagation life is used to determine intervals between periodic rail inspections or between the periodic removal of cracks (e.g., by grinding). The inspection intervals are often recommended to be less than half of the crack propagation life [38, 40].

The fatigue crack-growth life consists of three main stages as shown in Figure 2-7 [3, 38, 62]. The first stage is the long initiation stage that is also known as the initiation life or nucleation life [3]. This stage can be studied using mechanical-based models [34]. The second stage is the transition stage from the initiation to propagation stage and is hard to define due to uncertainty in crack-detection methods [3, 38]. The last stage is the propagation stage. This stage shows the cumulative tonnage (the number of load cycles) that causes a fatigue crack to grow from a barely detectable size to a critical size [3]. The propagation life and growth rate of fatigue defects under varying operational, structural, and environmental conditions can be determined using fracture mechanics principals [8, 38, 40]. The fatigue crack growth is sometimes analysed conservatively in terms of propagation life [3]. The crack initial size (detectable size), critical size, and propagation life are three main parameters in the damage tolerance concept [38].

The crack initial size is a size that is detectable by non-destructive inspection (NDI) techniques. The detection limit for NDI techniques is a statistical quantity rather than a fixed value. The NDI techniques such as visual, ultrasonic, and magnetic inspection methods have a certain level of accuracy. As a result, defects may remain undetectable at the time of the test because they are too small to be detected by the inspection methods, or they are masked under the rail surface cracks. For that reason, the crack initial size refers to the smallest size that NDI techniques can detect with a sufficiently high probability [3, 38].

The critical size for a crack is a size by which the crack is expected to fracture under the next train [3]. Alternatively, the critical crack size may be defined as a crack size which is expected to fracture within the next inspection interval [33]. The critical size may be also defined using equations from fracture mechanics. For instance, the critical crack size for the crack and component geometry shown in Figure 2-6 can be determined using Equation 2-6 provided that the applied stresses and the fracture toughness are known [62].

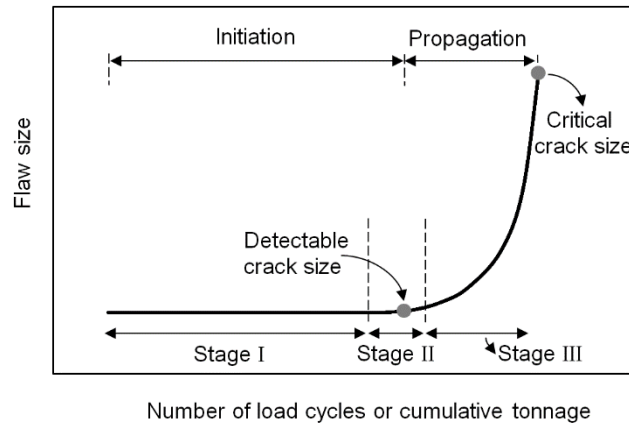


Figure 2-7 Growth trend of rail flaw.

$$a_f = \frac{1}{\pi} \left(\frac{K_C}{\sigma_{max}} \right)^2 \quad (2-6)$$

Under normal service conditions the critical size for a defect in the rail head could be 70 to 80% of the rail head area. In winter, this critical size could be reduced up to 10% of rail-head area due to lower fracture toughness and higher thermally induced tensile stresses [40].

The fatigue propagation life for steel elements is mainly associated with three parameters: the number of cycles of loading (or cumulative tonnage), the stress range at the location of the

defect, and the type of defect being examined. By definition, the number of load cycles (N) is inversely proportional to the stress range ($\Delta\sigma$). When the stress range is low, the crack size needs a higher number of cycles to reach the critical size ($N \propto 1/\Delta\sigma$).

The fatigue crack-growth rate (da/dN) from fracture mechanics approaches is widely used to estimate the fatigue propagation life of cracks [8, 32, 38, 62]. When the crack size (a) is plotted versus the number of cycles (N), the fatigue crack growth rate indicates the slope of the curve at a given number of cycles. This rate is correlated to the applied stress-intensity factor range (ΔK) during loading cycles. Figure 2-8 illustrates the correlation between fatigue crack-growth rate and ΔK [8, 32, 38, 62].

In Figure 2-8, Region I indicates a fatigue threshold value (ΔK_{th}) below which no crack growth is observed. ΔK_{th} for steel is usually between 5 and 15 ksi.in^{0.5}. This threshold depends on parameters such as stress ratio (R), frequency of loading, and environment. ΔK_{th} decreases as the stress ratio increases [62].

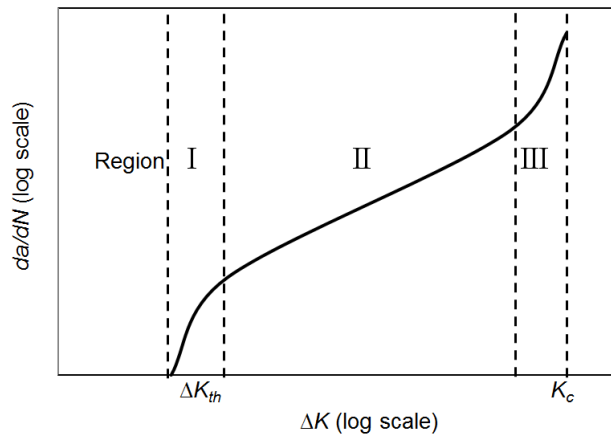


Figure 2-8 Fatigue crack growth rate (da/dN) vs. the applied stress intensity factor range (ΔK).

Region II shows a near linear correlation between crack growth rate and the applied stress intensity factor. This correlation is quantified using Equation 2-7, which is known in fracture mechanics as the Paris equation. Region II, which is also known as the Paris region crack-growth rate, corresponds to stable crack growth [62, 63].

$$\frac{da}{dN} = A (\Delta K)^n \quad (2-7)$$

where n is the slope of the line in the constant slope, and A is the value of da/dN at ΔK equal to 1 MPa.m^{1/2}. n and A are material constants that are addressed in Reference [8, 62].

The growth rate is not only dependent on the stress-intensity factor range, particularly, near Region I in which the crack growth rate is more dependent on the maximum stress intensity (K_{max}) rather than ΔK . Hence, modification factors have been proposed for Equation 2-7 to consider the effect of the stress ratio (R), the threshold stress intensity range (ΔK_{th}), and K_{max} during each load cycle [32, 33, 38, 62]. R is the ratio between minimum and maximum stresses during a load cycle. This ratio represents the effect of mean stress. By increasing the mean stress by increasing R , the number of cycles to crack initiation and failure is decreased. In fact, high mean stresses significantly increase the crack growth rate and reduce the critical crack size and therefore, reduce the fatigue life [61, 62].

As shown in Figure 2-8, very high crack growth rates occur at Region III, which indicates that the crack is approaching instability. Region III has little effect on the total fatigue life. Region II can be considered the only region affecting the fatigue propagation life [62].

Information about the fatigue crack-growth rate makes it possible to calculate the propagation life in terms of the number of cycles (N). To clarify the discussion, for the crack geometry and loading pattern shown in Figure 2-6, calculations for estimating the propagation life are presented below [61, 62].

$$\Delta k = K_{max} - K_{min} = \sigma_{max}\sqrt{\pi a} - \sigma_{min}\sqrt{\pi a} = \Delta\sigma \sqrt{\pi a} \quad (2-8)$$

$$\frac{da}{dN} = A (\Delta K)^n = A(\Delta\sigma \sqrt{\pi a})^n = A\Delta\sigma^n (\pi a)^{n/2} \quad (2-9)$$

$$N_f = \int_0^N dN = \int_{a_i}^{a_c} \frac{da}{A\Delta\sigma^n (\pi a)^{n/2}} = \frac{1}{A\Delta\sigma^n (\pi)^{n/2}} \int_{a_i}^{a_c} \frac{da}{(a)^{n/2}} \quad (2-10)$$

where a_i is the initial crack size and a_f is the critical crack size. With the assumption $n \neq 2$:

$$\int_{a_i}^{a_c} \frac{da}{(a)^{n/2}} = \frac{(a_f)^{-\frac{n}{2}+1} - (a_i)^{-\frac{n}{2}+1}}{-\frac{n}{2}+1} \quad (2-11)$$

$$N_f = \frac{2}{(n-2)A\Delta\sigma^n (\pi)^{n/2}} \left[\frac{1}{a_i^{(n-2)/2}} - \frac{1}{a_f^{(n-2)/2}} \right] \quad (2-12)$$

2.5 Track modulus: its meaning and its effects on rail deflections and stresses

Track foundation modulus, commonly referred to as track modulus, is a measure of the vertical stiffness of the rail foundation. It is defined as the supporting force per unit length of rail per unit deflection. According to the definition, track modulus is not influenced by rail properties [27, 28]. It includes the effects of fasteners, ties and substructure [68]. Track modulus continuously changes along the track. Spatial variation in local geology, layer properties, layer thickness and track construction procedures disturb the rail support uniformity along the track. Track modulus can also rapidly change over a short length of the track at transition zones between embankments and bridges, concrete and wood crossties, ballast and slab track, and at the locations of switches, turnouts, crossings, hanging or broken cross ties, and loose rail-seat fasteners [29, 31].

Track modulus is an indicator of the structural condition of the track and is related to track performance [7, 29, 31, 69]. A higher track modulus generally leads to better track performance by offering adequate resistance to applied loads. A relatively high track modulus leads to decreased rail deflections and bending stresses and, therefore, improves track performance and reduces track deterioration [7, 30, 69, 70]. However, a very high track modulus results in increased dynamic forces in the rail-wheel interface and triggers problems such as rolling contact fatigue and wear [7, 30, 69, 70]. Additionally, a spatially varying track modulus leads to significant variations in dynamic train-track interaction forces, which cause track differential settlement. A non-uniform permanent track deflection distorts the initially smooth rail surface and expedites the track deterioration, which in turn contributes to rail failure by further increasing the dynamic forces [29, 31].

The optimum value of track modulus is neither too low nor too high [7, 27]. Referring to a field data analysis, the track modulus value of less than 13.7 MPa (2000 psi) is associated with poor track performance. Values between 13.7 MPa (2000 psi) and 27.5 MPa (4000 psi) are associated with average performance and a value greater than 27.5 MPa (4000 psi) is associated with good performance [71]. The track modulus values of higher than 68.95 MPa (10000 psi) are too high to accommodate a dynamic train-track interaction [72, 73]. For an acceptable track performance, the AREMA manual recommends a rail vertical deflection of greater than 3.175 mm (0.125 in) and less than 6.35 mm (0.25 in) that can be reached by providing an optimised track modulus [59]. A study on vertical rail deflection and track life is presented in References [7, 74].

Knowledge about track modulus and its effect on rail life is still far from complete. New techniques developed to measure track modulus continuously from a moving car can significantly improve understanding in this field [22-25, 68, 70].

2.6 Train-mounted systems to measure track modulus and assess rail condition

A number of train-mounted measurement systems have been developed for the estimation of track stiffness continuously along rails [21, 22, 26, 70, 75-80]. This includes the Track Loading Vehicle (TLV) and the MRail system; that measure the VTD from moving railcars under axle loads that are representative of fully loaded railcars [21, 26, 75, 76]. There is also one system that can be attached to an ordinary track geometry car and measures VTD [22]. Moreover, Rolling Stiffness Measurement Vehicle (RSMV) is available for estimating the dynamic track stiffness through measuring the accelerations under known applied loads [69, 70].

The TLV system was developed by the Transportation Technology Center, Inc. (TTCI) [26, 76]. In a standard TLV test, VTD is calculated through subtracting two sets of measurements conducted using two different railcars. Each railcar has a suspended truck at the centre which is equipped with non-contact laser cameras for deflection measurements. The main railcar is about 20 m in length and 138 kN in weight which is distributed between the two end trucks. The long length prevents the end trucks having effects on the deflection profile beneath the centre truck. The actuator installed on the centre truck of the main railcar is capable of applying 4 to 267 kN (1 to 60 kips) loads. The other railcar consists of the same assembly as the main railcar. However, its weight is much lower (about 62-kN) and the actuator mounted on the centre truck applies vertical loads only up to 9 kN (2 kips). The application of this small load is to ensure the contact between the wheel and the rail. The test can also be implemented to evaluate the stiffness of the subgrade. This evaluation requires a second run with load of 44 kN (10 kips). Difference between the results of the two runs demonstrates the subgrade deflections. The speed of moving railcars in this test is about 16.1 km/hr (10 mph) which is relatively low for track evaluation over the long distances. Moreover, the test requires expensive equipment and special railcars. The technique was implemented in revenue service to identify locations with large track stiffness variation, abrupt transitional stiffness change, and low levels of track support. It was suggested that the system can be used for assessing the capability of existing tracks for upgrade for

economical handling of higher operating speeds and heavier axle loads, and can provide a better the understanding of track strength degradation over time which allows for an optimised allocation of maintenance resources [26, 76].

The MRail system is a laser and camera system that measures the relative deflection (Y_{rel}) between the rail surface and the rail-wheel contact plane at a distance of 1.22 m from the nearest wheel to the sensor system. This system was developed at the University of Nebraska-Lincoln in collaboration with the Federal Railroad Administration (FRA). Technical details and the principal of measurement for the MRail system are presented in Chapter 3. The simplicity of the measurement technology and the capability of measurements at full track speeds make the MRail system a practical option for assessing the rail deflections over long distances. The unprocessed Y_{rel} measurements has shown the ability to identify the local track issues such as muddy crossings, crushed rail heads, failing joints, and broken ties [81]. The results from 270 miles of Y_{rel} measurements on the Union Pacific Railroad's heavy haul coal line also suggested that the average and standard deviation of Y_{rel} data have the potential use for assessing the track condition [82]. Field data analyses demonstrated that the processed Y_{rel} measurements can be used for mapping the extent of soft foundations beneath a railway line [80]. Moreover, the VTD measurements from two Canada's high-traffic subdivisions [>50 million gross tonnes (MGT)/year] were used to derive two indices that represent the magnitude and variability of the subgrade stiffness. The comparison of these indices with historical records of track performance showed that the locations at which track geometry defects occur match with locations that have a low modulus and high variability in the modulus [83]. The Y_{rel} measurements were also used to estimate the maximum bending moments and stresses in rail. The correlations between Y_{rel} and bending stresses were developed using the Winkler model (proposed in 1867 [7, 10]) that assumes a constant track modulus along the track. The rail bending estimations were then verified using a controlled experiment on the Union Pacific Railroad's Yoder Subdivision [20].

A new innovative method for VTD measurements was also developed in Sweden. This was done by adding an extra system to an ordinary track recording car to measure the rail longitudinal level. The method uses two different measurement systems of longitudinal level on one axle which allow for extracting the loaded and unloaded longitudinal levels. It was suggested that the VTD measurements together with an estimation of applied loads can be analysed using the

Winkler model to estimate track modulus. The system was used on the iron-ore line in Sweden. The results demonstrated the ability of the system to locate hanging sleepers and soft tracks which are sources of large deflections and bending moments for a rail. A plan was presented to investigate whether there is a correlation between the VTD measurements from this technique and the ultrasonic testing of rails showing rail defects [22].

Swedish Rail Administration (Banverket) developed a new device for measuring dynamic track stiffness. The system, referred to as RSMV, dynamically excites the track using two oscillating masses above one wheel-set. The measured axle box forces and accelerations are then used to calculate the dynamic track stiffness. The RSMV can be employed for overall measurements at speeds up to 50 km/h. However, if detailed investigation is needed, the measurements should be performed at speeds lower than 10 km/h. The data from the RSMV system was analysed using statistical approaches to obtain a good understanding of track stiffness and its variation along Swedish railway lines [69, 70].

Although the developed VTD and track modulus measurements techniques form valuable database for the rail structural assessment, the current knowledge for the data interpretation is still insufficient to derive rail failure criteria. In this regard, a theoretical backbone is needed to correlate the measured data with rail performance. More details about the contribution of this study with respect to the state-of-the-art and related literature are given in Chapters 3, 4, 5 and 6.

2.7 Summary

This chapter presented a brief review on rail stresses. Rail bending, wheel-rail contact, and thermal and residual stresses were described as the dominant stresses generated in a rail. Then, damage mechanisms controlling rail life, including fatigue, wear, and plastic deformations, were discussed. This was followed by a brief review on the most common rail defects. The growth planes, origin, and stresses involved in the growth of rail defects were explained. The literature review showed that transverse defects in the rail head are the leading cause of broken rail derailments in North America, and rail bending stresses are one of the main factors affecting the propagation of these transverse defects. Furthermore, the two most common failure modes, including rail permanent plastic bending and rail fracture, were reviewed. There was also a discussion of the stress limits that have been proposed to ensure safe operation of railways.

Finally, a definition was given of track modulus as an important parameter affecting rail deflections and stresses, and there was a review of the track modulus measurement techniques and effects of track modulus on rail structural performance.

CHAPTER 3: Evaluating the Potential of a Train-Mounted Vertical Track Deflection Measurement System to Estimate Track Modulus¹

3.1 Overview

Over the past two decades, a train-mounted vertical track deflection (VTD) measurement system aiming to continuously measure the track modulus has been under development at the University of Nebraska–Lincoln under the sponsorship of the Federal Railroad Administration (FRA). This system measures the relative vertical distance (referred to as Y_{rel}) between the rail surface and the rail-wheel contact plane at a distance of 1.22 m from the nearest wheel to the sensor system. According to “*Objective 1*” presented in Chapter 1, the aim of this study was to investigate the potential of using the Y_{rel} measurement as an indicator of the track modulus for various rail foundation conditions. To meet this objective, a detailed finite element model (FEM) capable of simulating moving loads and track modulus variation was developed. One of the unique contributions of this study is that it presents a comprehensive study of the Y_{rel} –track modulus relationship by defining more realistic support conditions using discrete spring supports and by simulating the stochastic nature of the track modulus along a 160-m track length. The numerical model was employed to examine the accuracy of estimating the track modulus using the Y_{rel} measurements when foundation stiffness is variable. Furthermore, the correlation between the statistical properties of the track modulus and Y_{rel} was studied over different track segment lengths.

3.2 Introduction

Track modulus is widely accepted as an important indicator of the track condition, since its value and variation along the rail significantly affect the track performance [28-31]. This track

¹ A version of this chapter has been published in Proceedings of the Institution of Mechanical Engineers, Part F: Journal of Rail and Rapid Transit as Fallah Nafari S, Gül M, Roghani A, Hendry M.T, and Cheng J.J.R, *Evaluating the Potential of a Rolling Deflection Measurement System to Estimate Track Modulus*. doi: 10.1177/0954409716646404.

parameter indicates the vertical stiffness of the rail foundation and is defined as the ratio between the vertical deflection of the rail and the vertical foundation supporting force per unit of track length [27]. In order to study the correlation between the track modulus and track performance comprehensively, reliable methods for measuring the track modulus are needed. A number of trackside and on-train measurement approaches are available for estimating the track modulus. These approaches typically rely on measuring the vertical deflection of the rail when subjected to a known applied load. Mathematical models are then required to convert the deflection to the track modulus. Trackside measurement techniques (also known as point measurement techniques) are those in which the rail deflection is measured under single or multiple static loads at particular discrete locations, whereas on-train approaches are designed to measure the deflection from a moving car [24, 27, 28, 84-87]. There are instances when trackside approaches are necessary for obtaining detailed information at specific locations, and these types of approaches may give very accurate results for certain cases, such as soft tracks [85, 88]. However, this technique may not provide a practical approach for assessing the track condition when dealing with a large rail network. The application of on-train techniques for measuring the track modulus at revenue speed provides a comprehensive overview of railway line conditions over long distances of track [22, 26, 69, 89, 90]. Despite this significant advantage, measuring the vertical rail deflection from a moving car is a challenge due to the difficulty in defining a reference point. Moreover, the interpretation of the on-train deflection measurement data still needs more investigation.

Over the past two decades, two deflection/track modulus measurement techniques have been developed and tested in North America: the Track Loading Vehicle (TLV) developed by the Transportation Technology Center, Inc. (TTCI) and the University of Nebraska Real-Time VTD Measurement System (commercially known as MRail system) developed under the sponsorship of the FRA [23-26, 76]. The focus of this study is on the MRail system that has shown the potential to measure deflection at relatively higher speeds and at lower equipment costs [21].

The MRail system has been recently employed within Canada's railway lines to evaluate the potential of VTD measurement as an indicator of track performance and as a tool for mapping subgrade stiffness [77-80]. The possible correlation between the VTD data and track modulus allow a true interpretation of the VTD data. Although local trackside measurements and

numerical studies have shown the relationship between VTD and track modulus [91], further studies are still needed to address the relationship for various rail foundation conditions.

In this study, a series of detailed FEMs capable of simulating moving loads and track modulus variation was developed to investigate the potential use of VTD measurements for estimating the track stiffness under varying track modulus conditions. The track structure used in the simulations was 160 m in length. The stochastic nature of the track modulus and its effects on the VTD data were also addressed in the models by using discrete spring supports. In different simulations, the track modulus coefficient of variation (COV) along the 160 m track length varied from 0 to 0.75 for different average values, and the track modulus values changed between 0 and 83 MPa (12,000 psi). Using these advanced models, the accuracy of estimating track modulus using VTD measurements was investigated for a track structure with variable track modulus. In addition, the correlation between the statistical properties of the track modulus and VTD data was studied in detail.

Results presented in this chapter are applicable to continuous welded rail, since the rail is considered as the continuous element in all simulations. It should also be noted that the framework discussed in this chapter aims to be used for interpreting the MRail VTD data measured within freight lines in Canada along which trains mainly operate at speeds equal to or lower than 65 km/h (40 mile/h). Hence, dynamic response is not considered in the numerical models.

3.3 MRail: a real-time vertical track deflection measurement system

The MRail system measures the relative deflection (Y_{rel}) between the rail surface and the rail-wheel contact plane at a distance of 1.22 m from the nearest wheel to the sensor system (Figure 3-1a). The measurement system includes two line lasers and a camera that are attached to a rigid bracket (Figure 3-1b). The assembly is then installed to the side-frame of a rail car truck. The two laser beams intersect and mark two curves on the surface of the rail (Figure 3-1c). The minimum distance between these two curves, shown with (d) in Figure 3-1(c), is geometrically related to the distance between the rail surface and the camera (h). Moreover, the distance between the wheel/rail contact plane and the camera ($h + Y_{rel}$) is always constant due to the rigidity of the bracket. Therefore, Y_{rel} is calculated by subtracting (h) from ($h + Y_{rel}$) [92, 93]. As

shown in Figure 3-1d, a newer system can be also implemented, which uses one laser beam to shine a line on the head of the rail at the camera's field of view [78, 79]. The only difference between the old and new system is the method used to calculate the distance between the rail surface and the camera (h). In the new system, the distance between the projected laser line and the center of the camera's field of view on the running surface of the rail head ($0.5d$) is measured and converted into (h). Using the MRail system, deflection measurements can be collected with a reasonable sampling rate at speeds of up to 96 km/h (60 mile/h) [21].

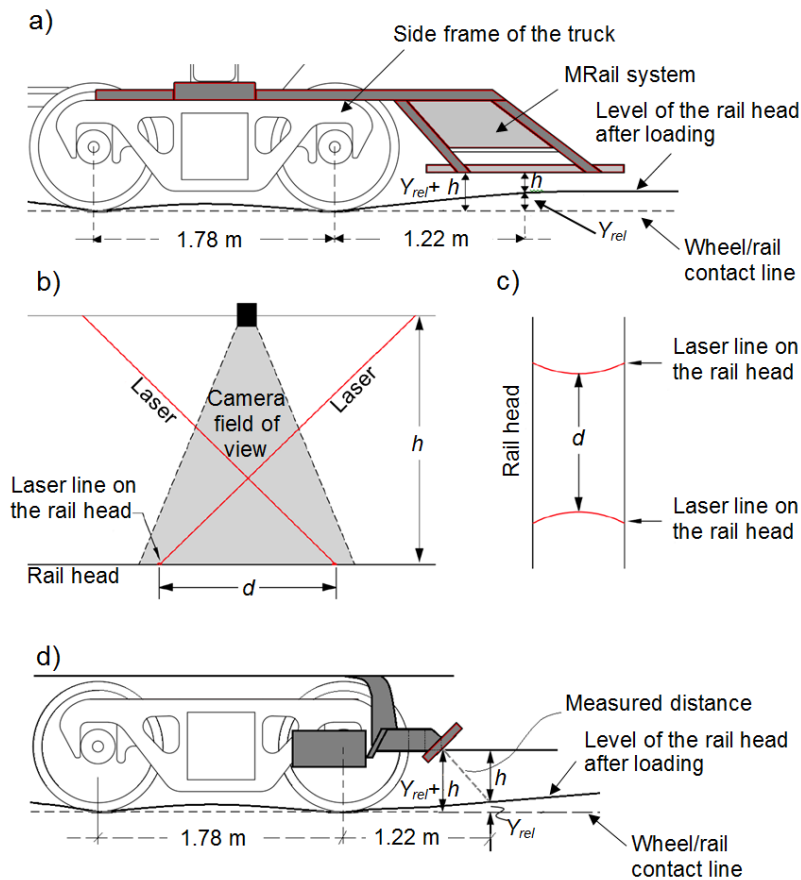


Figure 3-1 Schematic of the MRail system used to measure the relative vertical track deflection (Y_{rel}) (adapted from References [23, 79]), a) the original MRail system, b) sensor system, c) the top view of the laser lines on the rail head, d) the new MRail system.

The MRail system has shown the ability to detect the local track issues such as muddy crossings, crushed rail heads, failing joints, and broken ties [81]. Moreover, the field data analyses have demonstrated the ability of the system to map the relative stiffness of the subgrade [77-80]. The correlation between statistical properties of Y_{rel} data (i.e. average and standard deviation) and

track structural performance has also been shown using the preliminary field data analyses [77-79, 82].

3.4 Finite element model specifications and validation

The vertical rail deflection profile under the wheel loads can be calculated using a model based on the infinite beam on a continuous elastic foundation theory. This model, proposed by Winkler (1867), is widely accepted for estimating the rail bending response to vertical loads [94, 95]. According to the Winkler model, the vertical rail deflection, $Y(x)$, at distance x from a single point load (P) can be calculated using the Equation 3-1.

$$Y(x) = \frac{P\beta e^{-\beta x}}{2U} (\cos\beta x + \sin\beta x) \quad (3-1)$$

where U is the track modulus and β is the stiffness ratio equal to $(U/4EI)^{0.25}$, with EI being the rail bending stiffness. Even though the Winkler model provides accurate results for constant track modulus, its application for cases where the track modulus is not constant is limited. The limitations of the Winkler model can be overcome using the FEMs. Such models allow statistical variation of the track substructure to simulate the variability in VTDs. Hence, a detailed FEM to simulate the track structure consisting of two rails, crossties, and spring supports was developed using CSiBridge software [96], which is specialized software for 3D analysis and design of bridge-type structures. Although this software has specific capabilities to model bridge type structures, it can still be used for the 3D analysis of other types of structures and its capabilities in considering different types of springs and moving loads can be utilized for the railway track structure simulations. Figure 3-2 shows an image of the developed FEM.

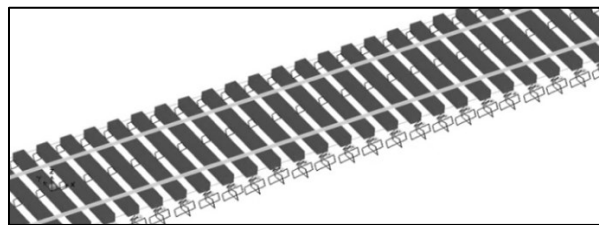


Figure 3-2 The track structure model developed for numerical study.

The definition of the variable track modulus within this FEM is possible through assigning different stiffness values to the discrete foundation springs. The load–deflection behaviour of

these springs can be either linear or nonlinear. The simulation of discrete spring supports and variable track modulus can significantly improve the accuracy of the numerical models [75]. Despite these significant advantages, simulation of the track–train dynamic interaction is not possible in this software. Considering the purpose of the study and the Y_{rel} measurements at low train speeds within freight lines in Canada (train speeds mainly equal to or lower than 65 km/h (40 mile/h)), this shortcoming is not a concern for this study due to the negligible effects of dynamic response on the track deflections when the train speed is low [23, 88, 97]. The effects of train speed and dynamic response on Y_{rel} interpretations should be taken into consideration if the train equipped with the measurement system travels at medium to high speeds. Addressing such dynamic effects is beyond the scope of this study.

Vertical deflections and bending moments in the rail can be calculated using the CSiBridge software. However, automated calculation of Y_{rel} along the track requires a complementary code for running simulations effectively and for post-processing data. The developed code in EXCEL Visual Basic for Application (VBA) uses the extracted vertical rail deflection profile from the software to obtain Y_{rel} at the predefined time steps. In the numerical models, the rail size and tie spacings were defined as RE100 and 0.508 m, respectively. It was assumed that the MRail system was installed in the back truck of a middle rail car, which is typical in tests (Figure 3-3). For this configuration, even though the two trucks in the rail car do not amplify the effect of each other due to large truck center spacing, the front truck of the trailing rail car affects the deflection profile and, thus, the Y_{rel} readings. The extent of effect depends on axle load, track modulus, and axle spacing. Loading condition considered in the simulations is as shown in Figure 3-4.

The simulated track structure was 180.8 m in length and included 357 crossties. Variable track modulus was considered for the mid-length, which was 160.5 m long and consisted of 317 crossties. A constant track modulus was assigned to the two remaining sections of track at both ends. The section with variable track modulus termed “mid-section” is the focus of the study. Having two sections approximately 10 m in length at both ends minimized the effects of the end boundary conditions on the midsection. The response of the track to the moving wheel load set shown in Figure 3-4 was derived using direct integration time history analysis. Train speed and output time steps were chosen so that Y_{rel} can be calculated at 0.3048 m (1 foot) intervals along the track.

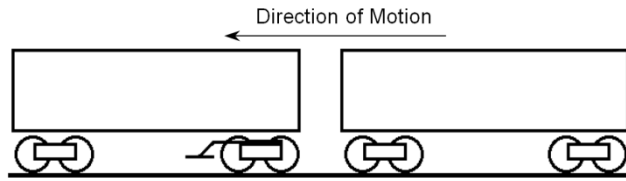


Figure 3-3 The MRail system installed in the back truck of a middle rail car.

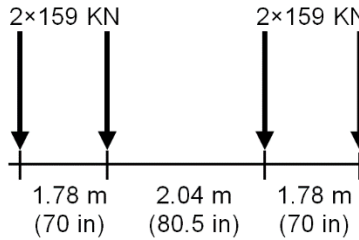


Figure 3-4 The wheel load set considered in the numerical models.

Since the track modulus has a stochastic nature along the track [98, 99], various track modulus distributions were considered for modelling this variability, as listed in Table 3-1. For each simulation, a track modulus distribution type was selected, and randomly generated numbers from this distribution were assigned as the spring coefficient values under the crossies along the rail. The procedure is graphically shown in Figure 3-5.

Table 3-1 Track modulus distributions considered in the numerical models.

	Average (MPa)	COV	No. of Simulations		Average (MPa)	Range (MPa)	No. of Simulations
	Normal Dist.	41.4	0.25		10	Uniform Dist.	41.4
0.5			10	10.3 to 72.4	10		
0.75			10	0 to 82.7	10		
27.6		0.25	10	27.6	13.8 to 41.4		10
		0.5	10		6.9 to 48.3		10
		0.75	10		0 to 55.2		10
13.8		0.25	10	13.8	6.9 to 20.7		10
		0.5	10		3.5 to 24.1		10
		0.75	10		0 to 27.6		10

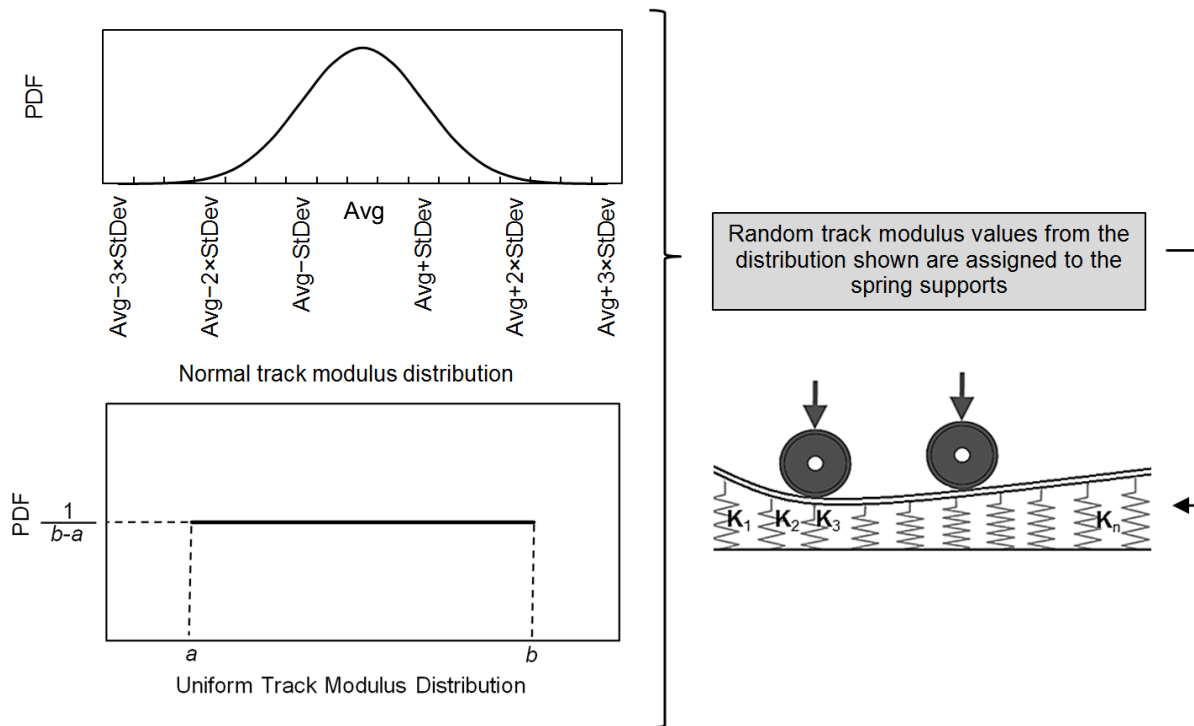


Figure 3-5 Assignment of randomly selected stiffness values to the springs under the crossies along the track (ninety models were developed using the normal track modulus distribution, and ninety models were developed using the uniform track modulus distribution), (k : Stiffness of the spring support, PDF: Probability distribution function).

The values randomly selected from a track modulus distribution are numerically independent. However, the values for each model come from a specific track modulus distribution, which makes them practically inter-related (i.e. the probability of values selecting from a distribution with low COV to be far apart is low). This modelling method allows simulation of abrupt changes in track modulus as well as global track modulus variation, as the randomly generated track modulus values can result in locations with a very low modulus even when the average modulus is relatively high. These locally low track modulus values can be representative of abrupt changes in rail foundation stiffness (e.g., broken ties, hanging ties).

Preliminary analyses revealed that the tensionless foundation affects the Y_{rel} data negligibly and increases the runtime significantly. Therefore, the spring supports' behaviour was defined as linear in the models, even though the real track foundation is tensionless and acts nonlinearly.

To confirm the modelling procedure, a constant track modulus of 41.4 MPa was considered along the track, and the resultant Y_{rel} were compared with the Winkler model results. Figure 3-6 demonstrates the extracted Y_{rel} from the FEM, only for a limited window of the track. Since the track modulus is constant, the pattern is repeated all over the full length of the track. The Y_{rel} data derived from the FEM vary between 3.15 mm and 3.25 mm, which are very close to the Y_{rel} value of 3.03 mm from the Winkler model for the corresponding rail size and loading conditions. At this point, the reason for the slight fluctuation in the Y_{rel} data is the discrete spring supports.

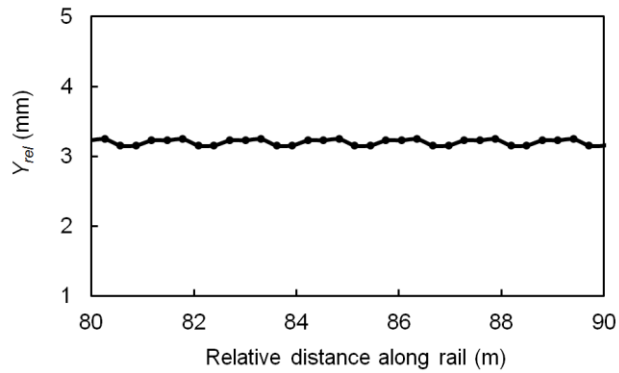


Figure 3-6 Distribution of the relative vertical track deflection (Y_{rel}) along the rail calculated using finite element modelling for a track structure with the constant track modulus of 41.4 MPa.

3.5 Correlation between Y_{rel} and track modulus

The correlation of Y_{rel} with track modulus is commonly explained using the Winkler model for “an infinite beam on a continuous elastic foundation” [81, 91]. Figure 3-7a illustrates the vertical deflection profile of a RE100 rail calculated using the Winkler model with a constant track modulus of 41.4 MPa and wheel loads of 159 kN. Y_{rel} is also shown in Figure 3-7a. The relationship between Y_{rel} and track modulus can be estimated by changing the constant track modulus value and calculating the deflection profile and Y_{rel} (Figure 3-7b). The established relationship between track modulus and Y_{rel} (Equation 3-2) is influenced by rail size and loading conditions. Figure 3-7b and Equation 3-2 correspond to the RE100 rail size and loading conditions shown in Figure 3-4.

$$U = 320.6 \times (Y_{rel})^{-1.85} \quad (3-2)$$

where U is the track modulus (in MPa) and Y_{rel} is the relative VTD measured by the MRail system (in mm).

The effect of variable foundation stiffness on the correlation between the track modulus and Y_{rel} can be investigated using the FEM technique described in the previous section. To examine the effect of track modulus variation, one of the numerical simulations (reported in Table 3-1) with an average track modulus of 41.4 and COV of 0.25 was selected. Figure 3-8(a) illustrates the distribution of track modulus defined as the model input for this simulation. The track modulus considered for the model input is termed “input track modulus” herein. The resultant Y_{rel} data calculated using the FEM analysis is also shown in Figure 3-8(b).

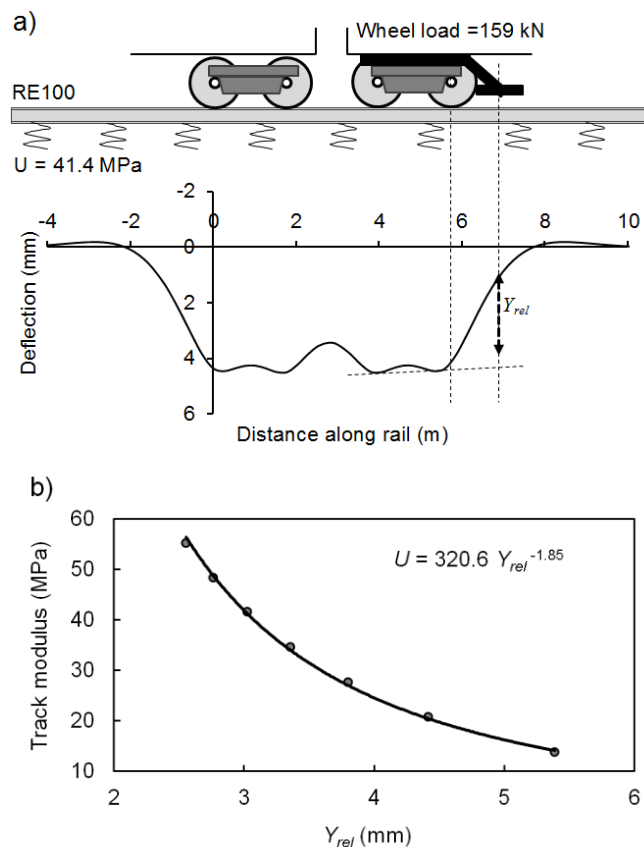


Figure 3-7 a) The vertical rail deflection profile under wheel loads and the relative vertical track deflection (Y_{rel}), b) correlation between the track modulus and Y_{rel} based on the Winkler model.

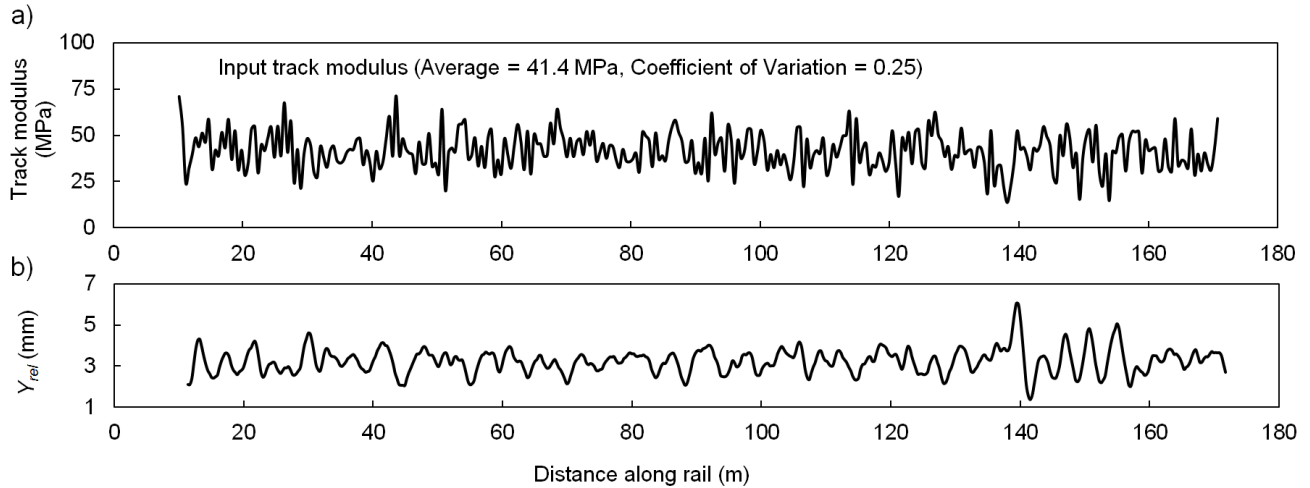


Figure 3-8 a) The track modulus distribution defined as input for the FEM, b) Distribution of the relative vertical track deflection (Y_{rel}) calculated using FEM.

Comparing the distributions of the input track modulus in Figure 3-8a with the calculated Y_{rel} along the track in Figure 3-8b clearly demonstrates a complicated relationship between these two parameters. As a result, converting Y_{rel} to the track modulus point-by-point along the track using simplified models creates significant inaccuracy when track modulus is not constant. Thus, even though the Winkler model is a well-proven model for calculating the vertical deflection and bending stress of a rail supported by constant track modulus, it is not applicable to the interpretation of the Y_{rel} data measured over a variable rail foundation. To show the level of inaccuracy in the track modulus estimation conducted point-by-point along the track using the Winkler assumption (Equation 3-2), two different cases are plotted in Figure 3-9. Case 1 depicts the input track modulus distribution shown previously in Figure 3-8a while Case 2 shows the track modulus distribution estimated using Equation (3-2) with the Y_{rel} data presented in Figure 3-8b.

In Figure 3-9, a significant difference can be noticed between the input and estimated track modulus. In general, the value of Y_{rel} depends on the rail deflection values at the locations of the two wheels and the sensor system. Therefore, Y_{rel} should not be expected to show the track modulus value at the same location where Y_{rel} is recorded. For instance, a high Y_{rel} value could be recorded at the location of the sensor due to the low track modulus value under the wheel nearest to the sensor system. Comparing Y_{rel} values with the input track modulus at every point along the rail (in Figures 3-8 and 3-9) clarifies that the value of Y_{rel} is significantly affected by the cluster

of track stiffness beneath and around the truck wheels and beneath the sensor. It should also be noted that the distribution of the Y_{rel} data is not only dependent on the track modulus distribution, but it also is significantly affected by the arrangement of the spring supports with different stiffness values.

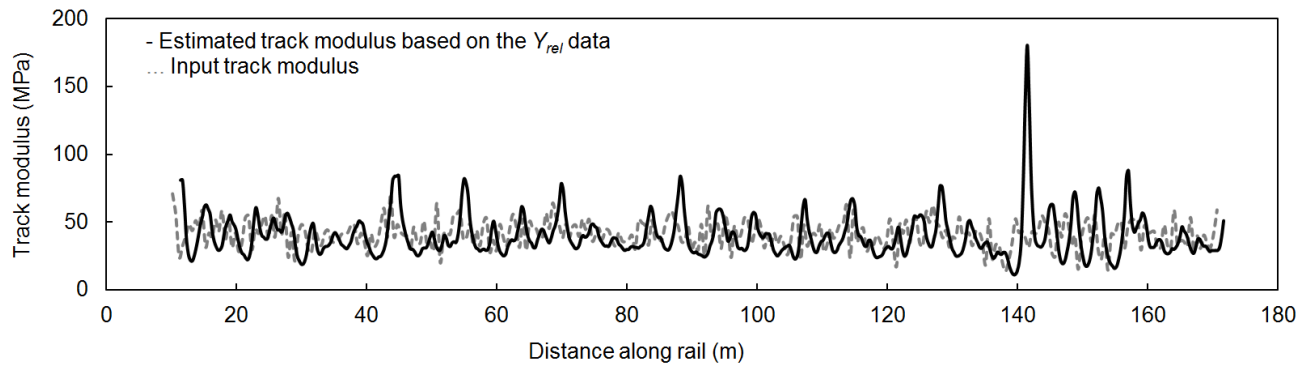


Figure 3-9 Estimation of the track modulus distribution based on the Y_{rel} data using the Winkler model (input track modulus distribution is normal with an average of 41.1 MPa and COV of 0.25).

Additionally, estimating the stiffness of individual rail supports is not usually important for the track maintenance purposes. For instance, from a maintenance point of view, a single damaged tie with good neighboring ties is often considered as acceptable in most locations, whereas a cluster of damaged ties are more of a concern. Moreover, estimation of the track modulus using Y_{rel} measurements point-by-point along the track would have inherent errors due to inevitable data problems, such as noise and offset, when dealing with thousands of miles of track. Individual Y_{rel} measurements can be influenced by different parameters. For example, track irregularities can affect the Y_{rel} measurements due to changes in the distance between the rail surface and the sensor system or changes in the dynamic load. The dynamic load can increase significantly because of the track irregularities, even when the train speed is low [100]. While it is hard to control the effect of such problems on individual Y_{rel} measurements, the evaluation of the Y_{rel} data over track segments, rather than point-by point, can be considered a practical solution and is investigated in the following section.

3.6 Correlation between track modulus average and Y_{rel} average

As mentioned, the vertical rail deflection profile under the wheel loads is affected not only by the individual vertical rail supports immediately below the wheels, but also by the adjacent supports.

Therefore, estimating the average track modulus over a track segment offers a significant advantage since it shows the behavior of clusters of vertical supports. Experimental results from previous studies also confirm the relationship between the Y_{rel} average and track structural performance [77-79]. In this section, the possible estimation of the track modulus average based on Y_{rel} average is investigated with respect to the window length. The window length refers to the track length along which average values of the track modulus and deflection are calculated.

As reported in Table 3-1, one hundred eighty models with different track modulus variations were simulated. Due to the simulated track length, the maximum window length was determined as 160 m, and the stiffness average for the vertical spring supports along the window was calculated and plotted against the Y_{rel} average for all one hundred eighty models. Results are reported in Figure 3-10a, where it is observed that the track modulus average is nonlinearly proportional to the Y_{rel} average. Moreover, it is evident that the average values for Y_{rel} over the 160-m track length (0.1 mi) remained practically unaltered as long as the track modulus average was kept constant. In other words, the Y_{rel} average was not dependent on the track modulus variation and distribution type. The nonlinear curve fitted to the FEM results was also compared with the corresponding Winkler model results. This comparison demonstrated that the Winkler model accurately shows the correlation of the track modulus average with the Y_{rel} average. In Figure 3-10a, slight differences between resultant graphs of the FEM and Winkler model are mainly due to the assumption of discrete supports in the FEMs.

It is valid to question whether the correlation between the track modulus average and Y_{rel} average can be affected by the window length. Therefore, the range of window length for which the Y_{rel} average has a strong relationship with the track modulus average needs to be determined. For instance, as shown in Figure 3-10b, an acceptable correlation cannot be established between average values of Y_{rel} and track modulus over a short track length of 4 m because of the high variations in the data.

To quantitatively investigate the effect of window length, average values of the track modulus and Y_{rel} were calculated and plotted for different window lengths. The best fit to the data was determined for each window length, and the corresponding equation is reported in Table 3-2. The coefficient of determination (R^2) and root mean square of errors (RMSE) are also presented to quantitatively show the goodness of the fitted curves. R^2 values close to 1 and low RMSE values

indicate a good match between the inputted and estimated track modulus averages. As can be seen in Table 3-2, the correlation between average values of the track modulus and Y_{rel} becomes stronger with increasing window length. It can also be observed that the Y_{rel} average is an indicator of the track modulus average when the window length is 8 m or longer ($R^2 \geq 0.9$). For the sake of simplicity, Equation 3-3 is proposed to explain the relationship between the Y_{rel} average ($(Y_{rel})_{Avg}$) and track modulus average (U_{Avg}) for all window lengths equal to or longer than 8 m. Using this equation for the worst case scenario of a 8-m window length, the R^2 between the inputted and estimated track modulus is an acceptable value of 0.87. Equation 3-3 can be employed as a tool to estimate the track modulus average using the Y_{rel} average for window lengths of 8 m or longer.

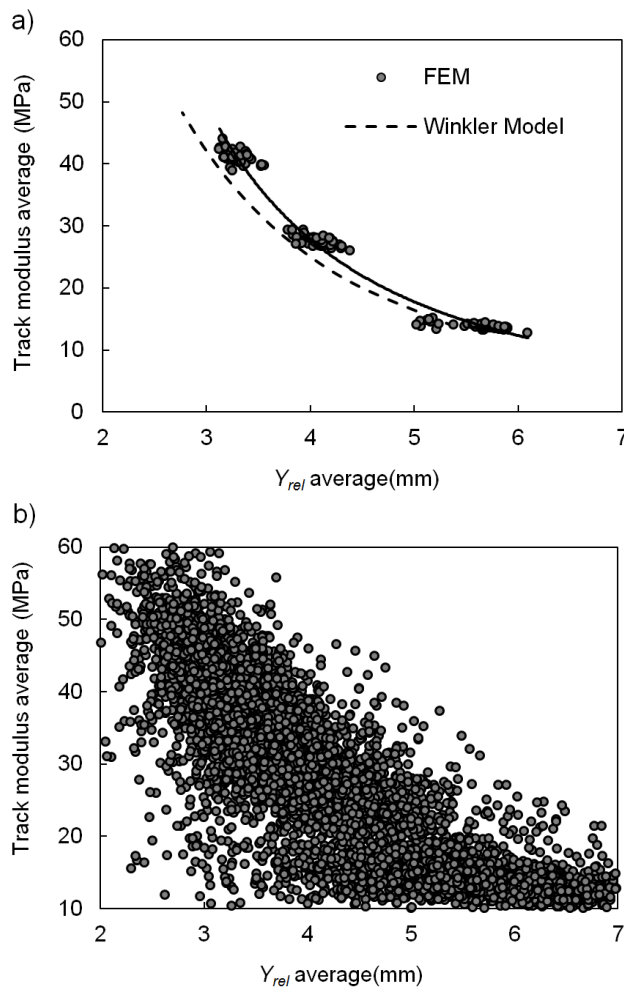


Figure 3-10 Track modulus average vs. Y_{rel} average for: a) 160-m window length and b) 4-m window length (Y_{rel} : relative vertical track deflection).

$$U_{Avg} = 450 \times (Y_{rel})_{Avg}^{-2} \quad (3-3)$$

Table 3-2 Correlation between the track modulus average and Y_{rel} average with respect to window size, (Y_{rel} : relative vertical track deflection).

Window Length (m)	Fitted Curve	R ²	RMSE (MPa)
160	$U_{Avg} = 449 \times (Y_{rel})_{Avg}^{-2.01}$	0.981	1.532
80	$U_{Avg} = 447 \times (Y_{rel})_{Avg}^{-2.00}$	0.98	1.598
40	$U_{Avg} = 440 \times (Y_{rel})_{Avg}^{-1.99}$	0.975	1.777
20	$U_{Avg} = 422 \times (Y_{rel})_{Avg}^{-1.97}$	0.963	2.2
10	$U_{Avg} = 377 \times (Y_{rel})_{Avg}^{-1.89}$	0.925	3.177
8	$U_{Avg} = 352 \times (Y_{rel})_{Avg}^{-1.85}$	0.896	3.778
5	$U_{Avg} = 269 \times (Y_{rel})_{Avg}^{-1.67}$	0.793	5.472
4	$U_{Avg} = 209 \times (Y_{rel})_{Avg}^{-1.50}$	0.521	8.471

Table 3-2 and Equation 3-3 are based on the FEM results extracted from the one hundred eighty simulations with either normal or uniform track modulus distribution (see Table 3-1). To investigate the accuracy of the proposed equations further, a new model with totally randomized stiffness at each support was generated. The distribution of the track modulus in this new model (shown with a dotted line in Figure 3-11) is neither uniform nor normal. In Figure 3-11, the moving average of the input track modulus is compared with the estimated track modulus average, which was calculated using Equation 3-3 and the Y_{rel} average data for window lengths of 8 m, 20 m, and 80 m. The coefficient of correlation between the inputted and estimated track modulus average calculated for the three window lengths of 8 m, 20 m, and 80 m is 0.995, 0.999, and 1.000, respectively. Considering that values close to 1 imply the accuracy of the estimation, it is deemed that the track modulus average can be accurately estimated for window lengths of 8 m and longer using Equation 3-3.

According to Figure 3-11, the local track modulus fluctuations can be observed more accurately when shorter window lengths are considered. Therefore, the appropriate window length for calculating Y_{rel} average values should be determined based on the required level of precision in estimating the local track modulus variations. Moreover, Equation 3-3 can be used for different

windows lengths with the same data to obtain information about the track modulus at different scales.

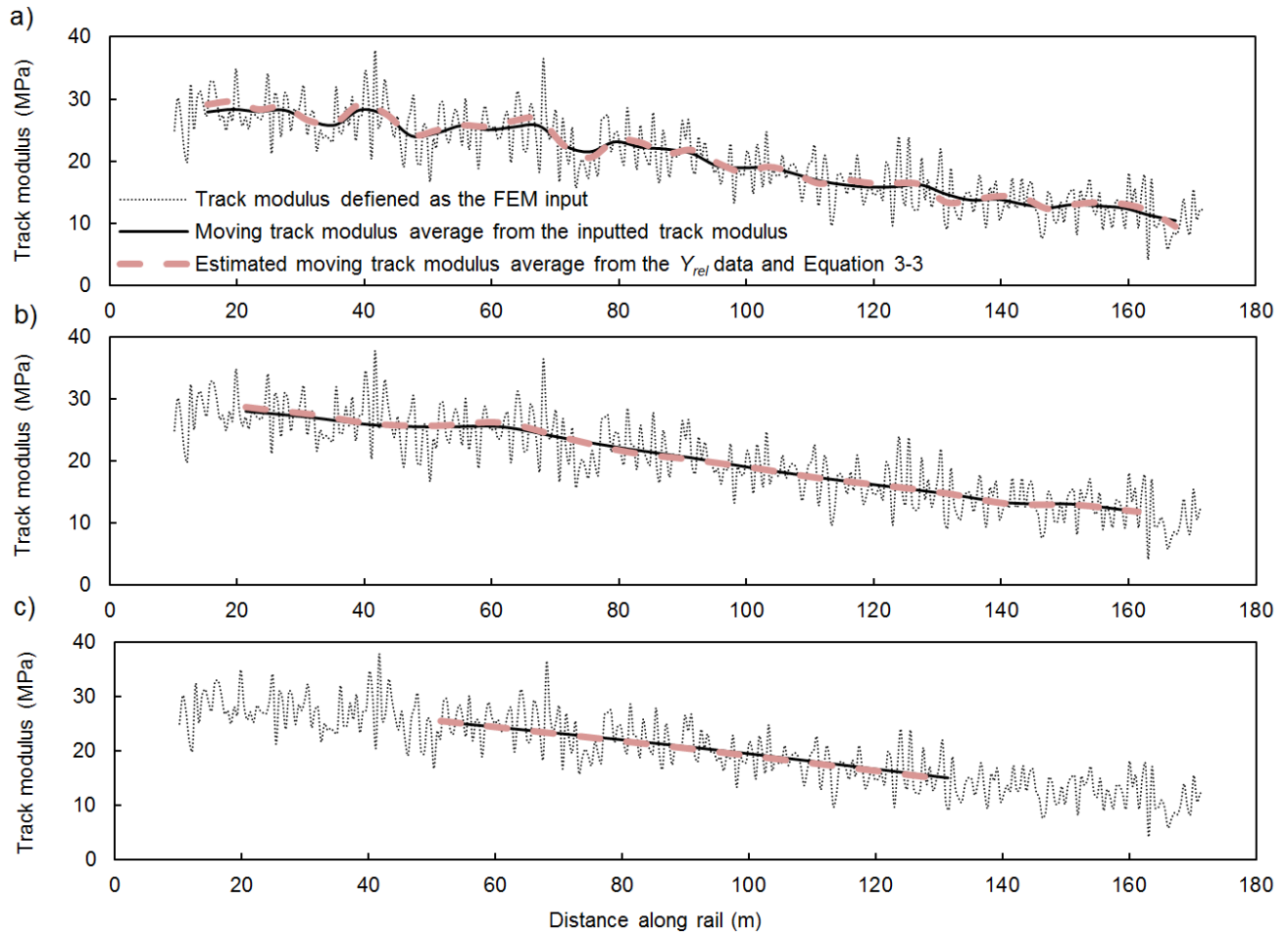


Figure 3-11 Comparison between the moving averages of inputted and estimated track modulus for: a) window length of 8 m, b) window length of 20 m, c) window length of 80 m.

3.7 Correlation between track modulus COV and Y_{rel} COV

In this section, the possibility of estimating the track modulus COV using Y_{rel} COV is investigated. The same procedure presented in the previous section was followed to examine the relationship between the track modulus COV and Y_{rel} COV. The track modulus COV is calculated and plotted against the Y_{rel} COV for different window lengths. For each window length, a nonlinear curve is fitted to the data point and the corresponding equation is reported in Table 3-3. The goodness of fit of the nonlinear regression is also evaluated using the R^2 and RMSE as before. Results for window lengths of 160 m and 4 m are shown in Figure 3-12 as

examples. In Figure 3-12, the discrepancy of the data points is higher when the Y_{rel} is highly variable. The correlation between the track modulus COV and Y_{rel} COV with respect to window size are summarized in Table 3-3.

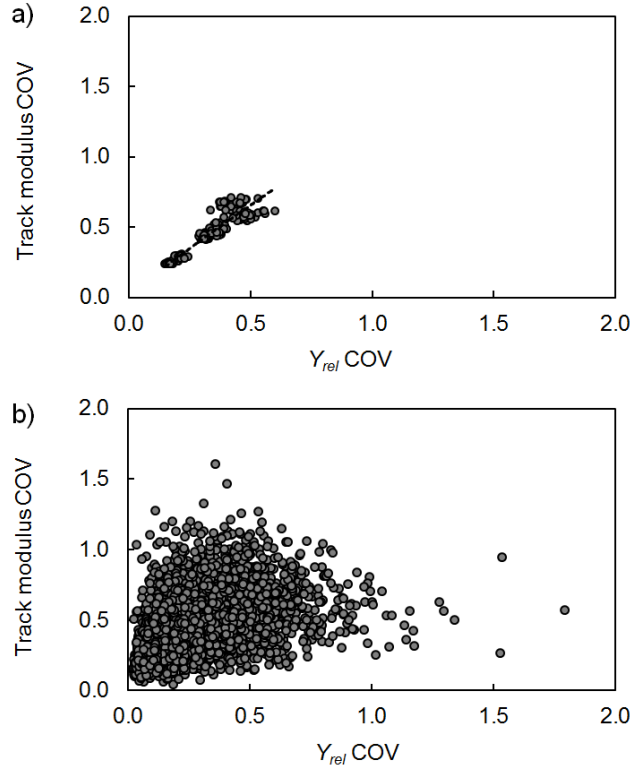


Figure 3-12 Track modulus COV vs. Y_{rel} COV for: a) 160-m window length and b) 4-m window length, (COV: coefficient of variation, Y_{rel} : relative vertical deflection).

According to the goodness of fit reported in Table 3-3, the correlation between the track modulus COV and Y_{rel} COV becomes significantly weaker with decreasing window length. Considering the value of R^2 , which is between 0.5 and 0.9 for window lengths from 8 m to 160 m, Y_{rel} COV is one of the parameters that can be used to estimate the track modulus COV to a certain extent. However, it is not precise enough to use Y_{rel} COV directly and individually to extract information about the track modulus COV when the window length is less than 80 m and the track modulus is highly variable.

Table 3-3 Correlation between track modulus COV and Y_{rel} COV with respect to window size, (COV: coefficient of variation, Y_{rel} : relative vertical deflection).

Window Length (m)	Fitted Curve	R ²	RMSE
160	$U_{COV} = 1.24 \times (Y_{rel})_{COV}^{0.91}$	0.857	0.056
80	$U_{COV} = 1.20 \times (Y_{rel})_{COV}^{0.88}$	0.821	0.063
40	$U_{COV} = 1.14 \times (Y_{rel})_{COV}^{0.83}$	0.748	0.076
20	$U_{COV} = 1.07 \times (Y_{rel})_{COV}^{0.77}$	0.658	0.092
10	$U_{COV} = 0.96 \times (Y_{rel})_{COV}^{0.66}$	0.528	0.114
8	$U_{COV} = 0.92 \times (Y_{rel})_{COV}^{0.62}$	0.468	0.125
5	$U_{COV} = 0.79 \times (Y_{rel})_{COV}^{0.50}$	0.310	0.152
4	$U_{COV} = 0.72 \times (Y_{rel})_{COV}^{0.43}$	0.217	0.171

3.8 Conclusions

In this chapter, the potential of the MRail system to quantify track modulus was studied using the numerical models. First, the accuracy of converting the MRail system's relative VTD measurement (Y_{rel}) to the stiffness of an individual rail support was examined. Second, the relationship between the statistical properties of the track modulus and Y_{rel} data was investigated for different window lengths. The study was conducted using a detailed FEM, in which the stochastic nature of the track modulus was addressed. Based on the numerical studies, three conclusions related to the measuring method under investigation and proposed approach can be made:

1. While the local stiffness issues are reflected in the Y_{rel} data, converting each Y_{rel} measurement to the exact stiffness value of an individual spring support is not accurate. This is due to the fact that Y_{rel} is strongly influenced by the cluster of vertical rail supports, which have different stiffness values beneath and around the truck wheels and beneath the sensor. For the same reason, it is not a precise approach to use numerical models assuming constant track modulus to interpret the Y_{rel} data.

2. An equation is proposed to estimate the track modulus average based on the Y_{rel} average. The purpose of this equation is to demonstrate the strong correlation between the track modulus average and Y_{rel} average. This correlation can be seen when the average values are calculated over track lengths of 8 m and longer. As a result, the Y_{rel} average, over track lengths of 8 m or longer, can be considered as an index of the track stiffness average. The longer the window length, the more accurate the track modulus estimate is. However, the ability to detect local track modulus variations decreases with increasing window length. The proposed equation is derived for a specific rail size and loading condition and, thus, it needs to be modified for other structural and operational conditions.

3. Y_{rel} COV and track modulus COV do not have a strong relationship, particularly when the window length is shorter than 80 m and Y_{rel} is highly variable; however, the relationship still provides useful information and shows the effect of track modulus COV on Y_{rel} COV over different window lengths. In other words, Y_{rel} COV is one of the parameters that can be considered for estimating the track modulus COV.

CHAPTER 4: Estimation of Rail Vertical Bending Stress using Train-Mounted Vertical Track Deflection Measurement Systems²

4.1 Overview

In Chapter 3, a new methodology was developed to investigate correlations between rail deflections and track modulus using finite element modelling. The stochastic nature of the track modulus, as one of the dominant factors influencing rail deflections and bending stresses, was simulated. The modelled data were analysed using statistical approaches and equations were proposed for estimating track modulus from VTD measurements. This chapter builds on that to develop a new methodology for estimating bending stresses over long sections of rail from VTD measurements (according to “*Objective 2*” presented in Chapter 1). The generated data from the models were used to investigate the correlations between track modulus, rail deflection, and rail bending stresses. The rail responses to applied loads were calculated and compared for scenarios of constant and variable track modulus values. The study resulted in a detailed framework that can be employed to estimate rail bending stresses from train-mounted VTD measurements. The framework allows estimation of the probability distributions of maximum tensile and compressive bending stresses in the rail head and base, which are necessary for calculating the rail reliability under applied loading.

4.2 Introduction

Rail breaks resulting from fatigue or overstressing are the leading cause of derailments on main tracks (defined as tracks of subdivisions extending through and between stations [5]) in North America [101-103]. The types of stresses identified to lead to rail breaks are residual, thermal, and live load stresses that result from the passing wheel loads [6, 9, 40, 60]. Estimating these stresses is often challenging due to the many uncontrollable environmental, operational, and

² A version of this chapter has been submitted to the Proceedings of the Institution of Mechanical Engineers, Part F: Journal of Rail and Rapid Transit for publication, Authors: Fallah Nafari S, Gül M, Hendry M.T, and Cheng J.J.R.

structural factors that affect the magnitude of these stresses along the thousands of miles of track [9, 10, 104, 105]. This chapter presents a methodology developed to estimate rail bending moments and resulting stresses continuously along the track.

Live bending stresses are one of the major modes by which transverse fatigue defects are propagated and become a major cause of rail breaks [9, 40, 44, 60, 104]. These stresses in the rail during the passage of trains have been quantified from cyclic strains measured by strain gauges.[20, 106, 107] Strain gauges provide only discrete measurements representative of local conditions and are not a practical approach for the characterization of these bending stresses over the length of the railway network. Train-mounted instruments that measure the VTD under train loading have become available over the last decade [21, 22, 26, 75, 76]. These instruments present an opportunity to estimate rail bending stresses over long distances and, thus, characterize the spatial variation of bending stresses [20, 21]. However, the effect of track modulus and its variability on the mathematical correlation between rail deflection and bending stresses has not been thoroughly investigated and, as a result, the method used to estimate rail bending stresses from VTD measurements is overly simplistic.

This study developed a framework that allows for the estimation of maximum bending stresses within the rail from VTD data, while considering the effect of a stochastically varying track modulus. Mathematical models of track structures are used to calculate rail deformed shape and corresponding bending stresses under applied wheel loads for a range of track modulus values. A mathematical correlation is then developed between the modelled VTD and rail bending stresses to allow for interpretation of the measured deflection data from train-mounted instrumentations. This new methodology results in probability distributions of maximum bending stresses in the rail head and base, which are intended for calculation of rail reliability under applied loading.

4.3 Train-mounted VTD measurement systems

A number of train-mounted measurement systems have been developed for the estimation of track stiffness continuously along rails [21, 22, 26, 70, 75-80]. This includes the Track Loading Vehicle (TLV) and the MRail system; that measure the VTD from moving railcars under axle loads that are representative of fully loaded railcars [21, 26, 75, 76]. These train-mounted VTD measurement systems have potential use for the estimation of maximum bending moments and

stresses in the rail by applying the mathematical correlation between rail deflections and bending stresses [20, 21]. This study used measurements from a MRail system because it measures vertical rail deflection at full track speeds [23-25]. Although the same concept is applicable to deflection data measured by TLV, frameworks for interpreting MRail and TLV deflection data would be slightly different due to the fact that MRail measures relative VTD and TLV measures maximum VTD under wheel loads.

The MRail system consists of a laser and camera-based system mounted on the side frame of a railcar truck. Using this system, the relative VTD (Y_{rel}) between the rail surface and the rail and wheel contact line is measured beneath the sensor, 1.22 m from the nearest axle (Figure 4-1) [21, 23-25, 75]. Y_{rel} is a relative deflection dependent on the vertical deflection of the rail at three points (i.e., the locations of two wheels and the sensor system) [23-25].

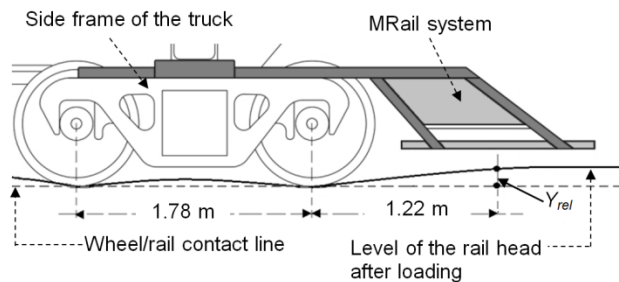


Figure 4-1 Illustration of the MRail system used to measure the relative vertical track deflection (Y_{rel}) (adapted from [77, 79]).

4.4 Estimating rail bending moment and stress from Y_{rel} measurements

The rail steel is cycled between maximum positive bending moments (M_{max}^+) and maximum negative bending moments (or maximum reverse bending moment, M_{max}^-) under moving wheel loads (Figure 4-2). This cycling results in an oscillation between tensile and compressive bending stresses in the rail head and base as the wheels pass over. Maximum tensile and compressive bending stresses and their respective magnitudes during each load cycle influence fatigue life of transverse defects [9, 40]. The fatigue life decreases due to tensile mean stresses and increases in the presence of compressive mean stress [44].

For a given rail type and axle load, the magnitude of the moments and stresses result from the magnitude of the rail displacement and, thus, the stiffness of the foundation of the track (track

modulus). Here, rail deflections and moments were calculated using both the Winkler model (proposed in 1867)[7, 10] and a finite element model (FEM).

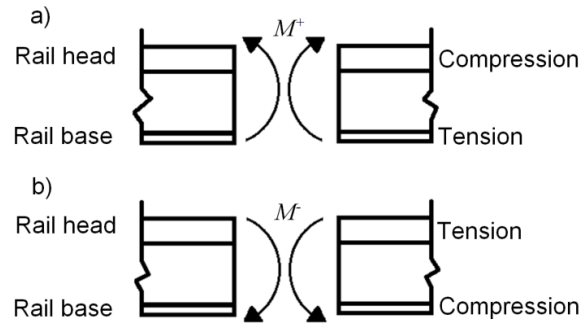


Figure 4-2 Tensile and compressive stresses in the rail head and base due to the positive and negative bending moments: a) positive bending moment (M^+), and b) negative or reverse bending moment (M^-).

The Winkler model has been used in the majority of studies on fatigue life and is recommended for estimating rail maximum bending moments based on Y_{rel} [9, 10, 23-25, 40, 60]. However, the Winkler model is limited as it can only model a constant track modulus along the length of track. FEMs are more versatile, and are used herein to simulate the rail deflection and moment for a track modulus that varies stochastically along the length of the track, thus resulting in stochastic M_{max}^+ and M_{max}^- values. The FEM results were examined for correlations between Y_{rel} and the modelled M_{max}^+ and M_{max}^- at each point along the track as well as between the probability distributions of Y_{rel} and those of M_{max}^+ and M_{max}^- . The FEM results were then compared with the Winkler model results to show the effect of stochastically varying track modulus on the correlation between rail deflections and stresses, and the importance of considering the track modulus variation in the estimation of bending moments and stresses from VTD measurements.

4.5 Correlation between Y_{rel} and rail bending moments based on Winkler modelling

The Winkler model considers the rail to be an infinite beam on a continuous elastic foundation [7, 10]. This model calculates the vertical rail deflection, $Y(x)$, and the bending moment, $M(x)$, at distance x from a single point load (P) using Equations 4-1 and 4-2.

$$Y(x) = \frac{P\beta e^{-\beta x}}{2U} (\cos\beta x + \sin\beta x) \quad (4-1)$$

$$M(x) = \frac{Pe^{-\beta x}}{4\beta} (\cos\beta x - \sin\beta x) \quad (4-2)$$

where U is the track modulus and β is the stiffness ratio equal to $(U/4EI)^{0.25}$, with EI being the rail bending stiffness. The linear elastic model allows for superposition to be used to calculate the response of the track beneath multiple wheel loads.

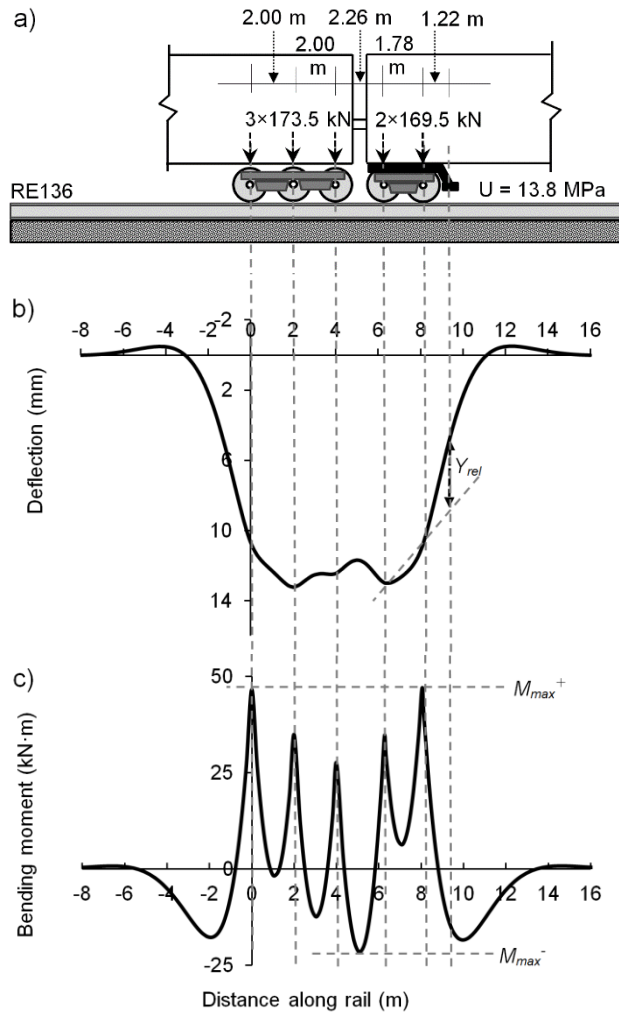


Figure 4-3 Relationship between the relative vertical track deflection (Y_{rel}) and bending moment calculated using the Winkler model: a) the train and axle loads on a track structure with an RE136 rail size and a constant track modulus of 13.8 MPa, b) resulting vertical track deflection profile and measured Y_{rel} , and c) resulting bending moment profile showing the maximum positive and negative bending moments (M_{max}^+ and M_{max}^-).

Figure 4-3 presents an example of the resulting deflection (Figure 4-3b) and the corresponding Y_{rel} (Figure 4-3b) and moment (Figure 4-3c) profiles derived from the use of the Winkler model

for a common freight railway loading condition in North America (Figure 4-3a). Figure 4-3c shows that M_{max}^+ occurs beneath the wheel loads while M_{max}^- occurs between the two trucks. M_{max}^+ always occurs beneath the wheels, whereas M_{max}^- shifts away from the trucks with decreasing track modulus. Table 4-1 and Figures 4-4 and 4-5 present Y_{rel} , M_{max}^+ , M_{max}^- , and maximum tensile and compressive stresses in the rail head and rail base calculated using the Winkler model for different track modulus values. Figure 4-4 shows the strong correlation between Y_{rel} , M_{max}^+ , and M_{max}^- from which relationships can be derived. Mathematical equations can be derived from a regression analysis of the data in Table 4-1 to quantify the Y_{rel} - M_{max}^+ and Y_{rel} - M_{max}^- relationships. These relationships could be also derived using the closed form solution; however, due to the lengthy derivation process involved, the data generated from the Winkler model were instead used in a regression analysis to calculate the relationships.

Table 4-1 Relative vertical track deflection (Y_{rel}), maximum positive and negative bending moments (M_{max}^+ and M_{max}^-), and maximum tensile and compressive stresses in the rail head ($\sigma_{max,h}^T$ and $\sigma_{max,h}^C$) and rail base ($\sigma_{max,b}^T$ and $\sigma_{max,b}^C$), respectively, calculated for different values of track modulus using the Winkler model ($\sigma_{max,h}^T = M_{max}^-/S_h$, $\sigma_{max,h}^C = M_{max}^+/S_h$, $\sigma_{max,b}^T = M_{max}^+/S_b$, and $\sigma_{max,b}^C = M_{max}^-/S_b$, where S_h and S_b are the rail head and base section modulus, respectively).

Track Modulus (MPa)	Y_{rel} (mm)	M_{max}^+ (kN·m)	M_{max}^- (kN·m)	$\sigma_{max,h}^T$ (MPa)	$\sigma_{max,h}^C$ (MPa)	$\sigma_{max,b}^T$ (MPa)	$\sigma_{max,b}^C$ (MPa)
6.90 (1000 psi)	5.95	54.1	-24.6	-63	139	-117	53
13.79 (2000 psi)	4.45	47.0	-21.6	-56	121	-102	47
20.69 (3000 psi)	3.67	43.4	-21.1	-54	112	-94	46
27.58 (4000 psi)	3.17	41.3	-20.4	-53	106	-89	44
34.47 (5000 psi)	2.82	39.7	-19.7	-51	102	-86	43
41.37 (6000 psi)	2.55	38.5	-19.1	-49	99	-83	41
48.26 (7000 psi)	2.33	37.6	-18.6	-48	97	-81	40
55.16 (8000 psi)	2.16	36.8	-18.1	-47	95	-80	39

From the results presented in Table 4-1, the value of M_{max}^- is approximately half that of M_{max}^+ for all values of track modulus, and the rail base is subjected to higher tensile stresses than the head. From Figure 4-5, the maximum tensile stress developed in the rail base in each load cycle

is much higher than the compressive stress and, as a result, the mean stress is tensile. Contrary to the stresses in the rail base, the tensile bending stresses in the rail head are not as large as compressive stresses and the mean stress is compressive.

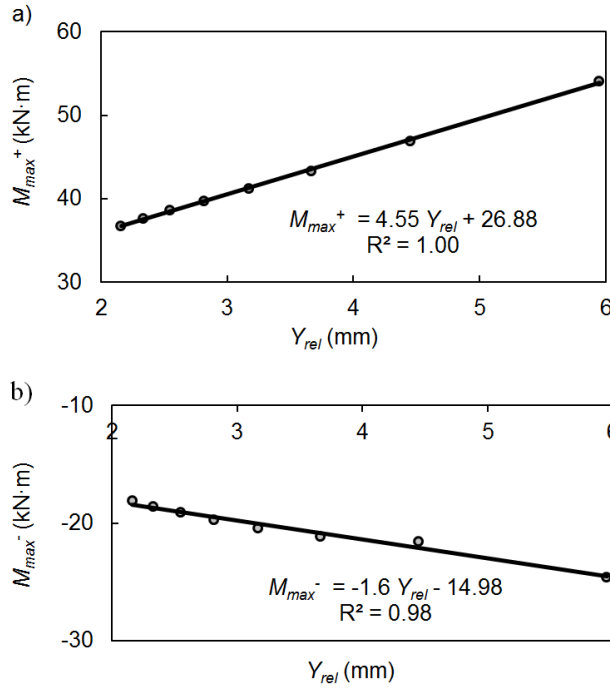


Figure 4-4 Relative vertical track deflection (Y_{rel}) and maximum positive and negative bending moments (M_{max}^+ and M_{max}^-) calculated for different values of track modulus using the Winkler model: a) correlation of Y_{rel} and M_{max}^+ , and b) correlation of Y_{rel} and M_{max}^- .

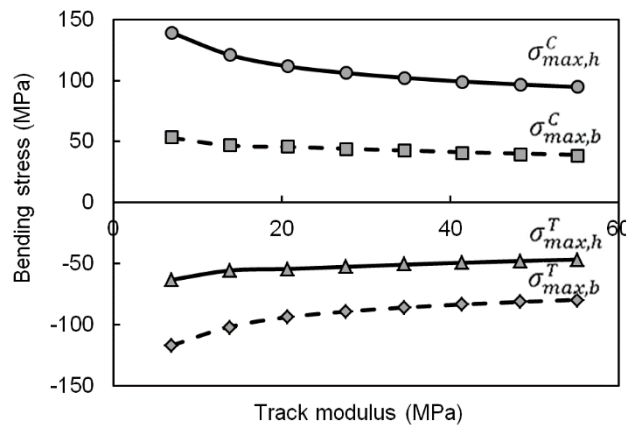


Figure 4-5 Maximum tensile and compressive bending stresses in the rail head ($\sigma_{max,h}^T$ and $\sigma_{max,h}^C$, respectively) together with the maximum tensile and compressive bending stresses in the rail base ($\sigma_{max,b}^T$ and $\sigma_{max,b}^C$, respectively), calculated for different values of track modulus using the Winkler model.

4.6 Finite element modelling

The FEM simulated the track structure including the two rails and cross ties. The support beneath the track structure was modelled as a spring applied to the base of the ties. This simulation was developed with CSiBridge software [96], which was used to calculate vertical deflections and bending moments in the rail. A complementary code was developed in EXCEL Visual Basic for Application (VBA) to calculate Y_{rel} at 0.3 (≈ 1 foot) intervals along the track from the modelled VTD profile at predefined time steps. The simulated track structure was 180.8 m in length and included 357 discrete crossties. Tie spacing was defined as 0.508 m while the rail size and loading conditions were the same as shown in Figure 4-3. Two approximately 10 m section lengths at both ends were assigned a constant track modulus and used to minimize the effects of end boundary conditions on the middle portion of the model; these ends were not included in the subsequent analysis.

A variable track modulus was assigned to the middle portion of the model which was 160.5 m long and consisted of 317 crossties. This assignment was done by defining different stiffness values for discrete spring supports. Track-train dynamic interaction was not considered in the models, and the response of the track to the moving wheel load was calculated using a direct integration time history analysis. More details about the modelling procedure are presented in Chapter 3 and Reference [108].

Local and global track modulus variations affect the magnitude of rail deflections and stresses [29, 69, 99]. Hence, ninety models with different track modulus distributions were considered (Table 4-2). For each simulation, a normal track modulus distribution from Table 4-2 was selected, and randomly generated numbers from this distribution were assigned as the coefficient values to the support springs. The procedure is graphically shown in Figure 4-6. This modelling method allows simulation of abrupt changes in track modulus as well as global track modulus variation, as the randomly generated track modulus values can result in locations with a very low modulus even when the average modulus is relatively high. These locally low track modulus values can be representative of abrupt changes in rail foundation stiffness (e.g., broken ties, hanging ties).

Table 4-2 Normal track modulus distributions considered in the numerical models.

Average (MPa)	COV	No. of Simulations
41.4	0.25	10
	0.5	10
	0.75	10
27.6	0.25	10
	0.5	10
	0.75	10
13.8	0.25	10
	0.5	10
	0.75	10

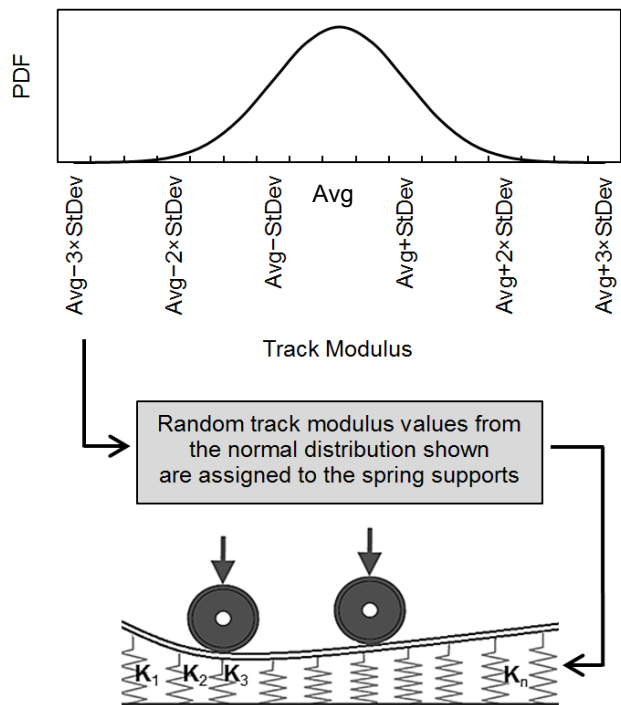


Figure 4-6 Assignment of randomly selected stiffness values to the support springs along the track (adapted from [108]), (Avg: Average, StDev: standard deviation, and K : stiffness of the spring support).

4.7 Validating the developed FEM

The results of the FEM with a constant track modulus were compared to those generated from the Winkler model to confirm that the method produced results consistent with what has been historically used for track design [7, 10]. As an example, a constant track modulus of 41.4 MPa was considered along the track in the FEM, and the resultant Y_{rel} , M_{max}^+ , and M_{max}^- values were compared with the Winkler model results. Figure 4-7 demonstrates the track response calculated using the FEM for a limited window of the track. Because the track modulus is constant, the pattern is repeated over the full length of the track. Y_{rel} data derived from the FEM vary between 2.63 and 2.69 mm, which is very close to the Y_{rel} value of 2.55 mm from the Winkler model (less than 5% difference) for the corresponding rail size and loading conditions. Similarly, the values of M_{max}^+ (varies between 36.6 and 39.5 kN·m) and M_{max}^- (varies between -18.3 and -20.6 kN·m) from the FEM are very close to values of 38.5 and -19.1 kN·m for M_{max}^+ and M_{max}^- , respectively, from the Winkler model (less than 8% difference). The reason for the slight fluctuation in the bending response is the discrete spring supports defined in the FEMs.

4.8 FEM results with a stochastically varying track modulus

Figure 4-8 shows an example of the track modulus applied to a model and the resulting Y_{rel} distribution along the track. The average track modulus and coefficient of variation (COV) from this example are 41.4 MPa and 0.5, respectively. Figure 4-8 shows the randomly generated track modulus value resulted in locations with a very low modulus, even though the average modulus was relatively high. In this example, the distribution of the resulting Y_{rel} is not normal, as evaluated with the “Lilliefors”, “Kolmogorov-Smirnov”, and “Anderson-Darling” tests, even though the distribution of the track modulus was generated to be normal. The reason is that arrangements of spring supports with different stiffness values affect the Y_{rel} data. Hence, Y_{rel} data may have any distribution type even though stiffness of the spring supports comes from a normal distribution. This example clearly shows that selecting random stiffness values from normal track modulus distributions does not impose limitations on the simulations.

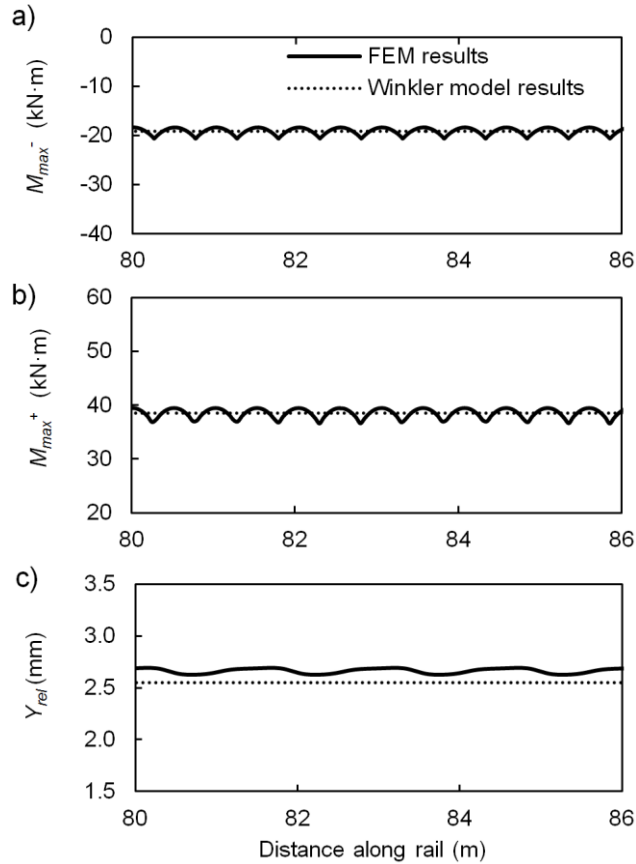


Figure 4-7 Response of a track structure with an RE136 rail size and constant track modulus of 41.4 MPa calculated using FEM and VBA code: a) envelope profile of maximum negative bending moment (M_{max}^-), b) envelope profile of maximum positive bending moment (M_{max}^+), and c) distribution of the relative vertical track deflection (Y_{rel}).

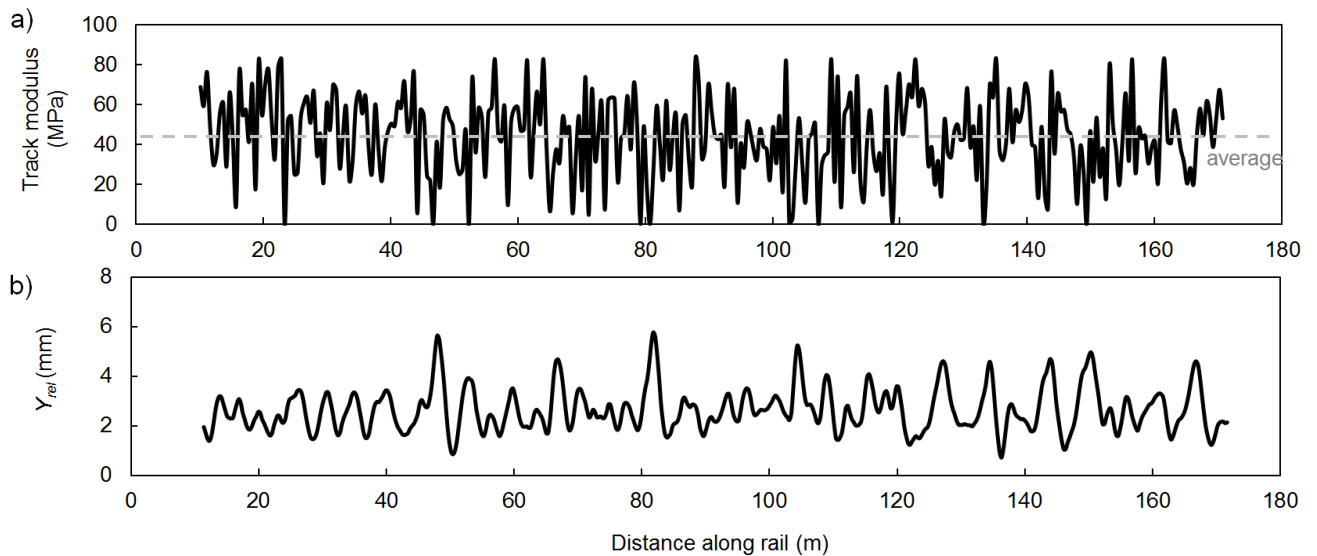


Figure 4-8 An example of numerical models: a) track modulus distribution defined as the model input, and b) distribution of the relative vertical track deflection (Y_{rel}) calculated using FEM and VBA code.

4.9 FEM with varying track modulus versus Winkler model results

Figure 4-9 depicts the envelope profile of M_{max}^+ and M_{max}^- as well as the maximum bending stresses in the rail head and base for the model with the track modulus distribution shown in Figure 4-8. These graphs show the high M_{max}^+ and M_{max}^- at locations with abrupt changes in the track modulus. Moreover, the locations with high maximum positive bending moments do not necessarily match the locations of high maximum negative bending moments. For instance, in Figure 4-9 the M_{max}^+ at section A_A is lower than the M_{max}^+ at section B_B, yet the rail underwent a higher M_{max}^- at section A_A compared to section B-B. Furthermore, in this simulation with an average track modulus of 41.4 MPa (6000 psi) and a COV of 0.5, the ratio of the M_{max}^- to M_{max}^+ magnitudes varies between 0.1 and 1.4 at different locations along the track. This indicates the rail is subjected to higher negative vs. positive bending moments at some locations (e.g., section A-A with M_{max}^+ of 26 kN·m and M_{max}^- of -36 kN·m). As illustrated in Figure 4-9c, the maximum tensile stress in the rail head at section A-A is higher than the maximum compressive stress, which causes tensile mean stress in the rail head during load cycles. These findings contradict the Winkler model results shown in Figure 4-5. With the assumption of constant track modulus in the Winkler model, the rail (under the loading condition shown in Figure 4-3a) sustains a higher maximum positive bending moment and also a higher maximum negative bending moment when the rail foundation becomes softer and the ratio of the maximum negative vs. positive bending moment is around 0.5, regardless of the rail support stiffness. Based on the Winkler model results, the rail is inferred to always be subjected to the tensile mean stress in the base and the compressive mean stress in the head during each load cycle. Differences between the results of the FEM with varying track modulus and the Winkler model show that the use of the Winkler model may result in inaccurate values of the maximum positive and negative bending stresses and their respective magnitudes when the track modulus varies along the track.

The correlation of Y_{rel} with M_{max}^+ and M_{max}^- in a track structure with variable foundation stiffness is more complex than for a constant track modulus (Figures 4-8 and 4-9). A comparison of the Y_{rel} versus M_{max}^+ and M_{max}^- at individual points along the track did not show a strong relationship, as was found using the Winkler model (Figure 4-4). However, Figures 4-8 and 4-9

show the trend of fluctuations in Y_{rel} data is very similar to the changes in the envelope profile of M_{max}^+ and M_{max}^- along the track.

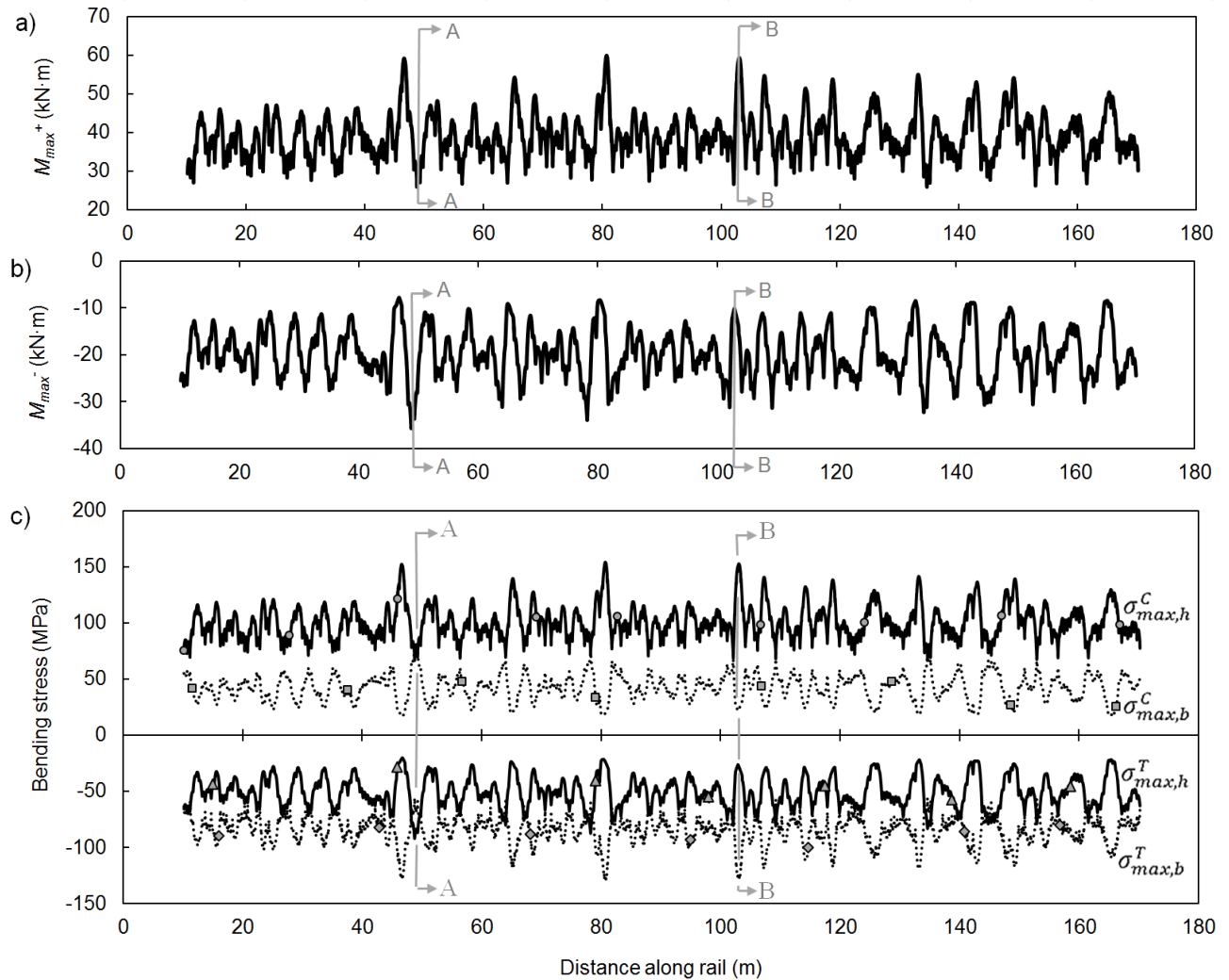


Figure 4-9 Bending response for one of the simulations, envelope profile of: a) rail maximum positive bending moment (M_{max}^+), b) rail maximum negative bending moment (M_{max}^-), and c) maximum bending stress in the rail head and base, ($\sigma_{max,h}^T$ and $\sigma_{max,h}^C$: maximum tensile and compressive stresses in the rail head, $\sigma_{max,b}^T$ and $\sigma_{max,b}^C$: maximum tensile and compressive stresses in the rail base).

4.10 Correlation between Y_{rel} and bending moments based on finite element modelling

For all ninety FEMs, the similarities between Y_{rel} fluctuations and M_{max}^+ and M_{max}^- fluctuations were quantitatively investigated by calculating cross-correlation (also known as sliding dot product) between the distributions of these parameters. Results suggest an approximate 1.22 m

lag of M_{max}^+ distribution relative to Y_{rel} readings in all ninety simulations. The physical interpretation of this finding is that any individual Y_{rel} measurement can be correlated to the maximum positive bending moment that the rail experiences at a distance 1.22 m from the sensor system (the location of the nearest wheel to the sensor system). This lies within the expectations that the rail undergoes the maximum positive bending moment under the farthest wheels, when a combination of wheels from the two adjacent trucks passes over the track (see Figure 4-3). Therefore, to examine the correlation between Y_{rel} and M_{max}^+ , the Y_{rel} data were calculated at 0.3 m intervals (527 discrete locations) along the 160-m track section. Then, each Y_{rel} was compared with the corresponding M_{max}^+ calculated at a distance 1.22 m from the location of the Y_{rel} reading. Figure 4-10 illustrates the results corresponding to the ninety simulations with various track modulus distributions. The equation of the best fit to the data points presented in Figure 4-10 is very close to the Winkler model result presented in Figure 4-4a. This indicates that a linear equation can be used to estimate maximum positive bending moment in rail using Y_{rel} data, regardless of variations in the rail foundation stiffness. However, considering the coefficient of determination (R^2) of 0.76 for the equation of the best fit line in Figure 4-10, estimations of M_{max}^+ using the Y_{rel} data at discrete locations along track are considered approximate.

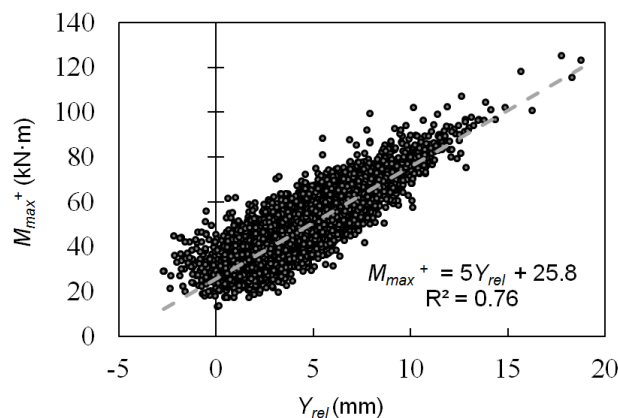


Figure 4-10 Rail maximum positive bending moment (M_{max}^+) vs. relative vertical deflection (Y_{rel}).

While the cross-correlation analysis of Y_{rel} and M_{max}^+ distributions over the 160-m track length had almost the same results for all ninety simulations, the lag between Y_{rel} and M_{max}^- distribution varied from one model to another. The outcome of the cross-correlation analysis of Y_{rel} and M_{max}^- distribution was not the same even for models with the same track modulus average and COV over the 160-m track length. Consequently, an individual Y_{rel} value cannot be correlated to

the maximum negative bending moment at a specific location along the track unless information about the stiffness of all individual rail supports at the loaded zone is available. Because gathering such detailed information is impractical for large railway networks, Y_{rel} measurements are not suitable for estimating M_{max}^- point-by-point along the track at the large scale.

4.11 Correlation between probability distributions of Y_{rel} and rail bending moments

The relationships between the cumulative distribution functions (CDFs) of Y_{rel} , M_{max}^+ , and M_{max}^- were investigated for 160-m track windows. While the probability distributions of the responses were calculated over the 160-m sections, the resolution of the Y_{rel} readings remained unaltered at 0.3 m. Therefore, the smaller scale variations in the track response are reflected in the CDFs. The 160-m window length was arbitrarily chosen; depending on the assessment or maintenance requirements, different window sizes may be selected. The window length can affect the correlation between the CDFs of Y_{rel} , M_{max}^+ , and M_{max}^- .

The CDFs of Y_{rel} , M_{max}^+ , and M_{max}^- were calculated separately for all ninety models to investigate the relationship between the probability distributions of these variables. Figure 4-11 depicts the CDFs of Y_{rel} , M_{max}^+ , and M_{max}^- calculated for the model with the track modulus distribution shown in Figure 4-8. Once the CDFs of Y_{rel} , M_{max}^+ , and M_{max}^- were computed for a model, the values of Y_{rel} , M_{max}^+ , and M_{max}^- at CDF levels of 0, 0.2, 0.4, 0.6, 0.8, and 1 were determined. The relationships between the CDFs of Y_{rel} , M_{max}^+ , and M_{max}^- were then separately investigated for each of these CDF levels to develop a mathematical tool for estimating the M_{max}^+ and M_{max}^- CDFs from the Y_{rel} CDF.

In Figure 4-12, the M_{max}^+ values calculated at CDF values of 0, 0.2, 0.4, 0.6, 0.8, and 1 were plotted against the Y_{rel} values at the same CDF levels. Each graph in Figure 4-12 contains data points from each of the ninety models. Figure 4-12 shows the strong correlation between the CDFs of Y_{rel} and M_{max}^+ that can be explained using numerical equations. The equations of best fit to the data points and corresponding R^2 values were calculated and reported separately for each graph. The closeness of R^2 to 1 for these equations evidently shows how well the mathematical equations describe the relationship between the CDFs of Y_{rel} and M_{max}^+ .

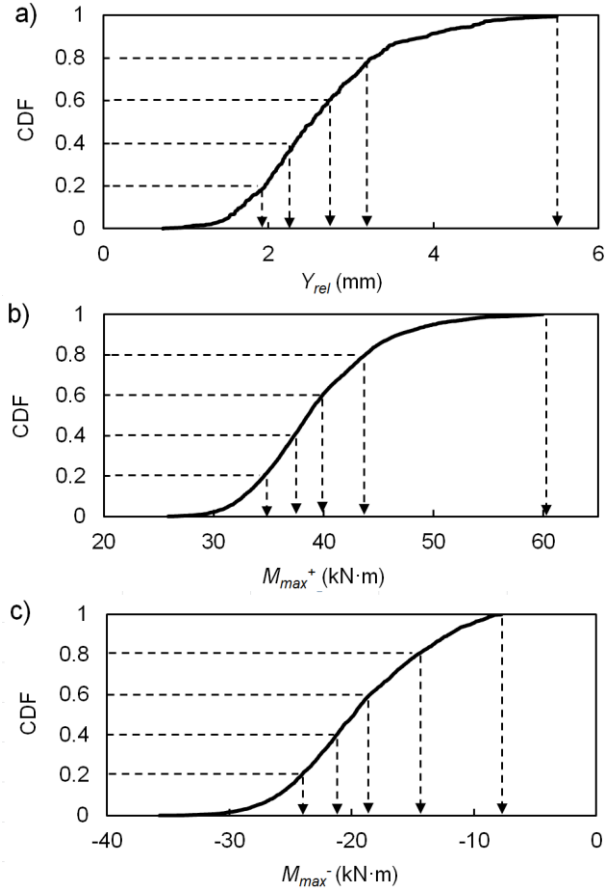


Figure 4-11 CDF of the rail responses for one of the simulations: a) CDF of Y_{rel} data, b) CDF of M_{max}^+ , and c) CDF of M_{max}^- (Y_{rel} : relative vertical deflection, M_{max}^+ : maximum positive bending moment, M_{max}^- : maximum negative bending moment).

Similarly, the correlation between the CDFs of Y_{rel} and M_{max}^- can be investigated by calculating the CDFs of Y_{rel} and M_{max}^- from all ninety models, determining the M_{max}^- and Y_{rel} at CDFs of 0, 0.2, 0.4, 0.6, 0.8, and 1, and plotting the M_{max}^- values calculated at the predefined CDF levels against the corresponding Y_{rel} values (Figure 4-13). Considering the poor correlation between the data points in Figure 4-13, other parameters evidently affect the relationship between the CDFs of Y_{rel} and M_{max}^- . A regression analysis was used to determine all predictor variables required for estimating the M_{max}^- CDF. The results of this multi-regression analysis revealed that the average and COV of Y_{rel} data impacted the M_{max}^- CDFs. Using the equations presented in Table 4-3, the CDF of M_{max}^- for a 160-m track length can be estimated from the Y_{rel} average, Y_{rel} COV, and Y_{rel} CDF over the same track window. The average and COV of Y_{rel} data over the 160-m track window are indicators of track modulus average and COV [108]. Hence, it is inferred that the

correlation between the CDFs of Y_{rel} and M_{max}^- is affected by the statistical properties of the track modulus.

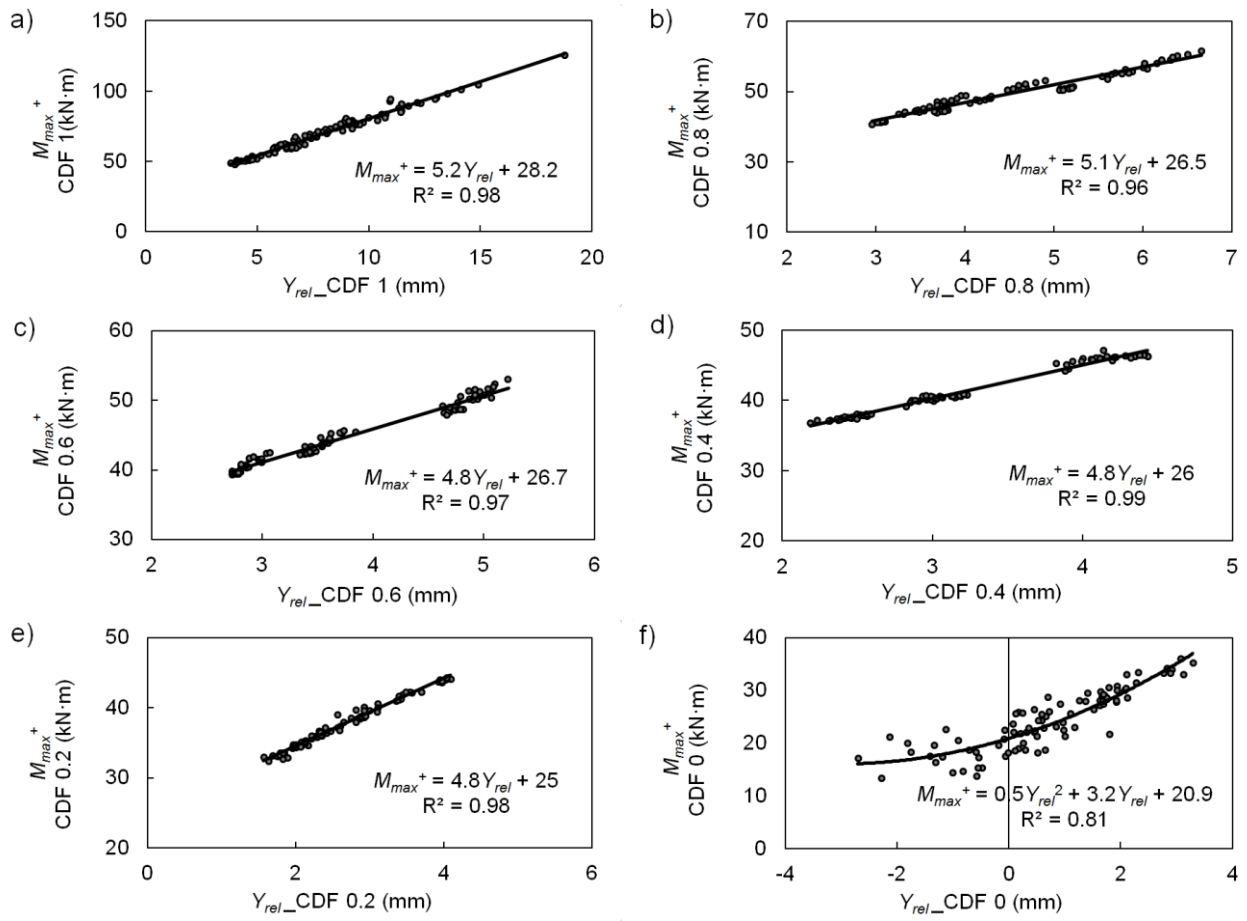
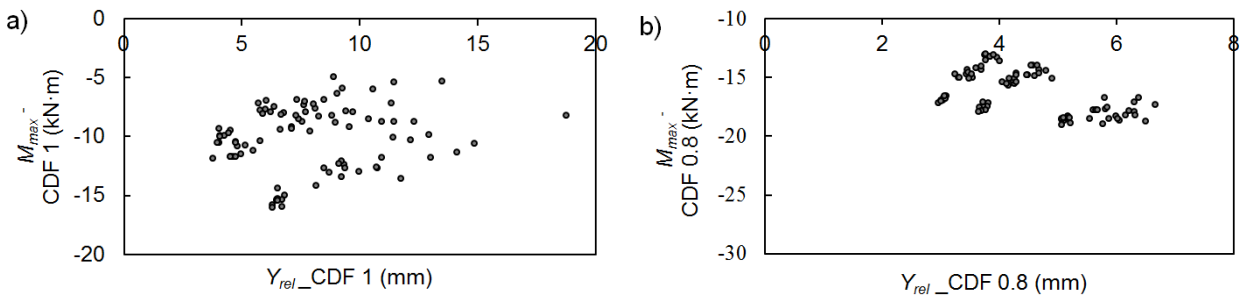


Figure 4-12 Correlation between the CDFs of Y_{rel} and M_{max}^+ calculated for ninety models with different track modulus distributions. These comparisons were made separately at CDF levels of: a) 0, b) 0.2, c) 0.4, d) 0.6, e) 0.8, and f) 1 (Y_{rel} : relative vertical track deflection, M_{max}^+ : maximum positive bending moment).



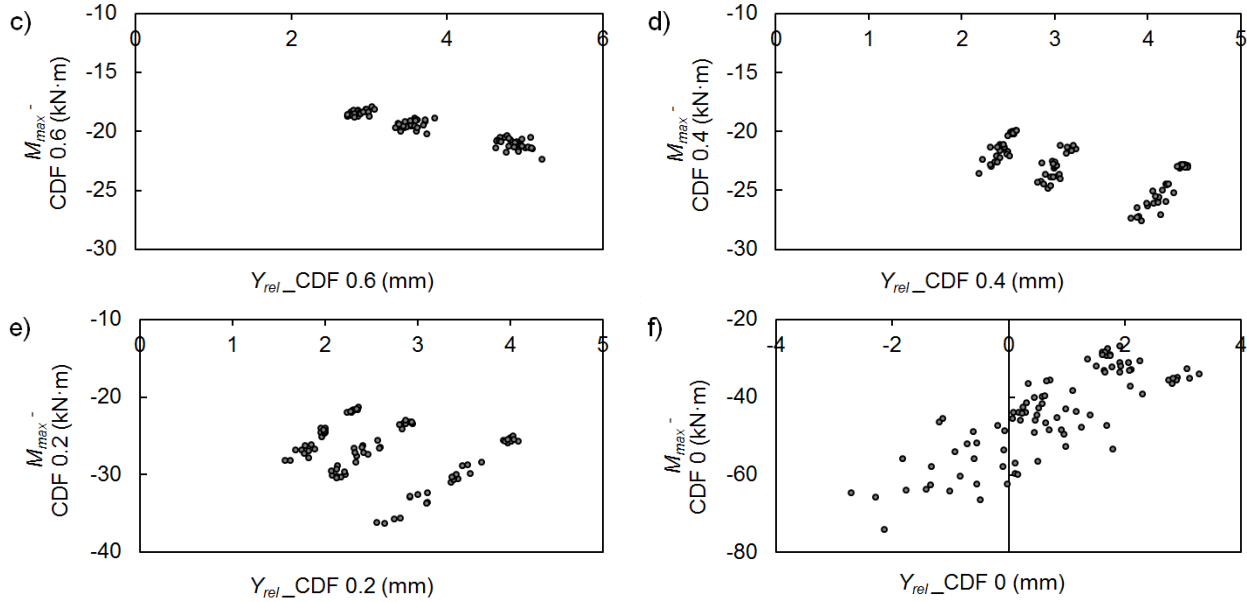


Figure 4-13 Correlation between the CDFs of Y_{rel} and M_{max}^- calculated for ninety models with different track modulus distributions. These comparisons were made separately at CDF levels of: a) 0, b) 0.2, c) 0.4, d) 0.6, e) 0.8, and f) 1 (Y_{rel} : relative vertical track deflection, M_{max}^- : maximum negative bending moment).

Table 4-3 Estimating the CDF of M_{max}^- using three predictor variables (Y_{rel} CDF, Y_{rel} average ($(Y_{rel})_{Avg}$), and Y_{rel} COV ($(Y_{rel})_{COV}$)) for a window length of 160 m (M_{max}^- : maximum negative bending moment, Y_{rel} : relative vertical track deflection, COV: coefficient of variation, CDF: cumulative distribution function).

M_{max}^- at different CDF levels	Equations based on three predictor parameters	R^2
M_{max}^- -CDF 0	$-12.33 - 6.89 (Y_{rel})_{Avg} - 32.52 (Y_{rel})_{COV} + 4.31 (Y_{rel} - CDF 0)$	0.94
M_{max}^- -CDF 0.2	$-15.76 - 7.90 (Y_{rel})_{Avg} - 1.21 (Y_{rel})_{COV} + 6.56 (Y_{rel} - CDF 0.2)$	0.99
M_{max}^- -CDF 0.4	$-15.1 - 6.56 (Y_{rel})_{Avg} - 1.86 (Y_{rel})_{COV} + 5.04 (Y_{rel} - CDF 0.4)$	0.97
M_{max}^- -CDF 0.6	$-14.68 - 1.77 (Y_{rel})_{Avg} + 0.25 (Y_{rel})_{COV} + 0.35 (Y_{rel} - CDF 0.6)$	0.91
M_{max}^- -CDF 0.8	$-14.76 + 0.88 (Y_{rel})_{Avg} + 12.67 (Y_{rel})_{COV} - 1.97 (Y_{rel} - CDF 0.8)$	0.9
M_{max}^- -CDF 1	$-4.60 - 2.77 (Y_{rel})_{Avg} + 10.97 (Y_{rel})_{COV} + 0.11 (Y_{rel} - CDF 1)$	0.94

4.12 Conclusions

This chapter presents a new methodology to estimate live vertical bending stresses in rail from train-mounted VTD measurements. The method allows for estimation of the maximum bending

stresses over long sections of rail. This was done by developing mathematical correlations between relative VTD (Y_{rel}), M_{max}^+ , and M_{max}^- values generated using finite element modelling. The resulting correlations show strong relationships between Y_{rel} , M_{max}^+ , and M_{max}^- when the track modulus is assumed to be constant along the track; these relationships are not applicable for interpreting Y_{rel} data when the track modulus is variable. Track models with a stochastically varying track modulus are more representative of real-world conditions. For a varying track modulus, the correlations do not provide strong estimates of M_{max}^+ and M_{max}^- at discrete locations along the track. The track modulus variation significantly affects M_{max}^+ , M_{max}^- , and their respective magnitudes. Hence, the assumption of a constant track modulus creates large inaccuracies in stress estimations. The results of the FEMs with a stochastically varying track modulus show that correlations between Y_{rel} , M_{max}^+ , and M_{max}^- must be quantified over track windows rather than at discrete locations along the track. From the results, the probability distributions of M_{max}^+ and M_{max}^- can be estimated from the probability distribution of Y_{rel} data. This indicates strong potential for estimating the probability distribution of maximum rail bending stresses using deflection data from train-mounted VTD measurement systems.

CHAPTER 5: An Investigation of the Correlation between Train-Mounted Vertical Track Deflection Measurements, Track Modulus, and Rail Bending Moments³

5.1 Overview

This chapter presents a complementary study to Chapter 4, in accordance with “*Objective 2*” presented in Chapter 1. The correlations between track modulus, train-mounted vertical track deflection (VTD) measurements, and vertical bending moments were investigated using the developed finite element model (FEM). Various track modulus distributions were simulated and the resulting VTD and rail bending moments under a moving wheel set were calculated. The mathematical correlation between the inputted track modulus, modelled VTD and rail bending moments were then quantified using statistical approaches. Based on the results, the track modulus average and standard deviation can be estimated over track windows using the VTD measurements. These estimations can then be used to quantify the average, standard deviation (StDev), and peak for the envelope profile of the maximum vertical bending moment in the rail over the same track windows. The accuracy of the method was verified using a numerical case study for which a random track modulus distribution was considered and artificial noise was added to the modelled VTD.

5.2 Introduction

Rail break has been among the main reasons for track-caused accidents and derailments in North America [101-103]. A major factor that leads to rail breaks is large bending stresses generated in the rail during the passage of wheels [6, 9, 60]. These stresses reduce the fatigue life of transverse defects in the rail by increasing the growth rate of cracks [9, 40, 60, 104]. Hence, estimating rail bending stresses is fundamental to assessing rail reliability and to minimising rail failures.

³ A part of this chapter was presented and published at the CSHM-6 workshop in Belfast in May 2015. The paper has been selected for publication in Structural and Geoinfrastructure Monitoring, a special issue of the Journal of Civil Structural Health Monitoring., Authors: Fallah Nafari S, Gül M, and Cheng J.J.R.

Quantifying rail bending stresses is often challenging for a large railway network. The magnitude of bending stresses in a rail significantly varies along the thousands of miles of track due to global and local changes in the track foundation stiffness (also referred to as track modulus) [29, 31, 69, 104]. A method that can be used to estimate the track modulus is to measure the deflection of the rail when subjected to a known applied known load [27]. Train-mounted VTD measurement systems that measure the rail deflection under fully loaded axles present an opportunity to estimate the track modulus along large railway networks [21, 22, 26, 76]. Once the track modulus is quantified, the range of bending moments and stresses developed in the rail under a known applied load can be estimated [7, 10]. In this method, the mathematical correlation between VTD, the track modulus, and the bending moment is needed to estimate the track modulus and rail bending moments from the deflection data measured using train-mounted instruments. The correlation between these parameters can be developed using mathematical models of the track structure and calculating the rail deformed shape and bending moments for different ranges of the track modulus.

The track structure can be modelled with different levels of complexity [95, 109]. If the track structure is modelled with the constant track modulus along the track [7, 10], the mathematical method for estimating the track modulus and bending moments from VTD measurements will be overly simplistic. The aim of this study is to address the effect of the stochastically varying track modulus on the mathematical correlation between the VTD, track modulus, and rail bending moments to develop a new detailed framework to estimate the maximum bending moments in the rail using VTD measurements. The objective was met by using a detailed FEM that allowed the simulation of the stochastically varying track modulus. Data generated using the FEM was used to investigate the mathematical correlation between the modelled VTD, track modulus, and rail bending moment for track structures with different track modulus distributions. The study focused on the use of the measurements from a real-time VTD measurement system that developed at the University of Nebraska-Lincoln under the sponsorship of Federal Railroad Administration [20, 23-25]. This laser and camera system, commercially known as MRail, is mounted on the side frame of a truck and measures the relative VTD (referred to as Y_{rel}) between the rail surface and the rail-wheel contact line under the sensor system, at a distance of 1.22 m from the nearest wheel [23-25]. The concept presented in this chapter is also applicable to other train-mounted VTD measurement systems. However, details of the process for interpreting the

VTD data would be slightly different for each system, depending on the type of deflection measurements.

5.3 FEM specifications

An FEM of the track structure developed with CSiBridge software was used [96, 108]. The rail size and tie spacing were defined as RE136 and 0.508 m, respectively. The stochastically varying track modulus was simulated by assigning different stiffness values to the spring supports along the track. Ninety models with different track modulus distributions were considered. For each simulation, a normal track modulus distribution was selected, and randomly generated numbers from this distribution were assigned as the spring coefficient to the spring supports. Table 5-1 shows the properties of normal track modulus distributions used for the study.

Table 5-1 Properties of the normal distributions considered for simulating the varying track modulus.

Average (MPa)	COV	No. of Simulations
41.4	0.25	10
	0.5	10
	0.75	10
27.6	0.25	10
	0.5	10
	0.75	10
13.8	0.25	10
	0.5	10
	0.75	10

The track's response to the moving wheel loads shown in Figure 5-1 was derived using direct integration time history analysis. The rail deflections and bending moments under the moving wheel loads were directly calculated using the software, while Y_{rel} at intervals of 0.3 m (≈ 1 foot) were calculated using a complementary code in EXCEL Visual Basic for Application (VBA). More details about the model specifications and validations are presented in Chapter 4 and Reference [108].

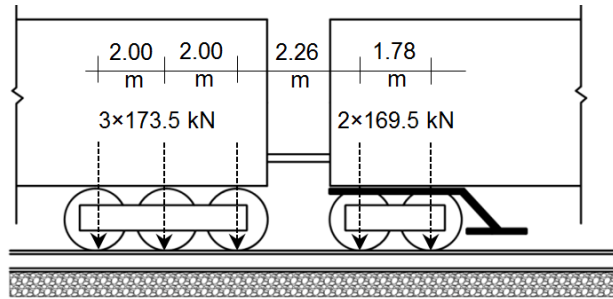


Figure 5-1 Wheel loads considered in the numerical models represent the two trucks in an adjacent railcar and locomotive.

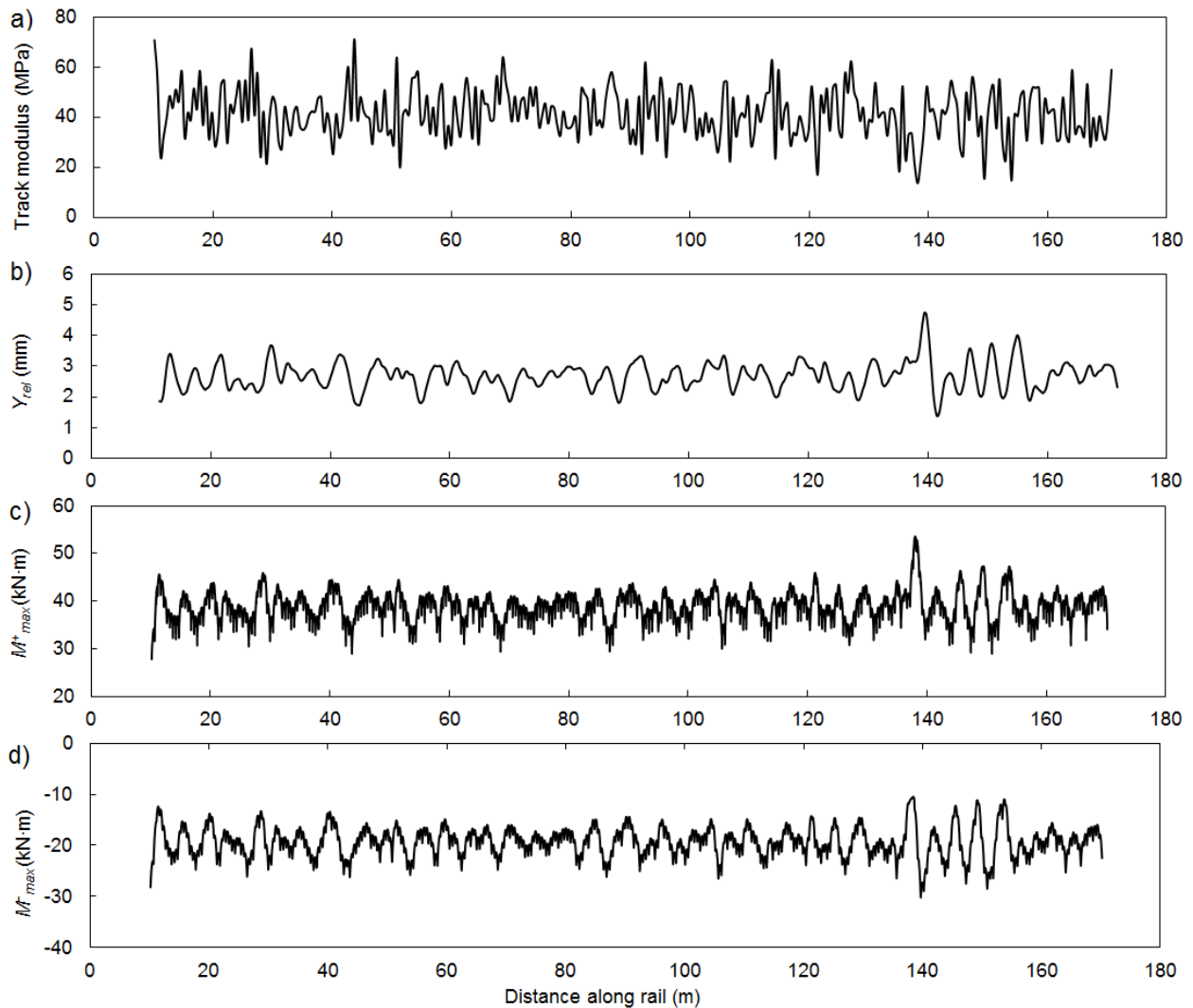


Figure 5-2 A typical example of a simulation: a) Inputted track modulus, b) resultant relative vertical track deflection (Y_{rel}), c) resultant envelope profile of maximum positive bending moment (M_{max}^+), and d) resultant envelope profile of maximum negative bending moment (M_{max}^-).

Figure 5-2 is a typical example of a simulation showing the inputted track modulus (Figure 5-2a), the resultant Y_{rel} (Figure 5-2b), and the envelope profile of the maximum positive and negative bending moments (M_{max}^+ , M_{max}^-) (Figure 5-2c and 5-2d). A positive bending moment results in longitudinal compressive and tensile stresses in the rail head and base, respectively, and a negative bending moment acts in the reverse direction. In Figure 5-2, the track modulus average and coefficient of variation (COV) were 41.4 MPa (6000 psi) and 0.25, respectively. The distributions of Y_{rel} and M_{max}^+ were similarly calculated for all models with different track modulus distributions to investigate the relationships between the Y_{rel} , track modulus and M_{max}^+ .

5.4 Correlation between statistical properties of track modulus and Y_{rel}

Comparing the inputted track modulus with the resultant Y_{rel} along the track in Figure 5-2 clearly demonstrates a complex relationship between these two parameters. In general, the value of Y_{rel} is dependent on the rail deflections at the locations of the two wheels and the sensor system and, thus, is affected by a cluster of track stiffness beneath and around the wheels and beneath the sensor. Therefore, the correlation between the track modulus and Y_{rel} needs to be studied over the track windows rather than at individual points along the track. The relationships of the Y_{rel} average-track modulus average and Y_{rel} coefficient of the variation (COV)-track modulus COV over different track window lengths were investigated in Chapter 4 and Reference [108]. That study showed that the Y_{rel} average has a strong correlation with the track modulus average over track lengths of 8 m and longer. The strong correlation was quantified and modelled using mathematical equations. It was also shown that Y_{rel} COV is not solely representative of the track modulus variation for track windows shorter than 80 m. For this chapter, complementary analyses were conducted to investigate how the track modulus variation can be estimated using the Y_{rel} data for a track window shorter than 80 m. A track window of 40 m was selected. Statistical properties of the track modulus and Y_{rel} , including the average, standard deviation (StDev), and COV over this track window, were calculated for all models. As mentioned earlier, ninety models with different track modulus distributions were considered. Each was 160 m long. These models provided 360 track windows with lengths of 40 m length. Figure 5-3a shows the track modulus average (U_{Avg}) versus the Y_{rel} average for all 360 track windows, along with the best fitted curve to the data points. The strong correlation between the track modulus average and the Y_{rel} average over the 40-m long track window was quantified using Equation 5-1.

Multivariate regression analyses were also conducted to find the parameters necessary to estimate the track modulus variation. The final results were plotted in Figure 5-3b. As shown in that figure, the track modulus StDev (U_{StDev}) correlates strongly with the Y_{rel} average and Y_{rel} StDev. Equation 5-2 is the equation of the best fitted surface to the data points in Figure 5-3b. The equation can be used to estimate the track modulus StDev from the Y_{rel} average and Y_{rel} StDev. It should be noted that Equations 5-1 and 5-2 correspond to the RE136 rail size and the loading condition shown in Figure 5-1 and could be modified for other loading conditions and rail sizes.

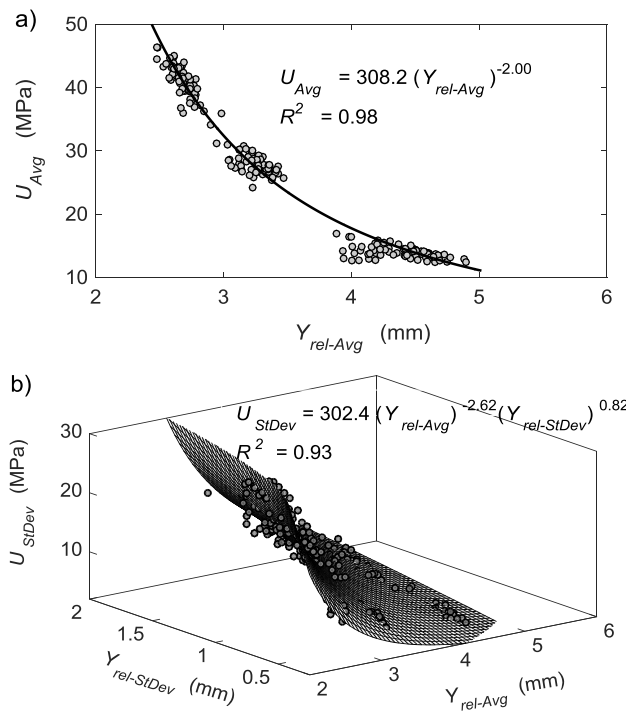


Figure 5-3 Correlation between track modulus and relative vertical track deflection (Y_{rel}) over 40-m long track windows: a) track modulus average (U_{avg}) vs. Y_{rel} average ($Y_{rel-Avg}$), and b) track modulus standard deviation (U_{StDev}) vs. Y_{rel} average and Y_{rel} standard deviation ($Y_{rel-StDev}$).

$$U_{Avg} = 308.2 \times (Y_{rel-Avg})^{-2.00} \quad (5-1)$$

$$U_{StDev} = 302.4 \times (Y_{rel-Avg})^{-2.62} \times (Y_{rel-StDev})^{0.82} \quad (5-2)$$

where U_{Avg} and U_{StDev} are the track modulus average and StDev over the 40-m track length (in MPa) and $Y_{rel-Avg}$ and $Y_{rel-StDev}$ are the average and StDev for the Y_{rel} over the 40-m track length (in mm).

5.5 Quantifying the spatial variation of the maximum rail bending moment

The numerical model results were used to investigate the correlation between the track modulus and M_{max}^+ for the RE136 rail size and the loading condition shown in Figure 5-1. Track windows of 40 m were selected and distributions of the inputted track modulus and the resulting M_{max}^+ envelope profile were compared. As shown in Figure 5-2c, the magnitude of M_{max}^+ varies along the track due to the spatially varying track modulus. For all ninety models, an average of the M_{max}^+ over each 40-m track length window was calculated and plotted versus the track modulus average (Figure 5-4a). As shown in Figure 5-4a, a higher track modulus average resulted in a lower M_{max}^+ average for a given rail size and loading condition. This correlation was quantified using a nonlinear regression analysis and the result is presented in Figure 5-4a and Equation 5-3. Multivariate regression analyses were also conducted to find the statistical properties of the track modulus that affected the M_{max}^+ StDev and peak M_{max}^+ along the 40-m track length. Figures 5-4b and 5-4c show that the M_{max}^+ StDev and peak M_{max}^+ correlate strongly with the track modulus average and StDev. The M_{max}^+ StDev and peak M_{max}^+ increased as the track modulus average decreased and the track modulus StDev increased. The correlations were quantified using multivariate regression analysis. The equations of the best fitted surfaces to the data points are presented in Figures 5-4b and 5-4c and Equations 5-4 and 5-5. Equations 5-3 to 5-6 correspond to the RE136 rail size and the loading condition shown in Figure 5-1.

The same procedure was followed to investigate the correlations between the statistical properties of the track modulus and M_{max}^- . The results are presented in Figure 5-5 and Equations 5-6 to 5-8. From Figure 5-5, the average, StDev, and peak for the M_{max}^- envelope profile increased as the track modulus average decreased and the track modulus StDev increased.

$$M_{max-Avg}^+ = 80.45 \times (U_{Avg})^{-0.19} \quad (5-3)$$

$$M_{max-StDev}^+ = 34.76 \times (U_{Avg})^{-1.35} \times (U_{StDev})^{1.10} \quad (5-4)$$

$$M_{max-peak}^+ = 151.5 \times (U_{Avg})^{-0.54} \times (U_{StDev})^{0.36} \quad (5-5)$$

$$M_{max-Avg}^- = -42.7 \times (U_{Avg})^{-0.30} \times (U_{StDev})^{0.12} \quad (5-6)$$

$$M_{max-StDev}^- = 20.35 \times (U_{Avg})^{-1.09} \times (U_{StDev})^{0.93} \quad (5-7)$$

$$M_{max-peak}^- = -115.6 \times (U_{Avg})^{-0.70} \times (U_{StDev})^{0.50} \quad (5-8)$$

where the $M_{max-Avg}^+$, $M_{max-StDev}^+$, and $M_{max-peak}^+$ are average, the StDev and peak for the envelope profile of the M_{max}^+ over the 40-m track length (in kN·m), $M_{max-Avg}^-$, $M_{max-StDev}^-$, and $M_{max-peak}^-$ are average, the StDev and peak for the M_{max}^- envelope profile over the 40-m track length (in kN·m), and U_{Avg} and U_{StDev} are as defined in Equations 5-1 and 5-2.

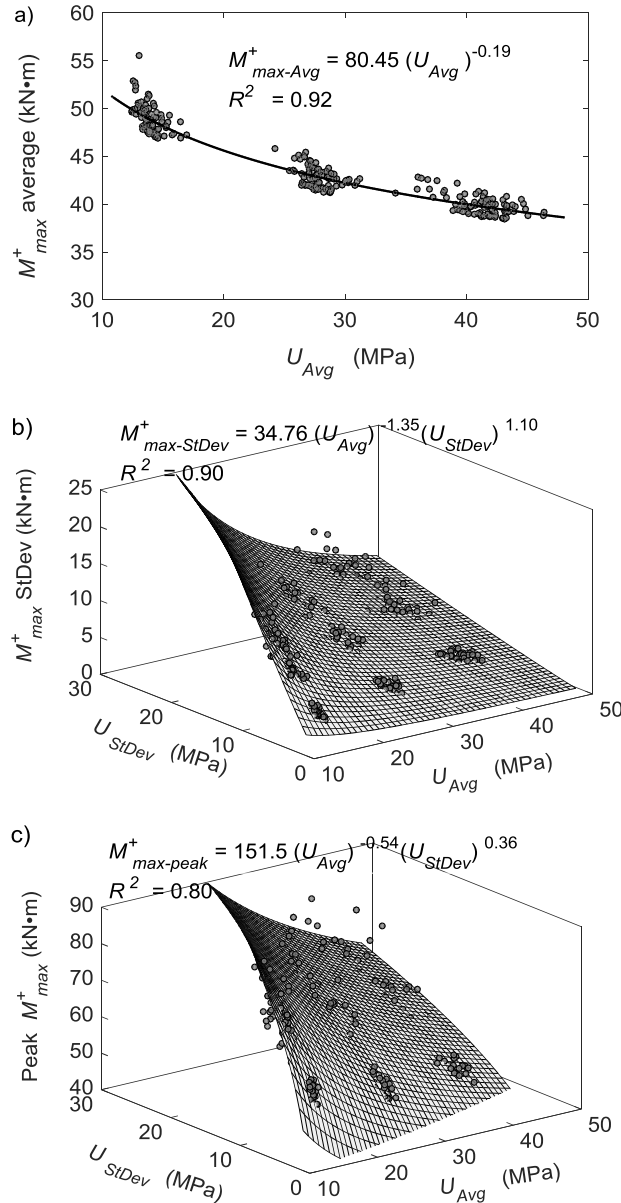


Figure 5-4 Correlation between track modulus and maximum positive bending moment (M_{max}^+) over track windows of 40 m: a) M_{max}^+ average ($M_{max-Avg}^+$) vs. track modulus average (U_{avg}), b) M_{max}^+ standard deviation ($M_{max-StDev}^+$) vs. track modulus average and standard deviation (U_{StDev}), and c) Peak M_{max}^+ ($M_{max-peak}^+$) vs. track modulus average and standard deviation.

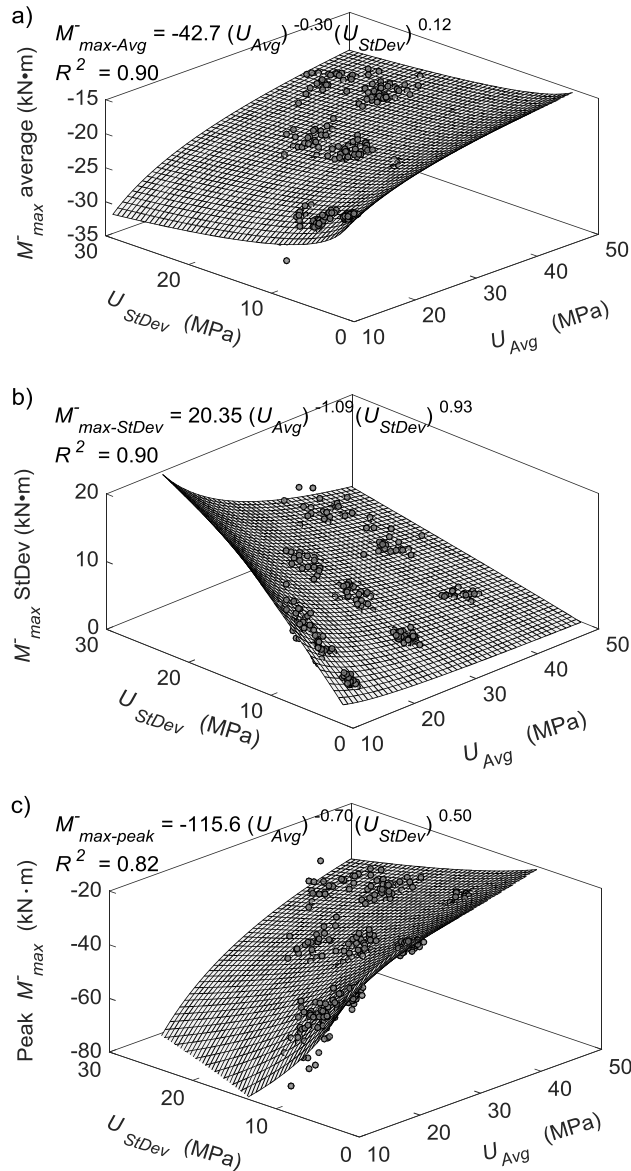


Figure 5-5 Correlation between track modulus and maximum negative bending moment (M_{max}^-) over track windows of 40 m: a) M_{max}^- average ($M_{max-Avg}^-$) vs. track modulus average (U_{avg}), b) M_{max}^- standard deviation ($M_{max-StDev}^-$) vs. track modulus average and standard deviation (U_{StDev}), and c) Peak M_{max}^- ($M_{max-peak}^-$) vs. track modulus average and standard deviation.

5.6 Numerical case study

The accuracy of Equations 5-1 to 5-8 for quantifying the spatial variation of the M_{max}^+ , M_{max}^- , and track modulus from Y_{rel} was investigated further using a new track model, which was not used while developing Equations 5-1 to 5-8. A track model with new randomised stiffness at

each support was developed and the resultant Y_{rel} and envelope profile of M_{max}^+ and M_{max}^- under the moving load (shown in Figure 5-1) were calculated using finite element analysis (FEA) and VBA codes. From the resultant Y_{rel} distribution and Equations 5-1 and 5-2, a track modulus average and StDev were estimated. These estimations were then compared with the inputted track modulus to verify the accuracy of Equations 5-1 and 5-2. Subsequently, the average, StDev, and peak for the envelope profile of M_{max}^+ were calculated by using the estimated track modulus average and StDev in Equations 5-3 and 5-5. The estimated statistical properties of M_{max}^+ were compared with the actual values of M_{max}^+ from the FEA to verify the accuracy of Equations 5-3 and 5-5. The same procedure was followed to verify the accuracy of Equations 5-6 and 5-8.

Unlike the previous models in which the stiffness of the spring supports along the track came from a normal track modulus distribution, in the new track model, the stiffness of the spring supports was randomly selected from a uniform track modulus distribution (also referred to as a rectangular probability distribution) that had constant probability on the interval between 6.5 MPa and 48 MPa. Using this method, the distribution of the track modulus for the new track model was totally different from the ninety normal track modulus distributions used while developing Equations 5-1 to 5-8. The inputted track modulus distribution for the new track model over a 40-m long track window of 40 m long is depicted in Figure 5-6a. The track modulus average and StDev for this track window were 26.80 MPa and 11 MPa, respectively. The solid black lines in Figures 5-6b to 5-6d show the resulting Y_{rel} and the envelope profile of M_{max}^+ and M_{max}^- that were calculated using FEA and VBA codes for the inputted track modulus.

To account for the effect of systematic errors and local disturbances on Y_{rel} data measured from train-mounted instruments in the field, artificial noise was added to the Y_{rel} distribution derived from FEM. The Y_{rel} distribution with artificial noise was then used to estimate the track modulus, M_{max}^+ , and M_{max}^- . Two components were considered for adding noise to the Y_{rel} distribution. The first component was adding a product of 0.12 mm and an evenly distributed random number between -1 and 1 to any individual Y_{rel} values. This component addressed the measurement resolution which is around 0.12 mm for the MRail system. The measurement resolution for the MRail system depends on the resolution of images captured by the camera system. The measurement resolution of 0.12 mm is based on the assumption that the system captures images

with a resolution of 782×582 pixels [21]. For the second component, one-tenth of each Y_{rel} value was multiplied by an evenly distributed random number between -1 and 1 and then added to the original Y_{rel} value. This component was intended to account for the effect of local disturbances on Y_{rel} data, such as the effect of track geometry irregularities. The procedure for adding artificial noise to each individual Y_{rel} value is presented in Equation 5-9. The noisy Y_{rel} distribution calculated using Equation 5-9 for the new track model is shown with the dotted black line in Figure 5-6b.

$$Y_{rel-noisy} = Y_{rel-Act} + RAND(-1, 1) \times 0.12 + RAND(-1, 1) \times 0.1 \times Y_{rel-Act} \quad (5-9)$$

where, $Y_{rel-noisy}$ is the relative VTD with the artificial noise (in mm), $RAND(-1, 1)$ is an evenly distributed random number between -1 and 1, and $Y_{rel-Act}$ is the actual relative VTD calculated using the FEM (in mm).

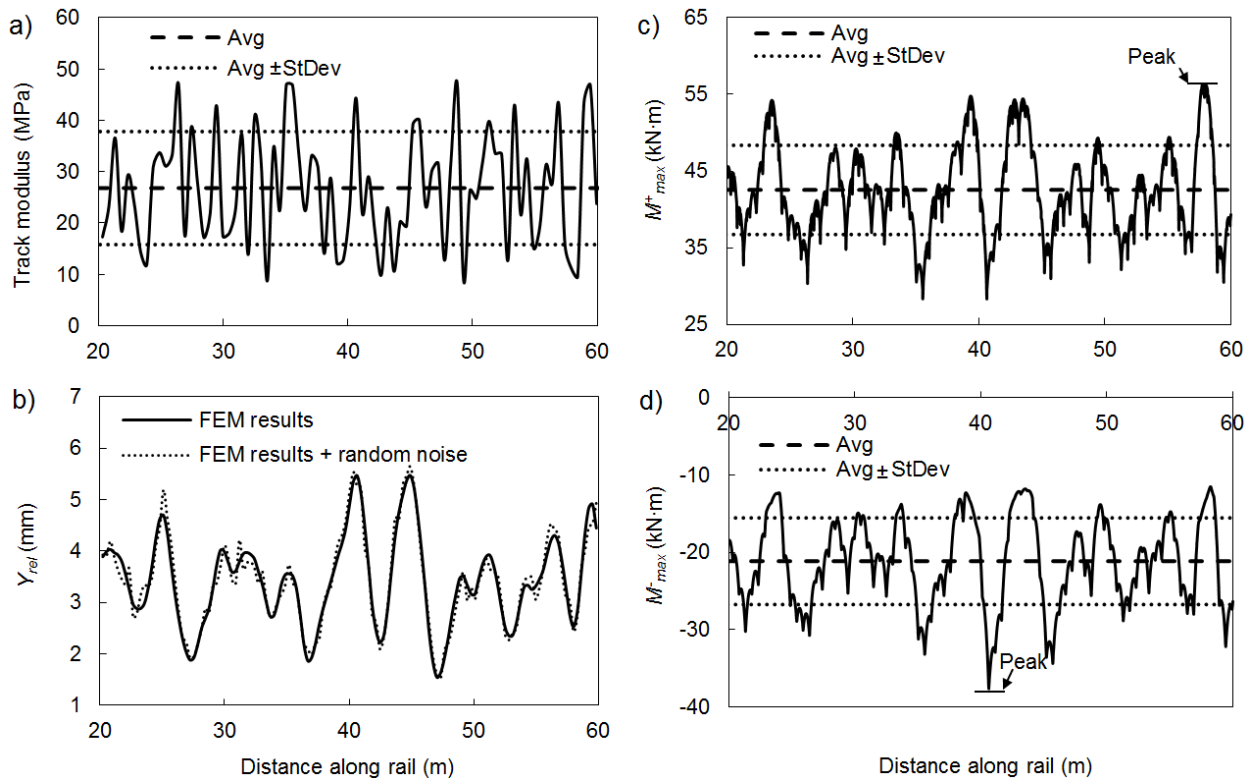


Figure 5-6 Input and output for a model with a 40-m track length: a) inputted track modulus distribution, b) resultant relative vertical track deflection (Y_{rel}) with and without artificial noise, c) resultant envelope profile of the maximum positive bending moment (M_{max}^+), and d) resultant envelope profile of the maximum negative bending moment (M_{max}^-) (Avg: average, StDev: standard deviation).

The average and StDev for the noisy Y_{rel} distribution depicted in Figure 5-6b are 3.43 mm and 0.90 mm, respectively. Calculations for estimating the track modulus, M_{max}^+ , and M_{max}^- from the noisy Y_{rel} distribution were summarized in Tables 5-2 to 5-4. Based on the results, the track modulus average and StDev were estimated from the noisy Y_{rel} distribution with less than 3% error, and from these estimations, the average, StDev, and peak for the envelope profile of M_{max}^+ and M_{max}^- were estimated with less than a 10% error.

Table 5-2 Summary of the calculations for quantifying the track modulus distribution from relative vertical track deflection (Y_{rel}) measurements (StDev: standard deviation).

Average for the noisy Y_{rel} distribution presented in Figure 5-6b	3.43 mm
StDev for the noisy Y_{rel} distribution presented in Figure 5-6b	0.90 mm
Inputted track modulus average presented in Figure 5-6a	26.80 MPa
Estimated track modulus average from the noisy Y_{rel} distribution and Equation 5-1	26.20 MPa
Difference between the estimated and inputted track modulus average	2.2 %
Inputted track modulus StDev presented in Figure 5-6a	11.00 MPa
Estimated track modulus StDev from the noisy Y_{rel} data and Equation 5-2	10.97MPa
Difference between the estimated and inputted track modulus StDev	0.3 %

Table 5-3 Summary of the calculations for quantifying the spatial variation of the maximum positive bending moment (M_{max}^+) from the relative vertical track deflection (Y_{rel}) measurements (StDev: standard deviation).

Average for the envelope profile of M_{max}^+ presented in Figure 5-6c	42.55 kN·m
Estimated M_{max}^+ average from the estimated track modulus average and Equation 5-3	43.25 kN·m
Difference between the estimated and actual M_{max}^+ average	1.6 %
StDev for the envelope profile of M_{max}^+ presented in Figure 5-6c	5.81
Estimated M_{max}^+ StDev from the estimated track modulus average and Equation 5-4	5.90
Difference between the estimated and actual M_{max}^+ StDev	1.5%
Peak for the envelope profile of M_{max}^+ presented in Figure 5-6c	56.32 kN·m
Estimated peak M_{max}^+ from Equation 5-5 and the estimated track modulus average and StDev	61.52 kN·m
Difference between estimated and actual peak M_{max}^+	9.1 %

Table 5-4 Summary of the calculations for quantifying the spatial variation of maximum negative bending moment (M_{max}^-) from relative vertical track deflection (Y_{rel}) measurements (StDev: standard deviation).

Average for the envelope profile of M_{max}^- presented in Figure 5-6d	-21.14 kN·m
Estimated M_{max}^- average from the estimated track modulus average and Equation 5-6	-21.37 kN·m
Difference between the estimated and actual M_{max}^- average	1.1%
StDev for the envelope profile of M_{max}^- presented in Figure 5-6d	5.60
Estimated M_{max}^- StDev from the estimated track modulus average and Equation 5-7	5.37
Difference between the estimated and actual M_{max}^- StDev	0.1%
Peak for the envelope profile of M_{max}^- presented in Figure 5-6d	-37.60 kN·m
Estimated peak M_{max}^- from Equation 5-8 and the estimated track modulus average and StDev	-38.93 kN·m
Difference between estimated and actual peak M_{max}^-	3.5%

5.7 Conclusions

In this chapter, the developed FEM was used to investigate the correlations between the track modulus, VTD, and maximum bending moments. The purpose was to develop a method that makes it possible to estimate the spatial variation of maximum rail bending moments from VTD measurements. Various track modulus distributions were simulated and the track's responses to a known applied load were calculated in terms of VTD and the maximum positive and negative bending moments' envelope profile. Statistical approaches were then used to quantify the correlations between the inputted track modulus, the modelled VTD, and the modelled maximum rail bending moments. The quantified correlations and proposed equations allow the estimation of the track modulus average and StDev using VTD measurements. Once the track modulus average and StDev are estimated, the average, StDev and peak for the envelope profile of the maximum positive and negative bending moments in the rail can be quantified using the developed correlations between the inputted track modulus and rail bending moments. Finally, a numerical case study was presented for which a random track modulus distribution was considered and artificial noise was added to the modelled VTD. The study further proved the accuracy of the proposed equations.

CHAPTER 6: A Case Study of the Assessment of Vertical Bending Stresses in Rail⁴

6.1 Overview

Train-mounted vertical track deflection (VTD) measurements offer new opportunities for estimating rail bending stresses over long distances. The estimations are possible due to mathematical correlations between rail deflections, rail bending stresses, and the loads applied to the rail. Previous numerical studies, presented in Chapters 3 to 5, resulted in a methodology that suggests the use of finite element models to develop the correlations. These models facilitate the simulation of a stochastically varying track modulus along the track and provide a strong basis for interpreting the deflection data. In this study, according to “*Objective 3*” presented in Chapter 1, datasets collected from a test site were employed to validate this methodology for estimating rail bending stresses under passing train loads. The rail-mounted strain gauges and the wheel impact load detector system at the test site provided information about the rail bending strains under known applied loads. This allowed validation of the maximum bending stresses estimated using train-mounted deflection measurements. The magnitude of rail bending stresses was assessed using measurements from different seasons; stress changes over time were also investigated.

6.2 Introduction

Rail issues such as broken rails, rail joint bars, and welds are the most common cause of main track derailments in Canada’s railway network [4]. Main tracks are the tracks of subdivisions extending through and between stations [5]. Any derailments on these tracks could have very serious consequences, including fatalities, injuries, and financial loss [4]. Figure 6-1 illustrates results from the analysis of broken rail derailments that occurred on Canada’s main tracks between 2000 and 2014. Rail head defects that propagated along the rail cross section, also

⁴ A version of this chapter will be submitted to the ASCE Journal of Transportation Engineering, Authors: Fallah Nafari S, Gül M, Hendry M.T, Otter D, and Cheng J.J.R.

referred to as transverse defects, are the leading cause (27%) of broken rail derailments. Transverse defects are categorised as detail fractures, transverse fissures, and compound fissures depending on the origin of the defect [36]. The initiation and early propagation of a transverse defect is often due to wheel-rail contact stresses. After the defect extends away from the rail surface, its propagation is mainly controlled by live bending stress, thermal stress, and residual stress [8, 35, 40]. The second leading cause of broken rail derailments (24%) is base defects (Figure 6-1). The growth of base defects along the rail cross section is also influenced by live bending stress, thermal stress, and residual stress.

The establishment of optimised solutions for rail issues requires reliable methods for estimating rail stresses along the track [6]. The estimation of rail stresses is challenging as the stresses continuously vary along the track due to operational, environmental, and structural factors [7, 9, 10]. Many attempts have been made to develop methods for measuring rail stresses [13-19]. However, the number of studies evaluating rail bending stresses over long distances is very limited [20, 21].

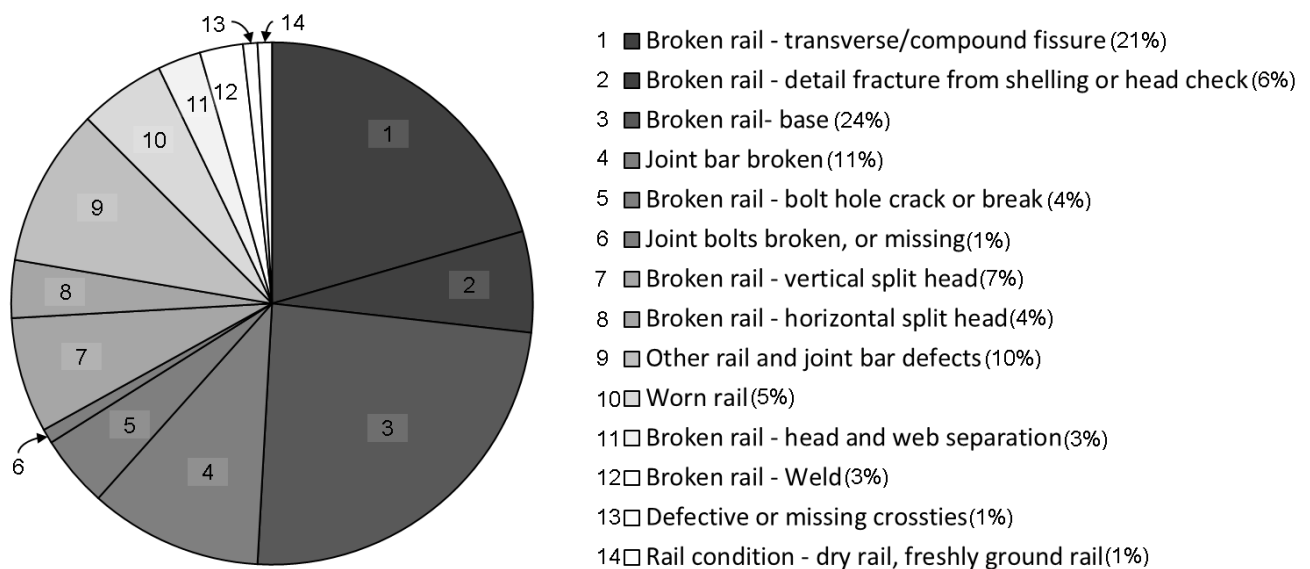


Figure 6-1 Causes of broken rail derailments on Canada's main tracks from 2000 to 2014.

New train-mounted systems that measure the vertical track deflection (VTD) under fully loaded axles offer new opportunities for estimating rail bending stresses over long distances [21, 22, 26]. The mathematical correlations between rail deflection, rail bending stress, and loads applied to the rail form the basis of the method. The potential of VTD measurements for the estimation

of rail bending stress has been studied and confirmed using field tests, but used a track model with a constant track modulus to develop the mathematical correlations between rail deflection and stress [20]. Experience with VTD data shows that interpretation of the data requires track models in which track modulus variation is addressed [80]. The track modulus varies stochastically along the track [29, 31] and, thus, track models with a constant track modulus have limited application for interpreting VTD data.

A newer methodology was developed and presented in Chapters 3 to 5 for establishing mathematical correlations between track modulus, rail deflections, and stresses using finite element models (FEMs) in which stochastically varying track modulus are considered [108, 110]. The methodology suggests developing track models with different track modulus distributions. This is possible by assigning different random stiffness values to the spring supports along the tracks. The finite element analysis is then used to calculate the profile of rail deflections and bending moments under known applied loading sets. For each model, the statistical properties for the distributions of the inputted track modulus, the modelled VTD, and the rail bending moments are calculated. The values calculated from the models with different track modulus distributions are analysed using statistical approaches to develop the correlations between track modulus, VTD, and rail bending moment. The developed correlations facilitate the interpretation of the deflection data measured using train-mounted instruments.

This chapter presents the results of a study conducted to validate this methodology. Ranges for the magnitude of maximum bending stresses and tensile strains in the rail base were estimated using relative VTD measurements (also referred to as Y_{rel}) from the MRail system. The estimated ranges were then compared with measurements from rail-mounted strain gauges that collected strain data under known applied loads. Although the study focused on the use of VTD measurements from the MRail system, the same concept is applicable to other VTD measurement systems.

6.3 Study site

The study site selected was Canadian National's (CN) Wheel Impact Load Detector (WILD) site at Calrin, located between Mile 20 and 21 at CN's Rivers Subdivision near Winnipeg, Manitoba, Canada. Transportation Technology Centre, Inc. (TTCI) has mounted a number of strain gauges

on both rails at several locations along the north track at this site for the purpose of research studies. The WILD system along with the strain gauges have allowed measurement of vertical wheel loads and resultant rail bending strains for passing trains. The datasets provided the information necessary to validate the rail bending strains estimated from the VTD measurements. TTCI collected salient WILD data and rail strains for hundreds of trains in both August 2015 and February 2016. For this study, one sample from each of the August and February datasets was analysed to investigate changes in the magnitude of rail bending strains over time. Each sample included six strain time histories measured at three cribs along the base of the north and south rails.

Figure 6-2 depicts the layout of the WILD system and TTCI's instruments location at the Calrin site. The track structure consists of 67.5 kg/m (136 lb/yd) continuous welded rail and concrete cross-ties. The spacing between consecutive cross-ties is close to 0.61 m (24 in), but varies somewhat to optimise the coverage of the WILD system for different wheel diameters. Figure 6-3 is a photo of the study site.

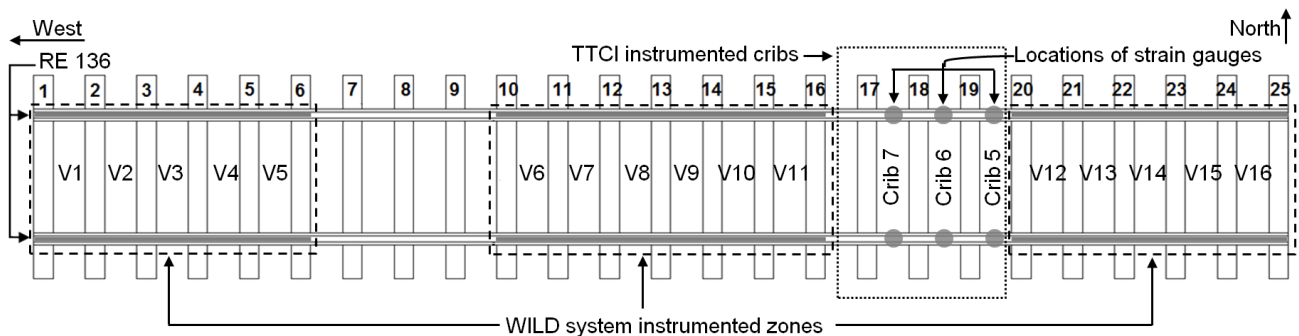


Figure 6-2 Layout of CN's Calrin WILD system including 16 instrumented cribs on both rails together with the location of rail base strain gauges.



Figure 6-3 A photo of the WILD system and instrumented cribs along the north track at the Calrin site.

A laser and camera-based system, commonly referred to as the MRail system, was employed for VTD measurements at the Calrin site. The MRail system was originally developed at the University of Nebraska-Lincoln in collaboration with the Federal Railroad Administration. Using the system, Y_{rel} between the rail surface and the wheel and rail contact plane is measured at a distance of 1.22 m from the nearest wheel to the sensor system [23, 25]. A new version of the MRail system was used for collecting the VTD data at Calrin (Figure 6-4), with the only difference being that the new system uses one laser line instead of the two in the original version [80].

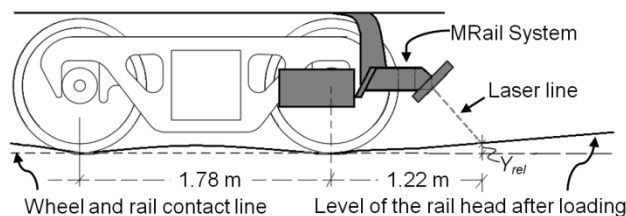


Figure 6-4 Illustration of the MRail system used for measuring vertical track deflections at Calrin (adapted from [80, 108]).

6.4 Load data collected using the WILD system

The WILD system is a hardened electronic data collection device that measures wheel impact forces using an array of strain gauges or accelerometers. The railway industry makes wide use of the system to detect damaged wheels that apply high impact forces to the rail. If any wheel generates an impact force greater than a predefined threshold, a report identifies that wheel for action. The WILD system at Calrin is a strain gauge-based system that measures rail shear strains using a series of rail-mounted strain gauge load circuits. The force applied to the rail is determined using a mathematical relationship between the shear strain and applied force. As shown in Figure 6-2, the Calrin WILD site is comprised of 16 instrumented cribs along the north and south rails. For each wheel that passes over a crib, many load data points are collected. The number of load measurements at one crib depends on the sample rate, train speed, and effective zone of the crib. The system outcome includes one average value and one peak (maximum) value for the load samples in a given crib. Figure 6-5 shows the average and peak loads recorded at 16 instrumented cribs when a wheel passed the Calrin WILD site in August 2015. Notably, the average and peak vertical loads recorded at each instrumented crib are different, even for one

wheel. One way to analyze the load data points is to determine the range for the average and peak vertical wheel loads using the measurements from all instrumented cribs.

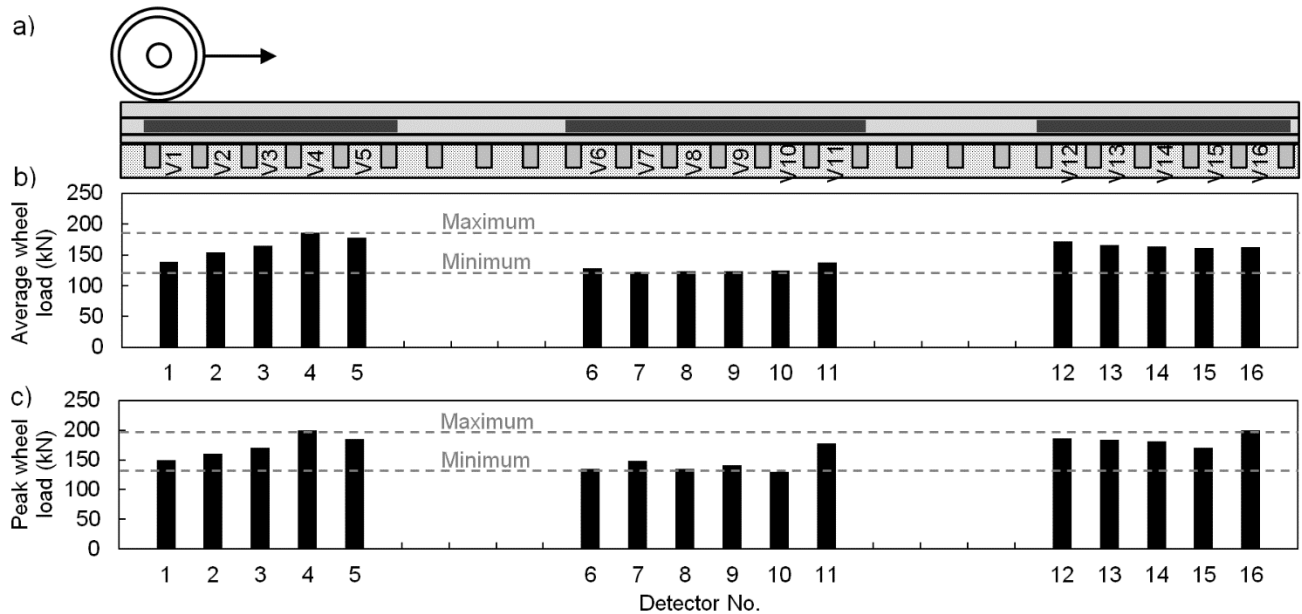


Figure 6-5 Measuring wheel impact forces using the WILD system: a) illustration of a wheel passing over WILD instrumented zones, b) average wheel loads recorded for the passing wheel at the Calrin WILD site in August 2015, and C) peak wheel loads recorded for the same passing wheel.

6.5 Strain data collected using strain gauges

TTCI has placed a number of strain gauges on both rails along the north track at the Calrin WILD site. Using the strain gauges, rail bending strains were measured under the passage of thousands of wheels in August 2015 and February 2016. Measurements in two different seasons allowed for an assessment of changes in the magnitude of rail bending strains over time. Each dataset (August 2015, February 2016) included six strain time histories collected using six rail base circuits at the locations of cribs No. 5, 6, and 7 along both rails (Figure 6-2). Rail base strain gauges were placed on top of the rail bottom flange to measure the average of strains from the field and gauge sides of the rail. The strain channels were all re-zeroed and rebalanced each day, sometimes multiple times per day if a large change in temperature occurred. Hence, the strain readings were the dynamic strain from the passing train only, with no need to make adjustments for temperature for any of the strain circuits. Figure 6-6 presents a strain time history from the rail base circuit at crib No. 5 along the north rail, recorded when a train with 216 axles traveled

across the site in August 2015. Relative positive peaks in the strain data indicate relative maximum tensile strains in the rail base when wheels passed over the rail base circuit. As demonstrated in Figure 6-6, two types of peaks were observed in the data: higher peaks correspond to fully loaded railcars while lower peaks correspond to partially loaded or empty railcars.

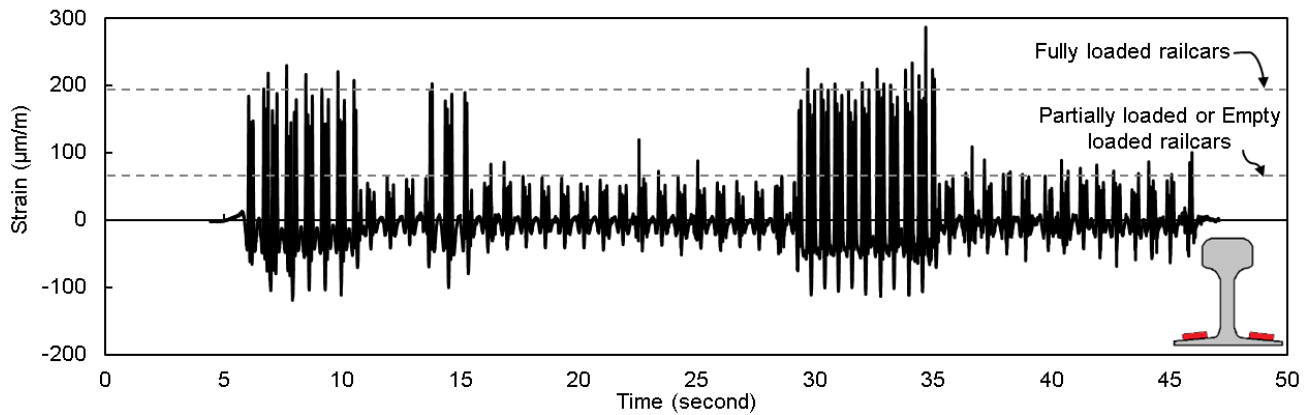


Figure 6-6 A sample strain time history from the August dataset collected using the rail base circuit at crib No. 5 long the north rail (tensile strains as positive values).

6.6 Analysis of datasets from the WILD system and strain gauges

The salient data from the Calrin WILD site along with the rail bending strain measurements provided information about the rail bending strains under known applied loads. This presented an opportunity to validate the rail bending strains estimated from the VTD measurements. Two tasks were completed to analyse the salient WILD data and bending strain measurements. First, maximum rail bending strains under a known applied load similar to the MRail loading set were extracted from the salient WILD data and strain datasets. Second, two strain datasets (August 2015, February 2016) were analysed to investigate possible changes in the magnitude of rail bending strains over time. The second analysis was conducted because the VTD measurements along the north track at the Calrin WILD site were not collected at the same time as the rail bending strain measurements. The two MRail runs were conducted in May and October 2015 and, thus, the estimated bending strains therefrom correspond to times when the track was not frozen. A notable consideration was whether the estimated bending strains from MRail measurements when the track was not frozen represent the magnitude of actual bending strains in the rail under the same loading throughout the year. Comparing the rail strain measurements

under similar loading sets in August and February demonstrated how the track stiffness and the magnitude of generated bending strains in rail changed over time (i.e., seasonally) at the Calrin Site.

The loading set depicted in Figure 6-7 was repeated three times in August 2015 and seven times in February 2016. This loading set represents two fully loaded trucks from two adjacent railcars and has a specific range for the average and peak wheel loads at WILD instrumented cribs. For each passage of the loading set, the maximum tensile strains generated in the south and north rails at cribs No. 5, 6, and 7 were extracted from the strain datasets; results are summarised in Table 6-1. The maximum tensile strains recorded in the rail base in August were approximately 55% higher than the February measurements. This implies that the track was significantly stiffer in the winter. Therefore, the estimations of rail bending strains from VTD measurements in May and October should only be compared with the bending strain measurements taken in August.

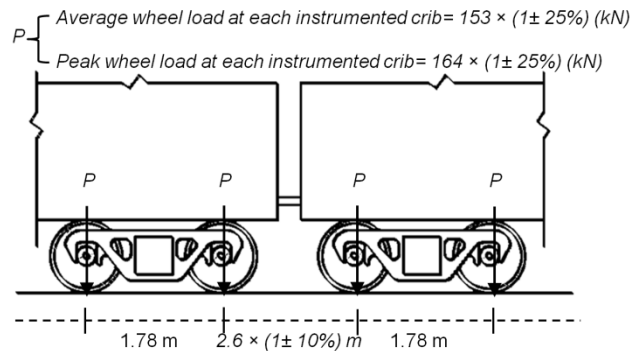


Figure 6-7 Loading set used for comparing the strain datasets from August and February.

Table 6-1 Range of the multiple measurements of maximum tensile strains in rail under the loading set shown in Figure 6-7.

Date	Crib No.	Average for north and south rail measurements ($\mu\epsilon$)
Aug. 2015	5, 6, and 7	$237 \times (1 \pm 10\%)$
Feb. 2016	5, 6, and 7	$107 \times (1 \pm 10\%)$

6.7 VTD measurements using the MRail System

Two MRail runs were conducted on the north track at the Calrin WILD site. The first run was in May 2015 with the MRail car next to a locomotive, and the second run was in October 2015 with

the MRail car next to a tank car. Information about the loading set for each run is presented in Figure 6-8. The axle spacings for the locomotive and railcars were determined using the North American car catalogue system (UMLER), and the wheel loads were estimated using the salient WILD data. To reduce uncertainties and simplify the calculations, the weight of each truck from the WILD system was evenly distributed between the truck wheels. The assumption of uniform wheel loads for each truck was acceptable because the study site is a tangent track (straight line). Moreover, the average of measurements on the north and south rails was used for the analysis of MRail and strain gauge data. The datasets from the MRail system consist of latitude and longitude coordinates of the measurements, the estimated milepost (MP), and Y_{rel} values for the right and left rails at approximately 0.305-m (1-ft) intervals. The accuracy level of the GPS system installed on the MRail car was ± 3.7 m with a 95% confidence level. The Y_{rel} data at the Calrin site were extracted from the datasets collected along the entire subdivision. This was initially done using the MRail GPS data and approximate GPS coordinates for the WILD site. To increase the accuracy of this data extraction, information about distances between the WILD site and nearby track elements were employed and fluctuation trends in the Y_{rel} data at and near the WILD site were examined. Using this procedure, the small error that might have occurred while extracting the Y_{rel} data should have insignificant influence on the results presented here. Figure 6-9 features a satellite map view of the study site together with Y_{rel} data from the May and October MRail runs.

The WILD system at Calrin is placed on a zone with concrete crossties. As shown in Figure 6-9b, the Y_{rel} data have very small fluctuations along the west half of the zone and high variations along the rest of zone. Investigation of this difference was beyond the scope of the study. Factors such as instruments installed on the track and changes in the track substructure may cause high variations in the Y_{rel} data. All calculations in this study are based on the average and standard deviation (StDev) of the Y_{rel} data over the full length of the 92.3-m zone with concrete crossties. This was done to consider the track condition along the entire zone; notably, shortening the track window to the length of the WILD instrumented zone (15.4 m) did not affect the results.

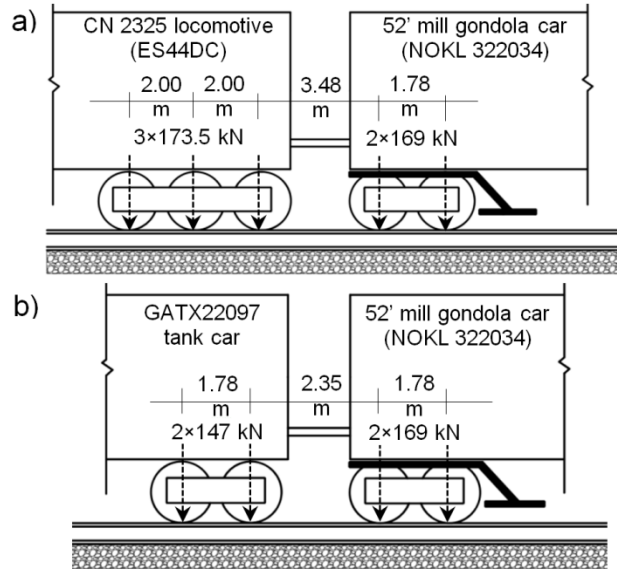


Figure 6-8 a) MRail next to a locomotive during the May run, and b) MRail next to a tank car during the October run.

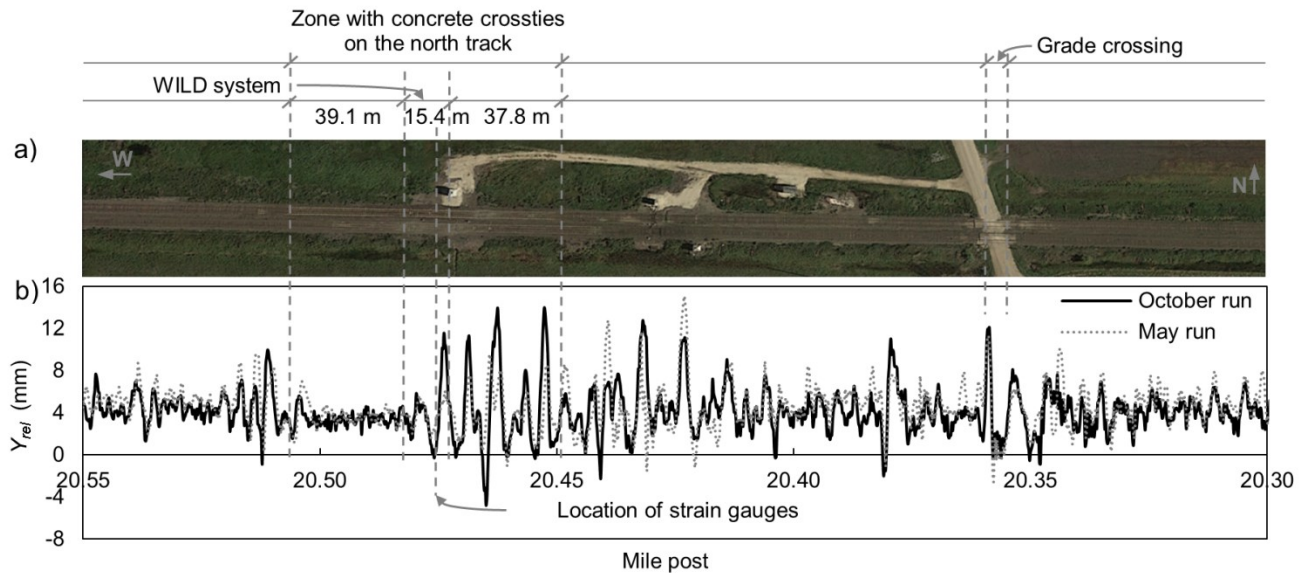


Figure 6-9 a) Satellite map view of the study site, b) Y_{rel} data from May and October MRail runs (average of measurements on the north and south rails).

6.8 Comparing the Y_{rel} datasets from two MRail runs

The Y_{rel} measurements from May and October runs had similar fluctuation patterns even though the magnitudes were often different. The runs were conducted under different loading sets and so the difference in magnitude was not only associated with changes in the track condition. A

detailed investigation of the changes was conducted through mathematical correlations between rail deflections, applied loads, and track modulus. The correlations facilitated the estimation of track modulus from Y_{rel} data and allowed for the investigation of changes in track modulus over time. A series of FEMs were used to develop mathematical correlations. One hundred and eighty models with different track modulus distributions were simulated using FEMs. The rail size and tie spacings in all models were defined to be similar to the track specifications at the Calrin WILD site. Distribution of Y_{rel} along the track was calculated under two different MRail loading sets. For each model, the average and StDev of inputted track modulus and resultant Y_{rel} were determined. The results from all models were then used in a regression analysis to quantify the correlations between the statistical properties of track modulus and Y_{rel} . An important parameter in calculations is the track window length along which the average and StDev of track modulus and Y_{rel} are calculated. A detailed discussion about the modelling procedure, regression analysis, and the effect of window length on the results is presented elsewhere [108]. The quantified correlations between track modulus and Y_{rel} corresponding to two different MRail loading sets are presented in Equations 6-1 to 6-4 and Figures 6-10 and 6-11. The correlations are applicable to track window lengths of 80 m and longer.

For the loading set shown in Figure 6-8a:

$$U_{Avg} = 303(Y_{rel-Avg})^{-1.74} \quad (6-1)$$

$$U_{StDev} = 272(Y_{rel-Avg})^{-2.3}(Y_{rel-StDev})^{0.9} \quad (6-2)$$

and for the loading set shown in Figure 6-8b:

$$U_{Avg} = 348(Y_{rel-Avg})^{-2} \quad (6-3)$$

$$U_{StDev} = 327(Y_{rel-Avg})^{-2.7}(Y_{rel-StDev})^{0.9} \quad (6-4)$$

where U_{Avg} and U_{StDev} are the track modulus average and StDev (in MPa), and $Y_{rel-Avg}$ and $Y_{rel-StDev}$ are Y_{rel} average and StDev (in mm) over a track window length of 80 m and longer.

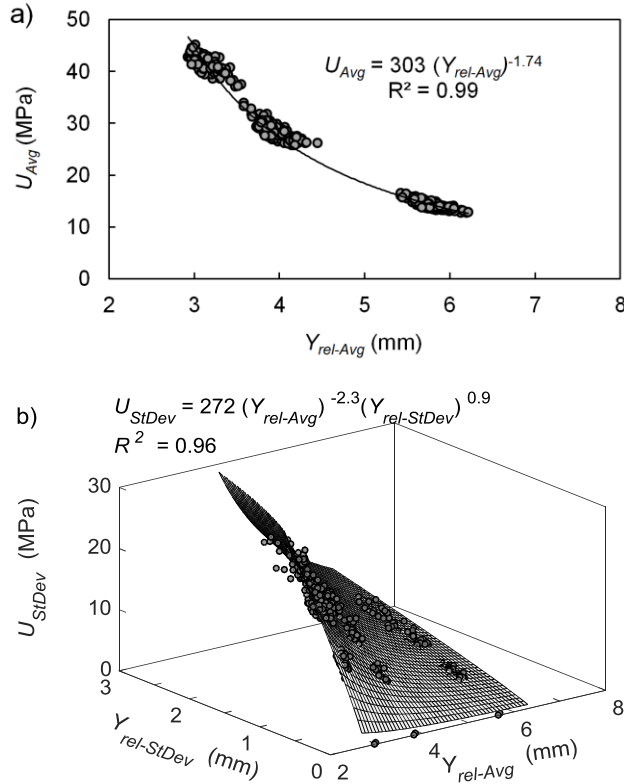


Figure 6-10 Correlations between statistical properties of track modulus and relative vertical track deflection (Y_{rel}) for the loading set shown in Figure 6-8a: a) track modulus average (U_{avg}) vs. Y_{rel} average ($Y_{rel-Avg}$), and b) track modulus standard deviation (U_{StDev}) vs. $Y_{rel-Avg}$ and Y_{rel} standard deviation ($Y_{rel-StDev}$).

The average and StDev of Y_{rel} data over the zone with concrete cross ties were calculated separately for each MRail run. As reported in Table 6-2, the Y_{rel} average for both runs was 3.8 mm. The average track modulus values for May and October were estimated using Equations 6-1 and 6-3 with respect to the MRail loading set. The track modulus average decreased by 20% from May to October 2015, which explains why the Y_{rel} average values from both runs were the same despite the MRail loading set being heavier in the May run. Track modulus StDev values were also estimated for the zone with concrete crossties using Equations 6-2 and 6-4, with results indicating a 20% increase from May to October 2015. Considering changes in the track condition from May to October, only the Y_{rel} data from the October run were used to estimate the rail bending strains; this is because the October MRail run was closer in time to August when the TTCI rail strain data were collected, and historical climate data for Calrin show that the ballast was not frozen in October. Additionally, the MRail loading set for the October run featured two

adjacent fully loaded trucks, similar to Figure 6-7 under which the TTCI measured rail bending strains.

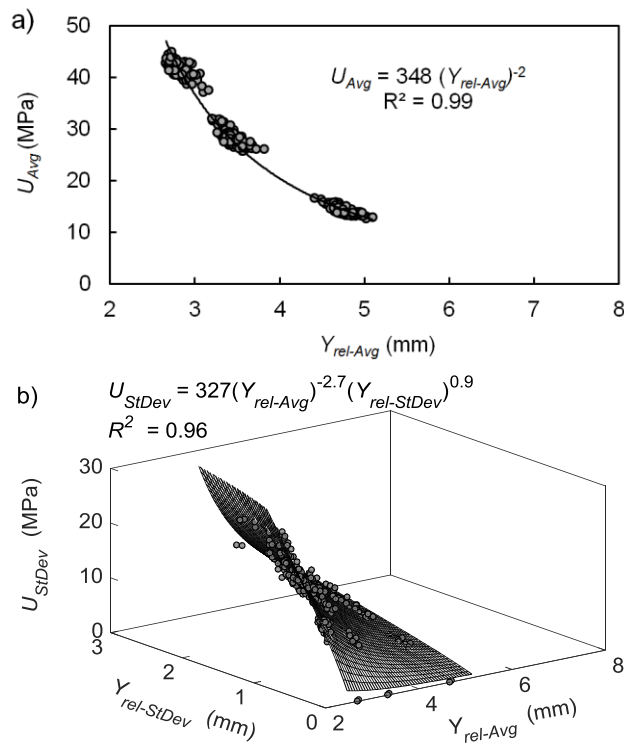


Figure 6-11 Correlations between statistical properties of track modulus and relative vertical track deflection (Y_{rel}) for the loading set shown in Figure 6-8b: a) track modulus average (U_{avg}) vs. Y_{rel} average ($Y_{rel-Avg}$), and b) track modulus standard deviation (U_{StDev}) vs. $Y_{rel-Avg}$ and Y_{rel} standard deviation ($Y_{rel-StDev}$).

Table 6-2 Statistical properties of track modulus and Y_{rel} for the zone with concrete cross ties at Calrin (Y_{rel} : relative vertical track deflection)

For zone with concrete crossties	May run	October run
Y_{rel} average (mm)	3.8	3.8
Y_{rel} StDev (mm)	1.7	3.0
Estimated track modulus average (MPa)	30	24
Estimated track modulus StDev (MPa)	20	24

6.9 Estimating rail bending strains from Y_{rel} data

Rail is considered an infinite beam resting on spring supports. Euler–Bernoulli beam theory defines the relationships between applied loads, rail deformed shape, and rail bending moment profile. These relationships form the basis for estimating rail bending moments from VTD measurements. Once the bending moment is estimated, bending stress and strain are calculated using Equations 6-5 and 6-6 [7, 24].

$$\sigma = \frac{MC}{I} \quad (6-5)$$

$$\sigma = E\varepsilon \quad (6-6)$$

where σ and ε are the bending stress and strain, respectively, I is the moment of inertia of the rail, E is the rail elastic modulus, and C is the distance to the rail neutral axis.

Y_{rel} is dependent on the vertical deflection of the rail at the locations of two wheels and the sensor system. Therefore, the rail deflection profile and, thus, rail bending profile cannot be derived using an individual Y_{rel} measurement. Despite this, Y_{rel} measurements correlate to the extreme bending moments that the rail experiences under wheel loads [24]. This is valuable information that facilitates the calculation of maximum tensile strains in rail. The rail steel is cycled between maximum positive bending moments (M_{max}^+) and maximum negative bending moments (reverse bending moment, M_{max}^-) under moving wheel loads. M_{max}^+ creates maximum tensile strains in the rail base while M_{max}^- generates maximum tensile in the rail head. The cycling results in an oscillation between tensile and compressive bending strains in the rail head and base as wheels pass over [7]. The magnitude of M_{max}^+ is often much greater than M_{max}^- , hence the correlation between Y_{rel} and M_{max}^+ is only studied here. One method to interpret Y_{rel} data is to develop mathematical correlations between the statistical properties of the Y_{rel} distribution and the envelope profile of M_{max}^+ . Figure 6-12 shows the correlations developed for interpreting the Y_{rel} data from the MRail October run. One hundred and eighty track models with different track modulus distributions, RE136 rail size, and tie spacings of 0.61 m were simulated using FEMs. The models were used to calculate the Y_{rel} distribution and envelope profile of M_{max}^+ . The calculations were based on the moving loading set shown in Figure 6-8b. Track window lengths of 80 m were selected and the average and StDev of the modelled Y_{rel}

distribution and envelope profile of M_{max}^+ were calculated for each 80-m section. The correlations between the calculated values were investigated using nonlinear regression analyses. Correlations developed using regression analyses are represented by

$$M_{max-Avg}^+ = 5.3 Y_{rel-Avg} + 24 \quad (6-7)$$

$$M_{max-StDev}^+ = 5.15 Y_{rel-StDev} + 1.3 \quad (6-8)$$

where $M_{max-Avg}^+$ and $M_{max-StDev}^+$ are the average and StDev, respectively, for the envelope profile of M_{max}^+ (in kN·m). These equations are applicable to track window lengths of 80 m or more.

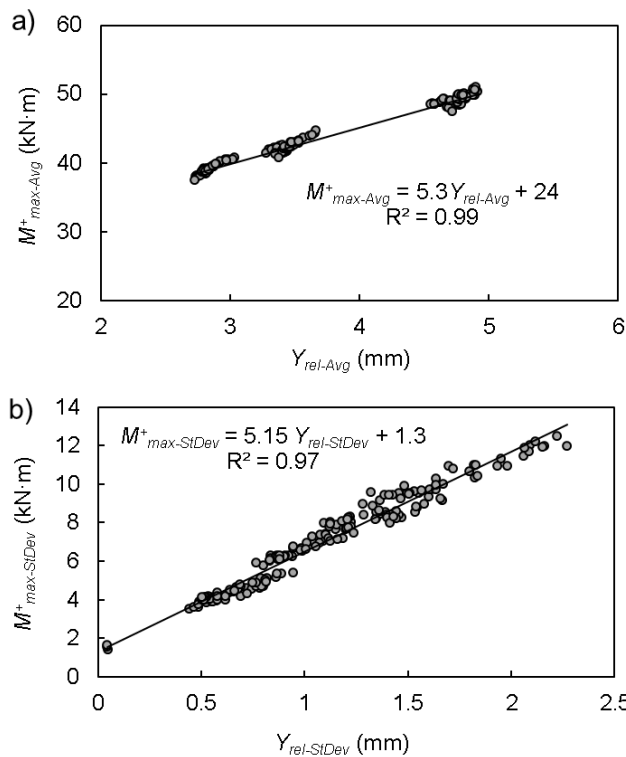


Figure 6-12 Correlations between statistical properties of the relative vertical track deflection (Y_{rel}) and the envelope profile of rail maximum positive bending moment (M_{max}^+) for the loading set shown in Figure 6-8b: a) M_{max}^+ average ($M_{max-Avg}^+$) vs. Y_{rel} average ($Y_{rel-Avg}$), and b) M_{max}^+ standard deviation ($M_{max-StDev}^+$) vs. Y_{rel} standard deviation ($Y_{rel-StDev}$).

Figure 6-13 depicts the distribution of Y_{rel} data collected during the October MRail run at Calrin. The Y_{rel} average and StDev for the zone with concrete cross-ties at the Calrin site are 3.8 and 3

mm, respectively. Equations 6-7 and 6-8 allowed for estimation of the average and StDev of the envelope profile of M_{max}^+ over this zone. Using Equations 6-5 and 6-6 and the estimated M_{max}^+ , the range for maximum tensile strains (ϵ_{max}^T) at the level of strain gauges (on top of the rail bottom flange) were calculated. Values for I , E , and C in the calculations were set at $3.9E-05 \text{ m}^4$ (92.4 in^4), 210 GPa, and 6.4 cm, respectively. Table 6-3 presents a summary of the calculations.

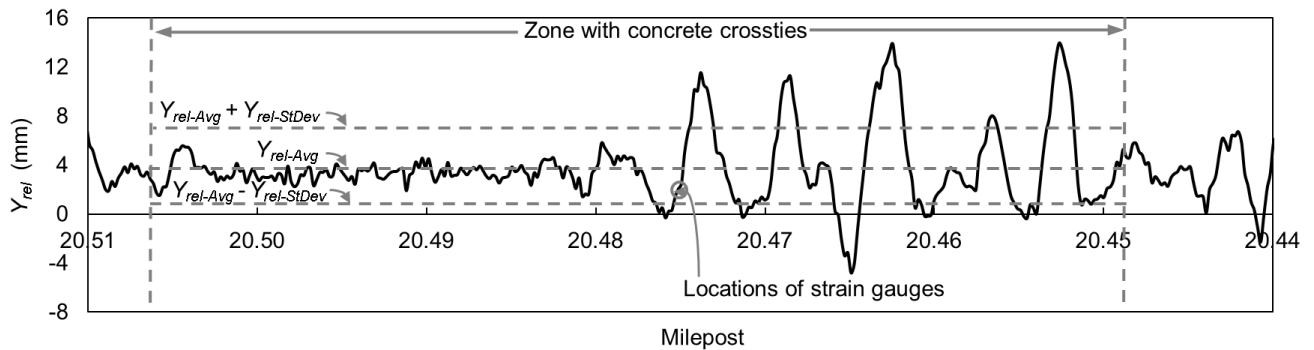


Figure 6-13 Y_{rel} data from the October MRail run at the Calrin site.

Table 6-3 Average and standard deviation for the MRail data at the Calrin site in October together with the estimated average and StDev for the envelope profile of rail maximum positive bending moment and tensile strain (Y_{rel} : relative vertical track deflection, M_{max}^+ : maximum positive bending moment, ϵ_{max}^T : maximum tensile strain, Avg: average, StDev: standard deviation).

$Y_{rel-Avg}$ (mm)	3.8
$Y_{rel-StDev}$ (mm)	3
Estimated $M_{max-Avg}^+$ from $Y_{rel-Avg}$ and Equation 6-7 (kN·m)	44
Estimated $M_{max-StDev}^+$ from $Y_{rel-StDev}$ and Equation 6-8 (kN·m)	17
Estimated $\epsilon_{max-Avg}^T$ from $M_{max-Avg}^+$ and Equations 6-5 and 6-6 ($\mu\epsilon$)	343
Estimated $\epsilon_{max-StDev}^T$ from $M_{max-StDev}^+$ and Equations 6-5 and 6-6 ($\mu\epsilon$)	133

6.10 Comparing the measured maximum tensile strains with the estimated range

The strain gauges at instrumented cribs No. 5, 6, and 7 provided an opportunity to validate the estimation of rail bending strains from the Y_{rel} data. The data points in Figure 6-14 present the maximum tensile bending strains recorded using the rail base strain gauges in August. These strain measurements were conducted under two adjacent fully loaded trucks (Figure 6-7). From

Table 6-3, ranges for M_{max}^+ and ε_{max}^T were estimated using the MRail data. The MRail loading set for the October run also featured two adjacent fully loaded trucks (Figure 6-8b). The Y_{rel} measurements at the locations of rail base strain gauges were within the range of 2 ± 0.6 mm. Considering the Y_{rel} average (3.8 mm) and StDev (3 mm) for the zone with concrete crossties, the Y_{rel} values at the locations of the strain gauges fell within one standard deviation below the Y_{rel} average (Figure 6-14). This suggests that the ε_{max}^T measured at the level of rail base strain gauges should be less than $\varepsilon_{max-Avg}^T$ and greater than $(\varepsilon_{max-Avg}^T - \varepsilon_{max-StDev}^T)$, where $\varepsilon_{max-Avg}^T$ and $\varepsilon_{max-StDev}^T$ are the average and StDev for the envelope profile of ε_{max}^T over the zone with concrete crossties, respectively. Estimated values for $\varepsilon_{max-Avg}^T$ and $\varepsilon_{max-StDev}^T$ from the Y_{rel} data are presented in Table 6-3. Figure 6-14 indicates that the measured tensile strains were within the expected range.

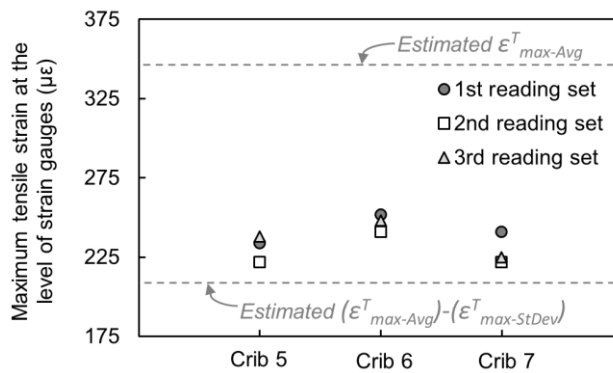


Figure 6-14 Maximum tensile strains measured three times using the rail base strain gauges compared with the range estimated from the Y_{rel} data (ε_{max}^T : maximum tensile strain, $\varepsilon_{max-Avg}^T$ and $\varepsilon_{max-StDev}^T$ are the average and StDev for the envelope profile of ε_{max}^T).

6.11 Conclusions

Train-mounted VTD measurements present an opportunity to estimate rail bending stresses over long distances. The estimations are possible due to mathematical correlations between rail deflections, rail stresses, and applied loads. A new methodology developed by the authors suggests the use of FEMs with stochastically varying track modulus for developing the correlations. The methodology developed using numerical studies facilitates the estimation of a range for the magnitude of maximum bending stresses in rail. The purpose of this study was to validate the methodology using field datasets. Different measurements at the study site were

utilised to meet the objective; specifically, rail-mounted strain gauges and the WILD system provided the information necessary to validate the rail bending stresses estimated from VTD measurements. Analysis of the datasets showed that the strain measurements lie within the estimated ranges. Datasets from different time periods were analysed to assess the rail bending stresses. The magnitude of maximum bending stresses in rail was found to be significantly lower in winter compared to summer. Frozen ballast and stiff track in the winter provide a stronger support for the rail that results in lower rail bending stresses. This suggests that VTD measurements should be conducted over different time periods to assess the overall magnitude of rail bending stress.

CHAPTER 7: Conclusions and Recommendations for Future Research

7.1 Summary and conclusions

In this study, a new methodology to estimate vertical bending stresses in rail from train-mounted vertical track deflection (VTD) measurements was developed and validated. The developed method facilitates the estimation of rail bending stresses over long distances. Mathematical correlations between track modulus, rail deflections, rail bending stresses, and applied loads form the basis of the methodology. The study focused on the use of the measurements from the MRail system that measures the relative VTD (referred to as Y_{rel}) between the rail surface and the rail-wheel contact line under the sensor system, at a distance of 1.22 m from the nearest wheel. The concept presented in this thesis is applicable to other train-mounted VTD measurement systems. However, details of the process for interpreting the VTD data would be slightly different for each system, depending on the type of deflection measurements.

Track modulus is a dominant factor that affects the correlations between rail deflections and bending stresses. Hence, first, the potential of using Y_{rel} measurements as an indicator of the track modulus was comprehensively investigated. The study showed that Y_{rel} is strongly influenced by the cluster of vertical rail supports, which have different stiffness values beneath and around the truck wheels and the sensor system. For this reason, it is not a precise approach to use track models assuming constant track modulus to interpret the Y_{rel} data. A series of finite element models (FEMs) were developed to simulate the stochastic nature of track modulus, and to investigate correlations between Y_{rel} and track modulus over different track window lengths. Data generated from FEMs were analysed using statistical approaches and a series of equations was proposed to quantify the correlation between the statistical properties of track modulus and Y_{rel} . The equations were developed for a specific rail size and loading condition and could be modified for other loading conditions and rail sizes. The data were analysed over different track window lengths. The longer the window length, the stronger the correlations were. However, the ability to detect local track modulus variations decreases with increasing window length. From

the results, different window sizes can be selected depending on the assessment or maintenance requirements. Using the quantified track modulus, a range for extreme bending stresses in rail can be estimated.

Y_{rel} is defined from the vertical deflection of the rail at the locations of two wheels and the sensor system. As a result, the rail deflection profile and, thus, rail bending profile cannot be derived using an individual Y_{rel} measurement. Despite this, Y_{rel} measurements correlate to the extreme bending moments that the rail experiences under wheel loads. This is valuable information that facilitates the calculation of maximum tensile and compressive strains in rail. The rail steel is cycled between maximum positive and negative bending moments under moving wheel loads. The cycling results in an oscillation between tensile and compressive bending strains in the rail head and base as wheels pass over. The magnitudes of maximum positive and negative bending moments vary along the track due to spatially varying track modulus. In this thesis, correlations between Y_{rel} and maximum bending moments in rail were comprehensively investigated. Data generated using the developed FEMs were used to investigate the correlations between statistical properties of Y_{rel} and envelope profile of maximum bending moments. The correlations were quantified using statistical approaches and a series of equations was proposed to estimate the average, standard deviation, and peak for the envelope profile of maximum bending moments from Y_{rel} measurements. The study also resulted in a detailed framework for estimating the probability distributions of rail bending stresses along the track. This indicates strong potential for calculating the reliability of rail under applied loading over large railway networks.

The accuracy of the proposed equations was first verified using a numerical case study for which a random track modulus distribution was considered and artificial noise was added to the modelled Y_{rel} . Subsequently, datasets collected from a study site were used to validate the methodology for estimating rail bending stresses. The rail-mounted strain gauges and the wheel impact load detector system at the study site provided information about the rail bending strains under known applied loads. This allowed validation of the maximum bending stresses estimated using MRail measurements.

The main contribution of this thesis is that it presents a detailed methodology for estimating track modulus and rail bending stresses from VTD measurements. This is the first study that addresses the effect of a stochastically varying track modulus on the correlation between VTD, track

modulus and rail bending stresses. The methodology developed for estimating track modulus and rail bending stresses over long distances is a major step towards evaluating the rail structural integrity which is a complex task and needs a number of pieces to be completed.

The results present a practical approach for interpreting VTD data and estimating track modulus and rail bending stresses over long distances. Information about track modulus and the way it varies along the track makes it easier to identify the root causes of the structural issues of the track. Furthermore, methods for estimating the spatial variation of rail bending stresses allow a more rigorous reliability analysis of rail, and therefore, the establishment of optimised solutions for rail issues.

7.2 Recommendations for future research

The application of the developed methodology needs to be addressed by further study. The VTD data along a railway subdivision can be analysed to identify the locations that experience large rail bending stresses under train passages. The results can be then compared with the historical performance of the rail at the subdivision to investigate the effect of large bending stresses on the rail performance. Historical record of rail defects and breaks from visual, ultrasonic and magnetic inspection methods along with records of maintenance activities (e.g. rail grinding, rail replacement) provide a good understanding about the historical performance of existing rails and indicate the problematic locations along the track.

The outcomes of this study may include:

- establishment of an empirical threshold for permissible stresses in rail;
- development of a new monitoring method for identifying rail sections prone to fracture;
- development of a decision-making tool for scheduling the intervals between rail inspections and more effective allocation of rail test resources;

For assessing the structural condition of the rail and calculating the rail reliability against fracture, information about rail bending stresses from VTD measurements should be used in combination with estimations of residual and thermal stresses. The effect of seasonal changes in rail bending stresses also needs to be addressed. Experience with the field data has shown that frozen ballast in winter can cause a significant reduction in rail deflections and bending stresses

under train passages. Conversely, low temperature in winter triggers high tensile thermal stresses in rail. Low temperature also influences the rail fracture toughness, which in turn affects the permissible rail stresses. Therefore, assessment of the rail condition requires a detailed framework that considers the effects of structural, environmental, and operational factors simultaneously.

References

- [1] Transportation Safety Board of Canada. Rail, <http://www.bst-tsb.gc.ca/eng/rail/index.asp> (accessed: 9 September 2016).
- [2] Jeong DY. Progress in Rail Integrity Research. Report no. DOT/FRA/ORD-01/18, Final Report, 2001.
- [3] Jeong DY and Perlman AB. Analysis of Minimum Rail Size in Heavy Axle Load Environment. In: 2013 Joint Rail Conference, Tennessee, USA, 2013.
- [4] Transportation Safety Board of Canada. Statistical Summary Railway Occurrences 2014. Report no. TU1-2E-PDF, 2015.
- [5] Transport Canada. Canadian Rail Operating Rules, 2015.
- [6] Cannon D, EDEL K, Grassie S, et al. Rail Defects: An overview. *Fatigue Fract Engng Mater Struct*, 2003; 26: 865-886.
- [7] Hay WW. *Railroad Engineering*. 2nd ed John Wiley & Sons, 1982.
- [8] Zerbst U, Schödel M and Heyder R. Damage Tolerance Investigations on Rails. *Eng Fract Mech*, 2009; 76 (17): 2637-2653.
- [9] Zerbst U, Lundén R, Edel K, et al. Introduction to the Damage Tolerance Behaviour of Railway Rails—a Review. *Eng Fract Mech*, 2009; 76: 2563-2601.
- [10] Esveld C. *Modern Railway Track*. 2nd ed. Netherlands: MRT-productions, 2001.
- [11] Mair R and Groenhout R. Prediction of Rail Steel Strength Requirements—A Reliability Approach. In: *Rail Steels—Developments, Processing, and use*, 1978.
- [12] Arbabi F and Loh C. Reliability Analysis of Railroad Tracks. *J Struct Eng*, 1991; 117: 1435-1447.
- [13] Koc W and Wilk A. Investigations of Methods to Measure Longitudinal Forces in Continuous Welded Rail Tracks using the Tamping Machine. *Proc Inst Mech Eng Pt F: J Rail Rapid Transit*, 2009; 223: 61-73.
- [14] Al-Nazer L and Sivathanu Y. In-Motion, Non-Contact Rail Temperature Measurement Sensor. Report no. RR 12-18, 2012.
- [15] Wegner A. Prevention of Track Buckling and Rail Fracture by Non-destructive Testing of the Neutral Temperature in CW-rails. In: *Proceedings International Heavy Haul Conference*, Kiruna, Sweden, 2007; 557-564.

- [16] Zhang Y, Clemenzi J, Kesler K, et al. Real Time Prediction of Rail Temperature. In: Proceedings of AREMA 2007 Annual Conference, Chicago, U.S., 2007.
- [17] Kelleher J, Prime M, Buttle D, et al. The Measurement of Residual Stress in Railway Rails by Diffraction and other Methods. *J Neutron Research*, 2003; 11: 187-193.
- [18] Deputat J, Szelazek J and Kwaszczyhska-Klimek AM. Experiences in Ultrasonic Measurement of Rail Residual Stresses. *Residual Stress in Rails*, 1992.
- [19] Groom J. Determination of Residual Stresses in rails. Report no. DOT/FRA/ORD-83/05, DOT-TSC-FRA-81-21, Final Report, 1983.
- [20] Greisen C, Lu S, Duan H, et al. Estimation of Rail Bending Stress from Real-time Vertical Track Deflection Measurement. In: 2009 Joint Rail Conference, 2009; 175-182.
- [21] Farritor S and Fateh M. Measurement of Vertical Track Deflection from a Moving Rail Car. Report no. Federal Railroad Administration, DOT/FRA/ORD-13/08, 2013.
- [22] Berggren EG, Nissen A and Paulsson BS. Track Deflection and Stiffness Measurements from a Track Recording Car. *Proc IMechE Part F: J Rail Rapid Transit*, 2014; 228(6): 570-580.
- [23] Norman CD. Measurement of Track Modulus from a Moving Railcar. Master Thesis, University of Nebraska -Lincoln, USA, 2004.
- [24] Lu S. Real-Time Vertical Track Deflection Measurement System. PhD Dissertation, University of Nebraska -Lincoln, USA, 2008.
- [25] Greisen CJ. Measurement, Simulation, and Analysis of the Mechanical Response of Railroad Track. Master Thesis, University of Nebraska -Lincoln, USA, 2010.
- [26] Li D, Thompson R, Marquez P, et al. Development and Implementation of a Continuous Vertical Track-Support Testing Technique. *Transp Res Rec*, 2004; 1863: 68-73.
- [27] Selig ET and Li D. Track Modulus: Its Meaning and Factors Influencing It. *Transp Res Rec*, 1994; 1470: 47-54.
- [28] Ebersohn W and Selig ET. Track Modulus Measurements on a Heavy Haul Line. *Transp Res Rec*, 1994; 1470: 73-82.
- [29] Sussman T, Ebersöhn W and Selig E. Fundamental Nonlinear Track Load-Deflection Behavior for Condition Evaluation. *Transp Res Rec*, 2001; 1742: 61-67.
- [30] Pita AL, Teixeira PF and Robusté F. High Speed and Track Deterioration: the Role of Vertical Stiffness of the Track. *Proc IMechE Part F: J Rail Rapid Transit*, 2004; 218: 31-40.

- [31] Dahlberg T. Railway Track Stiffness Variations-Consequences and Countermeasures. *International Journal of Civil Engineering*, 2010; Vol.8, No.1.
- [32] Mair R and Groenhout R. The Growth of Transverse Fatigue Defects in the Head of Railway Rails. *Rail Engineering International*, 1980.
- [33] Orringer O, Morris JM and Steele RK. Applied Research on Rail Fatigue and Fracture in the United States. *Theor Appl Fract Mech*, 1984.
- [34] Marich S. Rail Wear/Fatigue Limits. *Track Technology*, 1985: 179-189.
- [35] Zerbst U and Beretta S. Failure and Damage Tolerance Aspects of Railway Components. *Eng Failure Anal*, 2011.
- [36] Sperry Rail Service. Rail Defect Manual, 1964.
- [37] Transport RailCorp. Rail Defects Handbook. Version 1.2, 2012.
- [38] Zerbst U, Mädler K and Hintze H. Fracture Mechanics in Railway Applications—an Overview. *Eng Fract Mech*, 2005; 72(2), 163-194 .
- [39] Magel E, Sroba P, Sawley K, et al. Control of Rolling Contact Fatigue of Rails. In: AREMA 2004 Annual Conference, Nashville, USA, 2004.
- [40] Orringer O, Tang YH, Gordon JE, et al. Crack Propagation Life of Detail Fractures in Rails. Report no. DOT/FRA/ORD-88/13, DOT-TSC-FRA-88-1, Final Report, 1988.
- [41] Lim N, Park N and Kang Y. Stability of Continuous Welded Rail Track. *Comput Struct*, 2003; 81: 2219-2236.
- [42] Kish A and Samavedam G. Track Buckling Prevention: Theory, Safety Concepts, and Applications. Report no. DOT/FRA/ORD-13/16, Final Report, 2013.
- [43] Lyons M, Jeong D and Gordon J. Fracture Mechanics Approach to Estimate Rail Wear Limits. In: ASME 2009 Rail Transportation Division Fall Technical Conference, Texas, USA, 2009, 137-146.
- [44] Hasan N. Allowable Bending Fatigue Stress of Rails. *Pract Periodical Struct Des Constr*, 2014; 20(2): 04014033.
- [45] Sato Y, Matsumoto A and Knothe K. Review on Rail Corrugation Studies. *Wear*, 2002; 253: 130-139.
- [46] Olofsson U and Telliskivi T. Wear, Plastic deformation and Friction of Two Rail Steels—a Full-scale Test and a Laboratory Study. *Wear*, 2003; 254: 80-93.

- [47] Bower A and Johnson K. The Influence of Strain Hardening on Cumulative Plastic Deformation in Rolling and Sliding Line Contact. *J Mech Phys Solids*, 1989; 37: 471-493.
- [48] Van KD and Maitournam M. On Some Recent Trends in Modelling of Contact Fatigue and Wear in Rail. *Wear*, 2002; 253: 219-227.
- [49] Johnson K. The Mechanics of Plastic Deformation of Surface and Subsurface layers in Rolling and Sliding Contact. In: *Key Engineering Materials* , Trans Tech Publ, Switzerland, 1989; 33: 17-34.
- [50] Bower A and Johnson K. Plastic Flow and Shakedown of the Rail Surface in Repeated Wheel-rail Contact. *Wear*, 1991; 144: 1-18.
- [51] Vidaud M and Zwanenburg W. Current Situation on Rolling Contact Fatigue—a Rail Wear Phenomenon. In: *9th Swiss Transport Research Conference, Monte Verita, Ascona, 2009*.
- [52] Grassie SL. Rolling Contact Fatigue on the British Railway System: Treatment. *Wear*, 2005; 258: 1310-1318.
- [53] Sih GC and Tzou D. Three-dimensional Transverse Fatigue Crack Growth in Rail Head. *Theor Appl Fract Mech*, 1984; 1(1): 103-115.
- [54] Grassie S and Kalousek J. Rail Corrugation: Characteristics, Causes and Treatments. *Proc Inst Mech Eng Pt F: J Rail Rapid Transit*, 1993; 207: 57-68.
- [55] Grassie SL. Rail Corrugation: Advances in Measurement, Understanding and Treatment. *Wear*, 2005; 258: 1224-1234.
- [56] Transport Canada. Alternative Performance Measures for Rail-focused Track Safety . Report No. TP 15193E, 2013.
- [57] Mayville RA and Stringfellow RG. The Development and Application of Rail Defect Fracture Models to Assess Remedial Actions. Report no. DOT/FRA/ORD-93/33, Final Report, 1993.
- [58] Sih G and Tzou D. Rail-end Bolt Hole Fatigue Crack in Three Dimensions. *Theor Appl Fract Mech*, 1985; 3: 97-111.
- [59] American Railway Engineering and Maintenance-of-Way Association. *Manual for Railway Engineering*. Volume 4, 2011.
- [60] Jeong DY, Tang YH and Orringer O. Estimation of Rail Wear Limits Based on Rail Strength Investigations. Report no. DOT/FRA/ORD-98/07, DOT-VNTSC-FRA-98-13, Final Report, 1998.

- [61] Evans PRV, Owen NB and McCartney LN. Mean Stress Effects on Fatigue Crack Growth and Failure in a Rail Steel. *Eng Fract Mech*, 1974; 6: 183-193.
- [62] Bannantine J, Corner J and Handrock J. *Fundamentals of Metal Fatigue Analysis*. NJ: Prentice Hall, Englewood Cliffs, 1990.
- [63] Anderson TL and Anderson T. *Fracture Mechanics: Fundamentals and Applications*. CRC press, 2005.
- [64] Sih GC and Tzou D. Three-dimensional Transverse Fatigue Crack Growth in Rail Head. *Theor Appl Fract Mech*, 1984; 1: 103-115.
- [65] Shah RC and Kobayashi AS. Stress Intensity Factor for an Elliptical Crack under Arbitrary Normal Loading. *Eng Fract Mech*, 1971; 3: 71-96.
- [66] Shah RC and Kobayashi AS. Stress Intensity Factor for an Elliptical Crack Approaching the Surface of a Plate in Bending. In: *Stress Analysis and Growth of Cracks: Proceedings of the 1971 National Symposium on Fracture Mechanics: Part 1*, 1972.
- [67] Feddersen CE and Broek D. Fatigue Crack Propagation in Rail Steels. In: *Rail Steels—Developments, Processing, and Use*, Denver, 1976.
- [68] Narayanan RM, Jakub JW, Li D, et al. Railroad Track Modulus Estimation using Ground Penetrating Radar Measurements. *NDT E Int*, 2004; 37: 141-151.
- [69] Li M and Berggren E. A Study of the Effect of Global Track Stiffness and its Variations on Track Performance: Simulation and Measurement. *Proc IMechE Part F: J Rail Rapid Transit*, 2010; 224: 375-382.
- [70] Berggren E. *Railway Track Stiffness: Dynamic Measurements and Evaluation for Efficient Maintenance*. PhD Dissertation, Royal Institute of Technology (KTH), Sweden, 2009.
- [71] Ahlf RE. M/W Costs: How They Are Affected by Car Weights and the Track Structure. *Railw Track Struct*, 1975; 71 (3).
- [72] Redden J, Selig E and Zarembski A. Stiff Track Modulus Considerations. *Railw Track Struct*, 2002; 98: 25-30.
- [73] Raymond GP. Analysis of Track Support and Determination of Track Modulus. *Transp Res Rec*, 1985; 1022: 80-90.
- [74] Lundgren JR, Martin G and Hay W. A Simulation Model of Ballast Support and the Modulus of Track Elasticity. *Civil Engineering Studies, Transportation Series No. 14*, Department of Civil Engineering, University of Illinois, Illinois, 1970.

- [75] Farritor S. Real-Time Measurement of Track Modulus from a Moving Car. Report no. DOT/FRA/ORD-05/05, 2005.
- [76] Thompson R and Li D. Automated Vertical Track Strength Testing Using TTCI's Track Loading Vehicle. Technology Digest February, 2002; 1489: 17-25.
- [77] Roghani A, Macciotta R and Hendry MT. Combining Track Quality and Performance Measures to Assess Track Maintenance Requirements. In: Joint Rail Conference, San Jose, CA, 2015.
- [78] Roghani A, Hendry MT, Ruel M, et al. A Case Study of the Assessment of an Existing Rail Line for Increased Traffic and Axle Loads. In: International Heavy Haul Association, Perth, Australia, 2015.
- [79] Roghani A and Hendry MT. Assessing the Potential of a Technology to Map the Subgrade Stiffness Under the Rail Tracks. In: Transportation Research Board 94th Annual Meeting, Washington, DC, USA, 2015.
- [80] Roghani A and Hendry MT. Continuous Vertical Track Deflection Measurements to Map Subgrade Condition along a Railway Line: Methodology and Case Studies. J Transp Eng 2016; doi:10.1061/(ASCE)TE.1943-5436.0000892.
- [81] Lu S, Duan H, Greisen C, et al. Case Studies Determining the Effects of Track Stiffness on Vehicle Dynamics. In: Joint Rail Conference, 2010;145-154.
- [82] Lu S, Hogan C, Minert B, et al. Exception Criteria in Vertical Track Deflection and Modulus. In: ASME/IEEE 2007 Joint Rail Conference and Internal Combustion Engine Division Spring Technical Conference, 2007; 191-198.
- [83] Roghani A and Hendry MT. Quantifying the Impact of Subgrade Stiffness on Track Quality and the Development of Geometry Defects. J Transp Eng, 2017; doi:10.1061/JTEPBS.0000043.
- [84] Bowness D, Lock AC, Powrie W, et al. Monitoring the Dynamic Displacements of Railway Track. Proc Inst Mech Eng Part F: J Rail Rapid Transit, 2007. doi: 10.1243/0954409JRRT51.
- [85] Priest JA and Powrie W. Determination of Dynamic Track Modulus from Measurement of Track Velocity during Train Passage. J Geotech Geoenviron Eng, 2009. doi: 10.1061/(ASCE)GT.1943-5606.0000130.
- [86] Murray CA, Take WA and Hoults NA. Measurement of Vertical and Longitudinal Rail Displacements using Digital Image Correlation. Can Geotech J, 2015; 52: 141-155.
- [87] Cai Z, Raymond GP and Bathurst RJ. Estimate of Static Track Modulus Using Elastic Foundation Models. Trans Res Rec, 1994; 1470: 65-72.

- [88] Hendry MT, Hughes DA and Barbour L. Track Displacement and Energy Loss in a Railway Embankment. *Proceedings of the ICE - Geotechnical Engineering* 2010; 163: 3-12.
- [89] Berggren E, Jahlénius Å and Bengtsson B. Continuous Track Stiffness Measurement: an Effective Method to Investigate the Structural Conditions of the Track. In: *International Conference of Railway Engineering*, London, 2002.
- [90] Wolf G and Hogan C. Real Time Derailment Risk Assessment Using Vehicle and Track Fault Monitoring With Dynamic Simulation over Long Corridors. In: *International Railway Safety Conference*, Melbourne, Australia, 2011.
- [91] Farritor S, Arnold R, Lu S, et al. Real-time Vertical Track Modulus Measurement System from a Moving Railcar. Report no. FRA/RR06-08, 2006.
- [92] Norman C, Farritor S, Arnold R, et al. Design of a System to Measure Track Modulus from a Moving Railcar. In: *Proceeding of American Railway Engineering and Maintenance of Way Association Annual Conference*, 2004.
- [93] Lu S, Farritor S, Arnold, et al. Measurement of Vertical Track Modulus: Field Testing, Repeatability, and Effects of Track Geometry. In: *IEEE/ASME/ASCE 2008 Joint Rail Conference*, 2008; 151-158.
- [94] Sadeghi J and Barati P. Evaluation of Conventional Methods in Analysis and Design of Railway Track System. *International Journal of Civil Engineering*, 2010; 8: 44-55.
- [95] Feng H. 3D-Models of Railway Track for Dynamic Analysis. Master Thesis, Division of Highway and Railway Engineering, Department of Transport Science, School of Architecture and the Built Environment, Royal Institute of Technology, Stockholm, Sweden, 2011.
- [96] Computers and Structures Inc. CSiBridge 2014; Advanced W/Rating 16.1.0.
- [97] Madshus C and Kaynia A. High-speed Railway Lines on Soft Ground: Dynamic Behaviour at Critical Train Speed. *Jornal of Sound Vibration*, 2000; 231(3): 689-701.
- [98] Mahmoud A and El Tawil MA. Beams on Random Elastic Supports. *Appl Math Model*, 1992; 16(6): 330-334.
- [99] Moravcik M. Vertical Track Stiffness Effect on Dynamic Behaviour of Track Structure. *Komunikacie*, 2004; 6(3): 10-16.
- [100] Yang LA, Powrie W and Priest JA. Dynamic Stress Analysis of a Ballasted Railway Track Bed during Train Passage. *J Geotech Geoenviron Eng*, 2009. doi: 10.1061/(ASCE)GT.1943-5606.0000032.

- [101] Transportation Safety Board of Canada. Statistical Summary Railway Occurrences 2014. Report no. TU1-2E-PDF, 2015.
- [102] Saat MR, Barkan CPL and Liu X. Analysis of Causes of Major Train Derailment and Their Effect on Accident Rates. *Transp Res Rec*, 2012; No. 2289: 154-163.
- [103] Dick CT, Barkan CPL, Chapman ER, et al. Multivariate Statistical Model for Predicting the Occurrence and Location of Broken Rails. *Transp Res Rec*, 2003; No. 1825: 48-55.
- [104] Jeong DY and Perlman AB. Estimating Track Capacity Based on Rail Stresses and Metal Fatigue. In: *Proceedings of the 2011 ASME Rail Transportation Division Fall Technical Conference*, Minneapolis, Minnesota, USA, September 2011.
- [105] Sawley K and Reiff R. Rail Failure Assessment for the Office of the Rail Regulator. Report no. P-00-070, 2000.
- [106] Kouroussis G, Caucheteur C, Kinet D, et al. Review of Trackside Monitoring Solutions: from Strain Gages to Optical Fibre Sensors. *Sensors*, 2015; 15: 20115-20139.
- [107] Jaiswal J, Blair S, Stevens A, et al. A Systems Approach to Evaluating Rail Life. In: *Railway Engineering/ECS Publications*, London, 2002.
- [108] Fallah Nafari S, Gül M, Roghani A, et al. Evaluating the Potential of a Rolling Deflection Measurement System to Estimate Track Modulus. *Proc IMechE Part F: J Rail Rapid Transit*, 2015; doi: 10.1177/0954409716646404.
- [109] Kouroussis G, Caucheteur C, Kinet D, et al. Review of Trackside Monitoring Solutions: from Strain Gages to Pptical Fibre Sensors. *Sensors*, 2015. doi: 10.3390/s150820115.
- [110] Fallah Nafari S, Gül M, Hendry MT, et al. Estimation of Rail Vertical Bending Stress using Train-Mounted Vertical Track Deflection Measurement Systems. *Proc IMechE Part F: J Rail Rapid Transit*, 2017; submitted for publication.

Appendix A: Numerical Model Details

In this project, RE136 and RE100 rail sizes were used for developing the models. Rails are modeled using frame elements in CSiBridge. Cross section and material properties for these rail sizes are as follows:

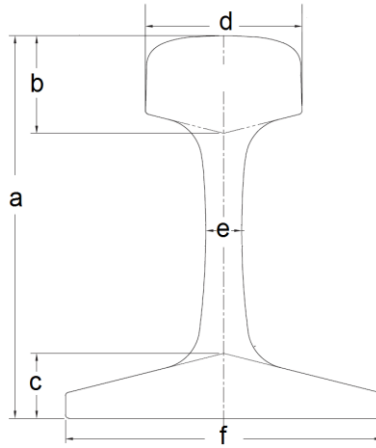


Figure A-1 Rail shape and guide for Table A-1

Table A-1 Cross section dimensions for RE136 and RE100 rail sizes (in mm)

Rail size	a	b	c	d	e	f
RE100	152.4	42.1	27.0	68.3	14.3	136.5
RE136	185.7	49.2	30.2	74.6	17.5	152.4

Table A-2 Cross section and material properties for RE136 and RE100 rail sizes (in mm)

Rail size	Area (mm ²)	Moment of inertia about the strong axis (mm ⁴)	Elastic modulus (GPa)
RE100	6419.3	2.04E07	210
RE136	8597.6	3.92E07	210